Published for SISSA by Springer

Received: October 13, 2010
Accepted: November 24, 2010
Published: December 14, 2010

Measurement of the $W \to \ell\nu$ and $Z/\gamma^* \to \ell\ell$ production cross sections in proton-proton collisions at $\sqrt{s} = 7$ TeV with the ATLAS detector

The ATLAS Collaboration[1]

Abstract: First measurements of the $W \to \ell\nu$ and $Z/\gamma^* \to \ell\ell$ ($\ell = e, \mu$) production cross sections in proton-proton collisions at $\sqrt{s} = 7$ TeV are presented using data recorded by the ATLAS experiment at the LHC. The results are based on 2250 $W \to \ell\nu$ and 179 $Z/\gamma^* \to \ell\ell$ candidate events selected from a data set corresponding to an integrated luminosity of approximately 320 nb^{-1}. The measured total W and Z/γ^*-boson production cross sections times the respective leptonic branching ratios for the combined electron and muon channels are $\sigma_W^{\text{tot}} \cdot \text{BR}(W \to \ell\nu) = 9.96 \pm 0.23(\text{stat}) \pm 0.50(\text{syst}) \pm 1.10(\text{lumi})$ nb and $\sigma_{Z/\gamma^*}^{\text{tot}} \cdot \text{BR}(Z/\gamma^* \to \ell\ell) = 0.82 \pm 0.06\,(\text{stat}) \pm 0.05\,(\text{syst}) \pm 0.09\,(\text{lumi})$ nb (within the invariant mass window $66 < m_{\ell\ell} < 116$ GeV). The W/Z cross-section ratio is measured to be $11.7 \pm 0.9(\text{stat}) \pm 0.4(\text{syst})$. In addition, measurements of the W^+ and W^- production cross sections and of the lepton charge asymmetry are reported. Theoretical predictions based on NNLO QCD calculations are found to agree with the measurements.

Keywords: Hadron-Hadron Scattering

ArXiv ePrint: 1010.2130

[1] See appendix for the list of collaboration members.

Open Access

doi:10.1007/JHEP12(2010)060

JHEP12(2010)060

Contents

JHEP12(2010)060

1 Introduction

Measurements of the inclusive production cross sections of the W and Z bosons at hadron colliders constitute an important test of the Standard Model. The theoretical calculations involve parton distribution functions (PDF) and different couplings of the partons to the weak bosons. They are affected by significant higher-order QCD corrections. Calculations of the inclusive W and Z production cross sections have been carried out at next-to-leading order (NLO) [1–3] and next-to-next-to leading order (NNLO) in perturbation theory [4–9].

The production of W and Z bosons at hadron colliders was measured previously by the UA1 [10] and UA2 [11] experiments at $\sqrt{s} = 0.63\,\text{TeV}$ at the CERN Sp$\bar{\text{p}}$S and by the CDF [12–14] and D0 [15–17] experiments at $\sqrt{s} = 1.8\,\text{TeV}$ and $\sqrt{s} = 1.96\,\text{TeV}$ at the Fermilab Tevatron proton-antiproton colliders. In contrast to proton-antiproton collisions, the cross sections for W^+ and W^- production are expected to be different in proton-proton collisions due to different valence quark distributions of the u and d quarks. Most recently, the RHIC collider experiments [18, 19] have reported the first observation of W production in proton-proton collisions at $\sqrt{s} = 0.5\,\text{TeV}$.

W and Z bosons are expected to be produced abundantly at the Large Hadron Collider (LHC) [20]. The projected large dataset and the high LHC energy will allow for detailed measurements of their production properties in a previously unexplored kinematic domain. These conditions, together with the proton-proton nature of the collisions, will provide new constraints on the parton distribution functions and will allow for precise tests of perturbative QCD. Besides the measurements of the W and Z boson production cross sections, the measurement of their ratio R and of the asymmetry between the W^+ and W^- cross sections constitute important tests of the Standard Model. The ratio R can be measured with a higher relative precision because both experimental and theoretical uncertainties partially cancel. With larger data sets this ratio can be used to provide constraints on the W-boson width Γ_W [14].

This paper describes the first measurement of the W^+, W^- and Z/γ^* boson production cross sections in proton-proton collisions at $\sqrt{s} = 7\,\text{TeV}$ by the ATLAS [21] experiment at the LHC. The measurements are based on data corresponding to an integrated luminosity of approximately 320 nb^{-1}. The inclusive Z/γ^*-production-cross section is measured within the mass range $66 < m_{\ell\ell} < 116\,\text{GeV}$. In addition to the individual cross-section measurements, first measurements of the ratio R of the W to Z cross sections and of the $W \to \ell\nu$ charge asymmetry are presented. Throughout this paper the label "Z" refers to Z/γ^*.

The paper is organized as follows: after a short description of the ATLAS detector, the data set and the Monte-Carlo samples in sections 2 and 3, the identification of electrons, muons and the measurement of the transverse missing energy are discussed in section 4. In section 5, the selection of $W \to \ell\nu$ and $Z \to \ell\ell$ candidates is presented. Section 6 is devoted to a detailed discussion of backgrounds in these samples. The measurement of the $W \to \ell\nu$ and $Z \to \ell\ell$ cross sections and of their ratio is presented in section 7 together with a comparison to theoretical predictions. The measurement of the $W \to \ell\nu$ charge asymmetry is discussed in section 8.

JHEP12(2010)060

2 The ATLAS detector

The ATLAS detector [21] at the LHC comprises a thin superconducting solenoid surrounding the inner-detector and three large superconducting toroids arranged with an eight-fold azimuthal coil symmetry placed around the calorimeters, forming the basis of the muon spectrometer.

The Inner-Detector (ID) system is immersed in a 2 T axial magnetic field and provides tracking information for charged particles in a pseudorapidity range matched by the precision measurements of the electromagnetic calorimeter; the silicon tracking detectors, pixel and silicon microstrip (SCT), cover the pseudorapidity range $|\eta| < 2.5$.[1] The highest granularity is achieved around the vertex region using the pixel detectors. The Transition Radiation Tracker (TRT), which surrounds the silicon detectors, enables track-following up to $|\eta| = 2.0$. Electron identification information is provided by the detection of transition radiation in the TRT straw tubes.

The calorimeter system covers the pseudorapidity range $|\eta| < 4.9$. It is based on two different detector technologies, with liquid argon (LAr) and scintillator-tiles as active media. The electromagnetic (EM) calorimeter, consisting of lead absorbers and liquid argon as the active material, is divided into one barrel ($|\eta| < 1.475$) and two end-cap components ($1.375 < |\eta| < 3.2$). It uses an accordion geometry to ensure fast and uniform response. It has a fine segmentation in both the lateral and longitudinal directions of the particle showers. At high energy, most of the EM shower energy is collected in the second layer which has a lateral cell granularity of $\Delta\eta \times \Delta\phi = 0.025 \times 0.025$. The first layer is segmented into eight strips per cell in the η direction which extend over four cells in ϕ. A third layer measures the tails of very high energy EM showers and helps in rejecting hadron showers. In the region $|\eta| < 1.8$, a presampler detector consisting of a thin layer of LAr is used to correct for the energy lost by electrons, positrons, and photons upstream of the calorimeter. The hadronic tile calorimeter is placed directly outside the EM calorimeter envelope. This steel/scintillating-tile detector consists of a barrel covering the region $|\eta| < 1.0$, and two extended barrels in the range $0.8 < |\eta| < 1.7$. The copper Hadronic End-cap Calorimeter (HEC), which uses LAr as active material, consists of two independent wheels per end-cap ($1.5 < |\eta| < 3.2$), located directly behind the end-cap electromagnetic calorimeter. The Forward Calorimeter (FCal), which also uses LAr as the active material, consists of three modules in each end-cap: the first, made of copper, is optimised for electromagnetic measurements, while the other two, made of tungsten, measure primarily the energy of hadronic interactions [22].

Muon detection is based on the magnetic deflection of muon tracks in the large superconducting air-core toroid magnets, instrumented with separate trigger and high-precision tracking chambers. A system of three toroids, a barrel and two end-caps, generates the

[1] The nominal interaction point is defined as the origin of the coordinate system, while the anti-clockwise beam direction defines the z-axis and the $x - y$ plane is transverse to the beam direction. The positive x-axis is defined as pointing from the interaction point to the centre of the LHC ring and the positive y-axis is defined as pointing upwards. The azimuthal angle ϕ is measured around the beam axis and the polar angle θ is the angle from the beam axis. The pseudorapidity is defined as $\eta = -\ln\tan(\theta/2)$. The distance ΔR in the $\eta - \phi$ space is defined as $\Delta R = \sqrt{(\Delta\eta)^2 + (\Delta\phi)^2}$.

JHEP12(2010)060

magnetic field for the muon spectrometer in the pseudorapidity range $|\eta| < 2.7$. Over most of the η-range, a precision measurement of the track coordinates in the principal bending direction of the magnetic field is provided by Monitored Drift Tubes (MDTs). At large pseudorapidities, Cathode Strip Chambers (CSCs) with higher granularity are used in the innermost plane (station) over $2.0 < |\eta| < 2.7$, to withstand the demanding rate and background conditions expected with the LHC operation at the nominal luminosity. The muon trigger system, which covers the pseudorapidity range $|\eta| < 2.4$, consists of Resistive Plate Chambers (RPCs) in the barrel ($|\eta| < 1.05$) and Thin Gap Chambers (TGCs) in the end-cap regions ($1.05 < |\eta| < 2.4$), with a small overlap in the $|\eta| = 1.05$ region.

The first-level (L1) trigger system uses a subset of the total detector information to make a decision on whether or not to record each event, reducing the data rate to a design value of approximately 75 kHz. Details about the L1 calorimeter and muon trigger systems used in the W and Z analyses are provided in section 3. The subsequent two levels, collectively known as the high-level trigger, are the Level-2 (L2) trigger and the event filter. They provide the reduction to a final data-taking rate designed to be approximately 200 Hz.

3 Data and Monte-Carlo samples

The data were collected over a four-month period, from March to July 2010. Application of basic beam, detector, and data-quality requirements resulted in total integrated luminosities of 315 nb^{-1} for the $W \to e\nu$, 310 nb^{-1} for the $W \to \mu\nu$, 316 nb^{-1} for the $Z \to ee$, and 331 nb^{-1} for the $Z \to \mu\mu$ channels. The absolute luminosity was calibrated using beam separation scans [23], yielding a total systematic uncertainty of $\pm 11\%$, dominated by the measurement of the LHC beam currents. Details on the methods and measurement results obtained with several detectors in ATLAS can be found in ref. [24].

Events in this analysis are selected using only the hardware-based L1 trigger, i.e. without use of the high-level trigger. The L1 calorimeter trigger selects photon and electron candidates within $|\eta| < 2.5$ using calorimeter information in trigger towers of dimension $\Delta\eta \times \Delta\phi = 0.1 \times 0.1$. The calorimeter trigger used in this analysis accepts electron and photon candidates if the transverse energy from a cluster of trigger towers is above approximately 10 GeV. The L1 muon trigger searches for patterns of hits within $|\eta| < 2.4$ consistent with high-p_{T} muons originating from the interaction region. The algorithm requires a coincidence of hits in the different trigger stations along a road which follows the path of a muon from the interaction point through the detector. The width of the road is related to the p_{T} threshold to be applied. The muon trigger used in this analysis corresponds to a threshold of approximately 6 GeV. As a result of these trigger decisions, a total of 6.5×10^6 and 5.1×10^6 events are triggered in the electron and muon channels, respectively.

In order to compare the data with theoretical expectations and to estimate the backgrounds from various physics processes, Monte-Carlo simulations were performed. For the W and Z signal processes, dedicated $W \to \ell\nu$ and $Z \to \ell\ell$ signal samples were generated. For the backgrounds the following processes were considered:

JHEP12(2010)060

- $W \to \tau\nu$: this process is expected to contribute, in particular via leptonic tau decays, $\tau \to \ell\nu\nu$, to both electron and muon final states in the W analysis.

- $Z \to \ell\ell$: $Z \to \mu\mu$ decays with one muon outside of the muon-spectrometer acceptance generate apparent missing transverse energy and constitute an important background in the $W \to \mu\nu$ analysis. Due to the larger η coverage of the calorimeter system, this effect is less severe for the corresponding $Z \to ee$ decays in the $W \to e\nu$ analysis.

- $Z \to \tau\tau$: these decays contribute a smaller background than $W \to \tau\nu$ and $Z \to \ell\ell$ decays to the W analysis. For the Z analysis, they are more important than the two aforementioned backgrounds.

- $t\bar{t}$ production: the production of top pairs constitutes an additional background to both the W and Z analyses. The relative size, compared to the backgrounds from W and Z decays, depends on the channel considered.

- Jet production via QCD processes: the production of jets via QCD processes (referred to as "QCD background" in the following) is another important background contribution. It has significant components from semi-leptonic decays of heavy quarks, hadrons misidentified as leptons and, in the case of the electron channel, electrons from conversions. For the $Z \to \mu\mu$ analysis, dedicated $b\bar{b}$ and $c\bar{c}$ samples were generated in addition, to increase the statistics for these background components.

An overview of all signal and background processes considered and of the generators used for the simulation is given in table 1. All signal and background samples were generated at $\sqrt{s} = 7\,\text{TeV}$, then processed with the GEANT4 [25] simulation of the ATLAS detector [26], reconstructed and passed through the same analysis chain as the data. For the comparison to data, all cross sections, except the dijet cross section, are normalised to the results of higher order QCD calculations (see table 1). More details on the calculations for the W and Z processes and on the assigned uncertainties are presented in section 7.6. For the $t\bar{t}$ production cross section, an uncertainty of $\pm 6\%$ is assumed.

For the QCD background, no reliable prediction can be obtained from a leading order Monte-Carlo simulation. For the comparisons of differential distributions to data, as presented in section 5, this background is normalised to data. However, for the final cross-section measurement, except for the $Z \to \mu\mu$ analysis, data-driven methods are used to determine the residual contributions of the QCD background to the final W and Z samples, as discussed in section 6.

During the period these data were recorded, the average pile-up varied from zero to about two extra interactions per event, with most of the data being recorded with roughly one extra interaction per event. To account for this, the $W \to \ell\nu$, $Z \to \ell\ell$, and QCD-dijet Monte-Carlo samples were generated with on average two extra primary interactions and then weighted to the primary vertex multiplicity distribution observed in the data.

All data distributions in this paper are shown with statistical uncertainties only, based on Poisson statistics [27], unless otherwise stated.

JHEP12(2010)060

Physics process	Generator	$\sigma\cdot$ BR [nb]		
$W \to \ell\nu \quad (\ell = e, \mu)$	PYTHIA [28]	10.46±0.52	NNLO	[5, 8, 9]
$W^+ \to \ell^+\nu$		6.16±0.31	NNLO	[5, 8, 9]
$W^- \to \ell^-\overline{\nu}$		4.30±0.21	NNLO	[5, 8, 9]
$Z/\gamma^* \to \ell\ell \quad (m_{\ell\ell} > 60\,\text{GeV})$	PYTHIA	0.99±0.05	NNLO	[5, 8, 9]
$W \to \tau\nu$	PYTHIA	10.46±0.52	NNLO	[5, 8, 9]
$W \to \tau\nu \to \ell\nu\nu\nu$	PYTHIA	3.68±0.18	NNLO	[5, 8, 9]
$Z/\gamma^* \to \tau\tau \quad (m_{\ell\ell} > 60\,\text{GeV})$	PYTHIA	0.99±0.05	NNLO	[5, 8, 9]
$t\bar{t}$	MC@NLO [29, 30], POWHEG [34]	0.16±0.01	NLO+NNLL	[31–33]
Dijet (e channel, $\hat{p}_{\text{T}} > 15\,\text{GeV}$)	PYTHIA	1.2×10^6	LO	[28]
Dijet (μ channel, $\hat{p}_{\text{T}} > 8\,\text{GeV}$)	PYTHIA	10.6×10^6	LO	[28]
$b\bar{b}$ (μ channel, $\hat{p}_{\text{T}} > 18\,\text{GeV}$, $p_{\text{T}}(\mu) > 15\,\text{GeV}$)	PYTHIA	73.9	LO	[28]
$c\bar{c}$ (μ channel, $\hat{p}_{\text{T}} > 18\,\text{GeV}$, $p_{\text{T}}(\mu) > 15\,\text{GeV}$)	PYTHIA	28.4	LO	[28]

Table 1. Signal and background Monte-Carlo samples as well as the generators used in the simulation. For each sample the production cross section, multiplied by the relevant branching ratios (BR), to which the samples were normalised is given. For the electroweak (W and Z boson production) and for the $t\bar{t}$ production, contributions from higher order QCD corrections are included. The inclusive QCD jet and heavy quark cross sections are given at leading order (LO). These samples were generated with requirements on the transverse momentum of the partons involved in the hard-scattering process, $\hat{p}_{\text{T}}$. No systematic uncertainties are assigned here for these cross sections, since methods are used to extract their normalisation and their systematic uncertainties from data (see text). All Monte-Carlo samples result in negligible statistical uncertainties, unless otherwise stated.

4 Reconstruction of electrons, muons and missing transverse energy

4.1 Track reconstruction in the inner detector

The reconstruction of both electrons and muons uses reconstructed charged tracks in the inner detector. A detailed description of the track reconstruction has already been presented in ref. [35]. The inner tracking system measures charged particle tracks at all ϕ over the pseudorapidity region $|\eta| < 2.5$ using the pixel, SCT and TRT detectors. Tracks are reconstructed using a pattern recognition algorithm that starts with the silicon information and adds hits in the TRT. This "inside-out" tracking procedure selects track candidates with transverse momenta above 100 MeV [36]. One further pattern recognition step is then run, which only looks at hits not previously used. It starts from the TRT and works inwards adding silicon hits as it progresses. In this second step, tracks from secondary interactions, such as photon conversions and long-lived hadron decays, with transverse momenta above 300 MeV are recovered.

JHEP12(2010)060

4.2 Electrons

The ATLAS standard electron reconstruction and identification algorithm [37] is designed to provide various levels of background rejection for high identification efficiencies for calorimeter transverse energy $E_{\mathrm{T}} > 20\,\mathrm{GeV}$, over the full acceptance of the inner-detector system. Electron reconstruction begins with a seed cluster of $E_{\mathrm{T}} > 2.5\,\mathrm{GeV}$ in the second layer of the electromagnetic calorimeter. A matching track, extrapolated to the second EM calorimeter layer, is searched for in a broad window of $\Delta\eta \times \Delta\phi = 0.05 \times 0.1$ amongst all reconstructed tracks with $p_{\mathrm{T}} > 0.5\,\mathrm{GeV}$. The closest-matched track to the cluster barycentre is kept as that belonging to the electron candidate. The final electron candidates have cluster sizes of $\Delta\eta \times \Delta\phi = 0.075 \times 0.175$ in the barrel calorimeter and 0.125×0.125 in the end-cap. The transverse energy of these electron candidates is obtained from the corresponding calorimeter clusters.

The electron identification selections are based on criteria using calorimeter and tracker information and have been optimised in 10 bins in η and 11 bins in E_{T}. Three reference sets of requirements ("loose", "medium", and "tight") have been chosen, providing progressively stronger jet rejection at the expense of some identification efficiency loss. Each set adds additional constraints to the previous requirements:

- *"Loose"*: this basic selection uses EM shower shape information from the second layer of the EM calorimeter (lateral shower containment and shower width) and energy leakage into the hadronic calorimeters as discriminant variables. This set of requirements provides high and uniform identification efficiency but a low background rejection.

- *"Medium"*: this selection provides additional rejection against hadrons by evaluating the energy deposit patterns in the first layer of the EM calorimeter (the shower width and the ratio of the energy difference associated with the largest and second largest energy deposit over the sum of these energies), track quality variables (number of hits in the pixel and silicon trackers, transverse distance of closest approach to the primary vertex (transverse impact parameter)) and a cluster-track matching variable ($\Delta\eta$ between the cluster and the track extrapolated to the first layer of the EM calorimeter).

- *"Tight"*: this selection further rejects charged hadrons and secondary electrons from conversions by fully exploiting the electron identification potential of the ATLAS detector. It makes requirements on the ratio of cluster energy to track momentum, on the number of hits in the TRT, and on the ratio of high-threshold hits[2] to the total number of hits in the TRT. Electrons from conversions are rejected by requiring at least one hit in the first layer of the pixel detector. A conversion-flagging algorithm is also used to further reduce this contribution. The impact-parameter requirement applied in the medium selection is further tightened at this level.

[2]The TRT readout discriminates at two thresholds. The lower one is set to register minimum-ionizing particles and the higher one is intended for the detection of transition radiation.

JHEP12(2010)060

$Z \to ee$ and $W \to e\nu$ signal Monte-Carlo samples were used to estimate the medium and tight electron identification efficiencies within the relevant kinematic and geometrical acceptance ($E_{\mathrm{T}} > 20\,\mathrm{GeV}$ within the range $|\eta| < 2.47$ and excluding the transition region between the barrel and end-cap calorimeters, $1.37 < |\eta| < 1.52$). The efficiencies are estimated to be 94.3% and 74.9% respectively, relative to the basic reconstruction efficiency of 97% which requires a very loose matching between the candidate electron track and the electromagnetic cluster. Using QCD dijet background Monte-Carlo samples, the corresponding rejections against background from hadrons or conversion electrons in generated jets with $E_{\mathrm{T}} > 20\,\mathrm{GeV}$ within the relevant kinematic and geometrical acceptance are found to be 5700 and 77000, respectively.

Given the limited available statistics of $Z \to ee$ decays, the electron performance cannot yet be evaluated in detail with collision data. The overall uncertainty on the electron energy scale is estimated to be $\pm 3\%$, based on extrapolations from test-beam measurements. The uncertainty on the electron energy resolution is also based on extrapolations from test-beam measurements and has a negligible impact on the measurements reported here.

The material in front of the electromagnetic calorimeter affects the reconstruction and identification efficiencies as well as the correct identification of the charge of the reconstructed electron. This has been studied in detail with dedicated simulations including additional material in the inner detector and in front of the electromagnetic calorimeter. The amount of additional material which might be present is currently best constrained by track efficiency measurements in minimum bias data [35] and studies of photon conversions. The probability for wrongly identifying the charge of the electron depends strongly on the amount of material it traverses in the inner detector and therefore on η. It is expected to be $(1.9 \pm 0.3)\%$ for the medium electron identification cuts (this affects the selection of Z-boson candidates as discussed in section 6.3) and $(0.6 \pm 0.3)\%$ for the tight identification cuts (this affects the measurement of the W-boson asymmetry as discussed in section 8).

The most precise current estimate of the electron identification efficiencies is obtained from a sample of $W \to e\nu$ candidates which were selected using tight cuts on the missing transverse energy and the topology of the event and requiring only that an electron candidate be reconstructed through the very loose match between a track and an electromagnetic cluster mentioned above. The residual background from QCD dijets was estimated using a calorimeter isolation technique similar to that described in section 6.1. The results obtained for the medium efficiency were $0.900 \pm 0.014(\mathrm{stat}) \pm 0.040(\mathrm{syst})$ compared to 0.943 from the Monte Carlo. For the tight efficiency, the corresponding results were $0.742 \pm 0.013(\mathrm{stat}) \pm 0.030(\mathrm{syst})$ compared to 0.749 from the Monte Carlo. These measurements confirm that, within the current uncertainties, the electron identification efficiencies are well modelled by the simulation and are used to evaluate the systematic uncertainties discussed in section 7.2.

4.3 Muons

The ATLAS muon identification and reconstruction algorithms take advantage of multiple sub-detector technologies which provide complementary approaches and cover pseudorapidities up to 2.7 [38].

JHEP12(2010)060

The *stand-alone muon* reconstruction is based entirely on muon-spectrometer information, independently of whether or not the muon-spectrometer track is also reconstructed in the inner detector. The muon reconstruction is initiated locally in a muon chamber by a search for straight line track segments in the bending plane. Hits in the precision chambers are used and the segment candidates are required to point to the centre of ATLAS. When available, the hit coordinate ϕ in the non-bending plane measured by the trigger detectors is associated to the segment. Two or more track segments in different muon stations are combined to form a muon track candidate using three-dimensional tracking in the magnetic field. The track parameters (p_{T}, η, ϕ, transverse and longitudinal distances of closest approach to the primary vertex) obtained from the muon spectrometer track fit are extrapolated to the interaction point taking into account both multiple scattering and energy loss in the calorimeters. For the latter, the reconstruction utilises either a parameterisation or actual measurements of calorimeter energy losses, together with a parameterisation of energy loss in the inert material. The average muon energy loss in the calorimeters is 3 GeV. The stand-alone muon reconstruction algorithms use the least-squares formalism to fit tracks in the muon spectrometer, with most material effects directly integrated into the χ^2 function.

The *combined muon* reconstruction associates a stand-alone muon-spectrometer track to an inner-detector track. The association is performed using a χ^2-test, defined from the difference between the respective track parameters weighted by their combined covariance matrices. The parameters are evaluated at the point of closest approach to the beam axis. The combined track parameters are derived either from a statistical combination of the two tracks or from a refit of the full track. To validate the results presented in this paper, these two independent reconstruction chains were exercised and good agreement was observed. The results presented here are based on the statistical combination of muon-spectrometer and inner-detector measurement.

Detailed studies of the muon performance in collision data were performed. The muon momentum scale and resolution were extracted by fitting the invariant mass distribution of the Z candidates described in section 5.4 to a Breit-Wigner function convolved with a Gaussian function. The fitted mean value indicates that the muon-momentum scale is within $\pm 1\%$ around the nominal value. From the fitted width the muon-momentum resolution, for muons from Z decays, is extracted to be $(4 \pm 2)\%$ in the barrel and $(7 \pm 3)\%$ in the end-cap regions. These results are consistent with those obtained from the single muon studies reported in ref. [39].

Two complementary approaches were used to measure the muon reconstruction efficiency in data. The first technique determines the efficiency of isolated combined muons relative to inner-detector tracks matched to muon hits in the muon spectrometer, resulting in an efficiency measured in data of $0.994 \pm 0.006(\mathrm{stat}) \pm 0.024(\mathrm{syst})$, compared to 0.986 from the Monte-Carlo simulation. In the second approach, events are selected requiring an isolated combined muon passing the same selection as for the Z analysis (see section 5.4). The second muon of the Z candidate is then selected as an inner-detector track with opposite charge. The invariant mass of the muon-track pair is required to be within 10 GeV of the nominal Z mass. The combined muon efficiency, measured relative to this sample

JHEP12(2010)060

of tracks, is 0.933 ± 0.022(stat) ± 0.013(syst), while the value from Monte-Carlo simulation is 0.924. The difference in the efficiency values obtained from the two methods is due to the different sensitivity to the geometrical acceptance of the muon spectrometer, as the first method explicitly requires muon hits. Both techniques confirm that the reconstruction efficiency is well modelled by the simulation and the results are used to assign a ±2.5% systematic uncertainty on this efficiency.

4.4 Missing transverse energy

The transverse missing energy ($E_{\mathrm{T}}^{\mathrm{miss}}$) reconstruction used in the electron channel is based on calorimeter information. It relies on a cell-based algorithm which sums the electromagnetic-scale energy deposits of calorimeter cells inside three-dimensional topological clusters [40]. The EM scale corresponds to the energy deposited in the calorimeter calculated under the assumption that all processes are purely electromagnetic in nature. These clusters are then corrected to take into account the different response to hadrons than to electrons or photons, dead material losses and out of cluster energy losses [41]. These topological clusters are built around energy $E > 4\sigma_{\mathrm{noise}}$ seeds, where σ_{noise} is the Gaussian width of the cell energy distribution in randomly triggered events, by iteratively gathering neighbouring cells with $E > 2\sigma_{\mathrm{noise}}$ and, in a final step, by adding all direct neighbours of these accumulated secondary cells.

For the electron channel, the components of the missing transverse energy are calculated by summing over all topological cluster cell energy components $E_{x,y}^{i}$:

$$E_{x,y}^{\mathrm{miss}}|_{e} \;=\; -\sum_{i} E_{x,y}^{i} \;. \tag{4.1}$$

The $E_{\mathrm{T}}^{\mathrm{miss}}$ used in the muon channel is calculated by adding the reconstructed momenta of isolated and non-isolated muons measured in the pseudorapidity range $|\eta| < 2.7$:

$$E_{x,y}^{\mathrm{miss}}|_{\mu} \;=\; -\sum_{i} E_{x,y}^{i} \;-\; \sum_{k}^{\mathrm{isolated}} p_{x,y}^{k} \;-\; \sum_{j}^{\mathrm{non-isolated}} p_{x,y}^{j}, \tag{4.2}$$

where non-isolated muons are those within a distance $\Delta R \leq 0.3$ of a jet in the event. The p_{T} of an isolated muon is determined from the combined measurement of the inner detector and muon spectrometer, as explained in section 4.3. The energy lost by an isolated muon in the calorimeters is removed from the calorimeter term. For a non-isolated muon, the energy lost in the calorimeter cannot be separated from the nearby jet energy. The muon-spectrometer measurement of the muon momentum after energy loss in the calorimeter is therefore used, unless there is a significant mismatch between the spectrometer and combined measurements. In this case the combined measurement minus the parameterised energy loss in the calorimeter is used. For values of the pseudorapidity outside the fiducial volume of the inner detector ($2.5 < |\eta| < 2.7$), there is no matched track requirement and the muon spectrometer stand-alone measurement is used instead.

JHEP12(2010)060

Systematic uncertainties on the measurement of $E_{\mathrm{T}}^{\mathrm{miss}}$ result mainly from uncertainties on the energy scale of topological clusters. From a comparison of the momentum and energy measurement of charged particles [42], the topological cluster energy scale is known to $\pm 20\%$ for $p_{\mathrm{T}} \sim 500\,\mathrm{MeV}$ and $\pm 5\%$ at high p_{T}. Other contributions result from uncertainties due to the imperfect modelling of the overall $E_{\mathrm{T}}^{\mathrm{miss}}$ response (low energy hadrons) and resolution, modelling of the underlying event and pile-up effects.

5 Selection of $W \to \ell\nu$ and $Z \to \ell\ell$ candidates

5.1 Event selection

Collision candidates are selected by requiring a primary vertex with at least three tracks, consistent with the beam-spot position. To reduce contamination from cosmic-ray or beam-halo events, the muon analysis requires the primary vertex position along the beam axis to be within 15 cm of the nominal position (this primary vertex distribution has a measured longitudinal RMS of 6.2 cm).

An analysis of a high-statistics sample of minimum-bias events has shown that events can occasionally contain very localised high-energy calorimeter deposits not originating from the proton-proton collision, but e.g. from sporadic discharges in the hadronic end-cap calorimeter or, more rarely, coherent noise in the electromagnetic calorimeter. Cosmic-ray muons undergoing a hard bremsstrahlung are also a potential source of localised energy deposits uncorrelated with the primary proton-proton collisions. The occurrence of these events is very rare but can potentially impact significantly the $E_{\mathrm{T}}^{\mathrm{miss}}$ measurement by creating high-energy tails [43]. To remove such events, dedicated cleaning requirements have been developed using a minimum-bias event sample. Using Monte-Carlo simulation, it was verified that these criteria remove less than 0.1% of minimum-bias events, 0.004% of $W \to \ell\nu$, and 0.01% of dijet events.

For the electron channel only, the event is rejected if the candidate electromagnetic cluster is located in any problematic region of the EM calorimeter. Due to hardware problems [22], the signal cannot be read out from $\sim$2% of the EM calorimeter cells.

5.2 Selection of high transverse-energy leptons

Electron candidates selected with the identification level "tight" for the W analysis and "medium" for the Z analysis (according to the algorithm described in section 4.2) are required to have a cluster $E_{\mathrm{T}} > 20\,\mathrm{GeV}$ within the range $|\eta| < 2.47$, excluding the transition region between the barrel and end-cap calorimeters ($1.37 < |\eta| < 1.52$). Muon candidates selected according to the algorithm described in section 4.3 are required to have a combined muon with $p_{\mathrm{T}} > 20\,\mathrm{GeV}$ and a muon-spectrometer track with $p_{\mathrm{T}} > 10\,\mathrm{GeV}$ within the range $|\eta| < 2.4$. To increase the robustness against track reconstruction mismatches, the difference between the inner-detector and muon-spectrometer p_{T} corrected for the mean energy loss in upstream material, is required to be less than 15 GeV. The difference between the z position of the muon track extrapolated to the beam line and the z coordinate of the primary vertex is required to be less than 1 cm, given that the RMS of this distribution in data is 2 mm.

JHEP12(2010)060

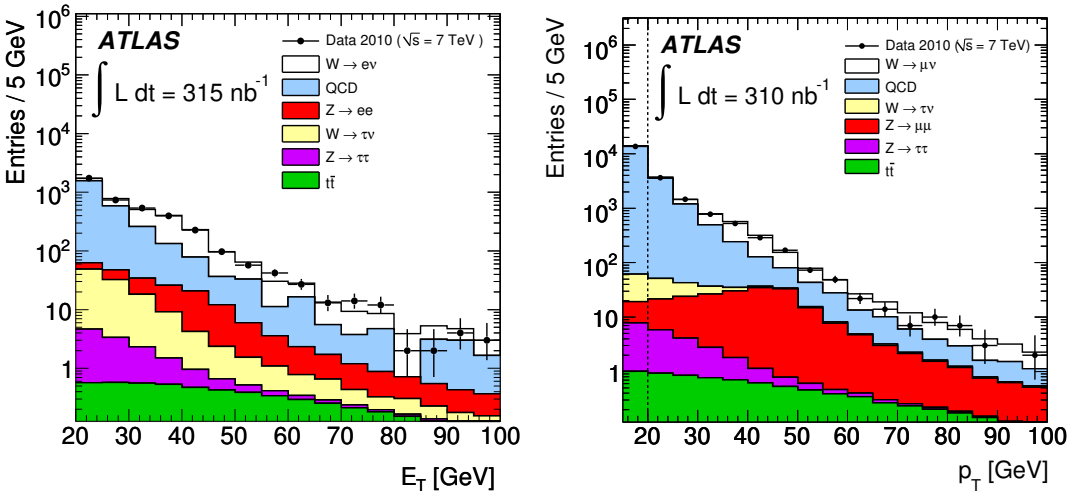

(a) (b)

Figure 1. Calorimeter cluster E_T of "tight" electron candidates (a) and combined p_{T} of muon candidates (b) for data and Monte-Carlo simulation, broken down into the signal and various background components. The vertical line in (b) indicates the analysis cut. The transverse momentum region between 15 and 20 GeV of the muon sample is used in the estimation of the QCD background (see section 6.2). The values of the integrated luminosities for the two channels have uncertainties of ±11%, see section 3.

Figure 1 shows the E_{T} and p_{T} spectra of these "tight" electron and combined muon candidates and compares these to the signal and background Monte-Carlo samples described in section 3. Comparisons of the dijet Monte-Carlo distributions to equivalent data distributions have shown that the dijet Monte Carlo for this high-p_{T} lepton selection over-estimates the amount of background by a factor of approximately 2.4 for the electron channel and a factor of 1.6 for the muon channel. The difference between these values is likely explained by the different composition of the QCD background in the two analyses. For the electron case, this normalisation factor is obtained by comparing data and Monte-Carlo samples of high transverse-momentum electron candidates which are dominated by QCD background (candidates satisfying the "loose" electron selection as defined in section 4.2). For the muon case, this normalisation factor is obtained from the comparison of a control sample of mostly QCD background events, obtained by reversing the isolation requirement (as defined in section 5.3) on muons passing the transverse-momentum selection, with the corresponding Monte-Carlo samples.

Unless otherwise stated, all Monte-Carlo distributions shown in this paper have been normalised to the integrated luminosity of the data as described in section 3, using the cross sections as given in table 1 and taking into account these scale factors for the QCD background. At this stage of the selection, the event samples are dominated by QCD background. These distributions show agreement in shape between data and Monte-Carlo simulation.

JHEP12(2010)060

5.3 Lepton isolation

The use of an isolation parameter to enhance the signal-to-background ratio was investigated. Separate isolation requirements must be considered for the electron and muon channels, since the electron can undergo bremsstrahlung, while a muon is primarily defined by its track.

A calorimeter-based isolation parameter defined as the total calorimeter transverse energy in a cone of $\Delta R < 0.3$ surrounding the candidate electron cluster, divided by the cluster E_{T}, is considered for the electron channel. This variable is exploited for background estimations in this channel, but is not used in the event selection.

In the muon analysis, a track-based isolation is defined using the sum of the transverse momenta of tracks with $p_{\mathrm{T}} > 1\,\mathrm{GeV}$ in the inner detector within a cone of $\Delta R < 0.4$ around the muon track, $\sum p_{\mathrm{T}}^{\mathrm{ID}}$. An isolation requirement of $\sum p_{\mathrm{T}}^{\mathrm{ID}}/p_{\mathrm{T}}^{\mu} < 0.2$ is imposed in the muon selection given that, after all other selections are made to identify W candidates, this requirement rejects over 84% of the expected QCD background while keeping (98.4±1.0)% of the signal events.

5.4 Kinematic selection

Additional requirements beyond those in sections 5.2 and 5.3 are imposed to better discriminate $W \to \ell\nu$ and $Z \to \ell\ell$ events from background events. A summary of all requirements is as follows:

- An electron with $E_{\mathrm{T}} > 20\,\mathrm{GeV}$ or a combined muon with $p_{\mathrm{T}} > 20\,\mathrm{GeV}$;
  For the $W \to e\nu$ analysis, events containing an additional "medium" electron are vetoed. If more than one combined muon candidate is reconstructed, the one with the highest p_{T} is chosen.
- Isolation for the muon channel: $\sum p_{\mathrm{T}}^{\mathrm{ID}}/p_{\mathrm{T}}^{\mu} < 0.2$;
  For the electron channel, no isolation criterion is used.
- For the W analysis only:
  - Missing transverse energy $E_{\mathrm{T}}^{\mathrm{miss}} > 25\,\mathrm{GeV}$;
  - Transverse mass of the lepton-$E_{\mathrm{T}}^{\mathrm{miss}}$system, $m_{\mathrm{T}} > 40\,\mathrm{GeV}$;
    The transverse mass is defined as $m_{\mathrm{T}} = \sqrt{2\, p_{\mathrm{T}}^{\ell}\, E_{\mathrm{T}}^{\mathrm{miss}}\, (1 - \cos\Delta\phi)}$, where $\Delta\phi$ is the azimuthal separation between the directions of the lepton and the missing transverse energy.
- For the Z analysis only:
  - A pair of oppositely-charged leptons (each lepton with $p_{\mathrm{T}} > 20\,\mathrm{GeV}$) of the same flavour;
  - Invariant mass window of lepton pair: $66 < m_{\ell\ell} < 116\,\mathrm{GeV}$;
  - Veto on events with three or more "medium" electrons (for the $Z \to ee$ analysis).

Figure 2 shows the $E_{\mathrm{T}}^{\mathrm{miss}}$ distributions of electron and muon candidates passing the requirements described above, except the $E_{\mathrm{T}}^{\mathrm{miss}}$ and m_{T} criteria. Both distributions indicate

JHEP12(2010)060

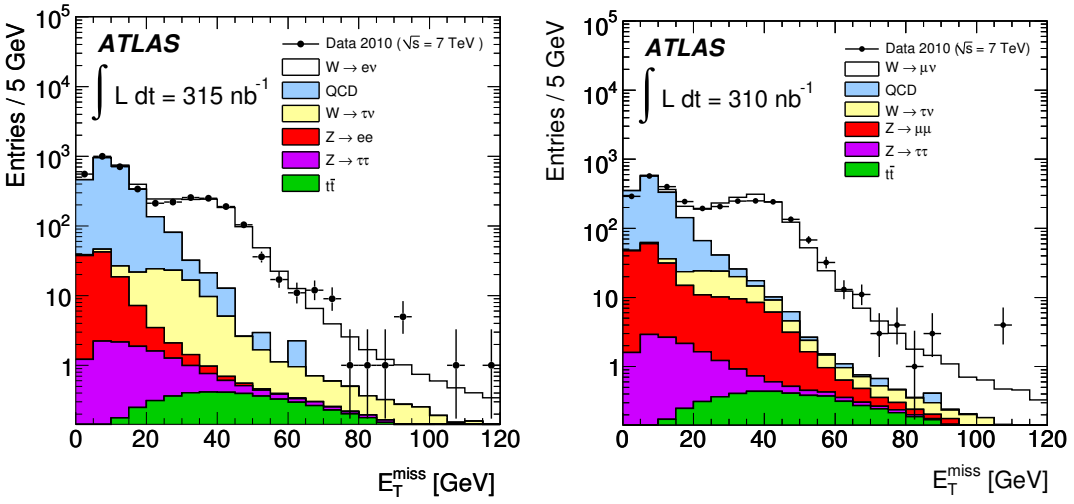

(a) (b)

Figure 2. Distributions of the missing transverse energy, $E_{\mathrm{T}}^{\mathrm{miss}}$, of electron (a) and muon (b) candidates for data and Monte-Carlo simulation, broken down into the signal and various background components. The values of the integrated luminosities for the two channels have uncertainties of $\pm 11\%$, see section 3.

that applying a minimum requirement on $E_{\mathrm{T}}^{\mathrm{miss}}$ greatly enhances the W signal over the expected background. True $W \to \ell\nu$ events in the Monte Carlo are predominantly at high $E_{\mathrm{T}}^{\mathrm{miss}}$ due to the escaping neutrino in the event. Although some of the QCD background events may also have neutrinos in their final state, they mostly populate the regions of small $E_{\mathrm{T}}^{\mathrm{miss}}$. Figures 3 and 4 show the m_{T} distributions without and with the requirement of $E_{\mathrm{T}}^{\mathrm{miss}} > 25\,\mathrm{GeV}$.

5.5 W and Z candidates after final selection

Table 2 summarises the number of $W \to \ell\nu$ candidates remaining after each major requirement in the respective analyses. A total of 1069 candidates (637 e^+ and 432 e^-) pass all requirements in the electron channel and 1181 candidates (710 μ^+ and 471 μ^-) in the muon channel. Figure 5 shows the electron cluster E_{T} and muon combined p_{T} of the lepton candidates, while figure 6 shows the p_{T} spectrum of the $W \to \ell\nu$ candidates. Both channels demonstrate a clear W signal over a small background.

Table 3 summarises the number of $Z \to \ell\ell$ candidates remaining after each major requirement has been imposed. A total of 70 candidates pass all requirements in the electron channel and 109 candidates in the muon channel, within the invariant mass window $66 < m_{\ell\ell} < 116\,\mathrm{GeV}$. Figure 7 shows the electron cluster E_{T} and muon combined p_{T} of the lepton candidates. The breakdown of the various background contributions are also shown in this figure. Due to the small size of the backgrounds in both channels, backgrounds are not shown in the subsequent distributions for the Z analysis. Figure 8 shows the p_{T} spectrum of the $Z \to \ell\ell$ candidates. The invariant mass distribution of the lepton pairs is presented in figure 9. The observed resolution degradation in the muon data compared to design expectations is currently under investigation. It has been taken into account in the systematic uncertainties of the cross-section measurement.

JHEP12(2010)060

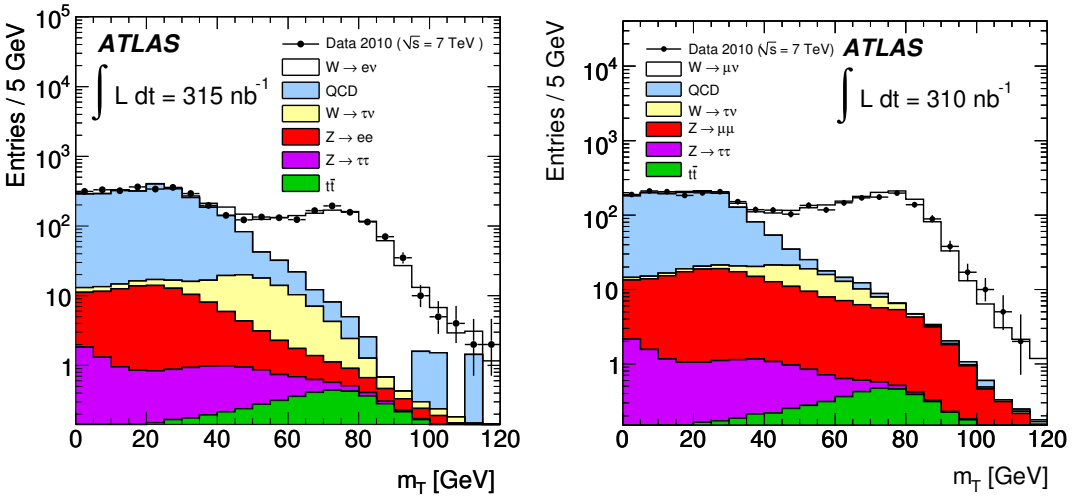

(a) (b)

Figure 3. Distributions of the transverse mass, m_{T}, of the electron-$E_{\mathrm{T}}^{\mathrm{miss}}$ system (a) and muon-$E_{\mathrm{T}}^{\mathrm{miss}}$ system (b) without an $E_{\mathrm{T}}^{\mathrm{miss}}$ requirement. The data are compared to Monte-Carlo simulation, broken down into the signal and various background components. The values of the integrated luminosities for the two channels have uncertainties of ±11%, see section 3.

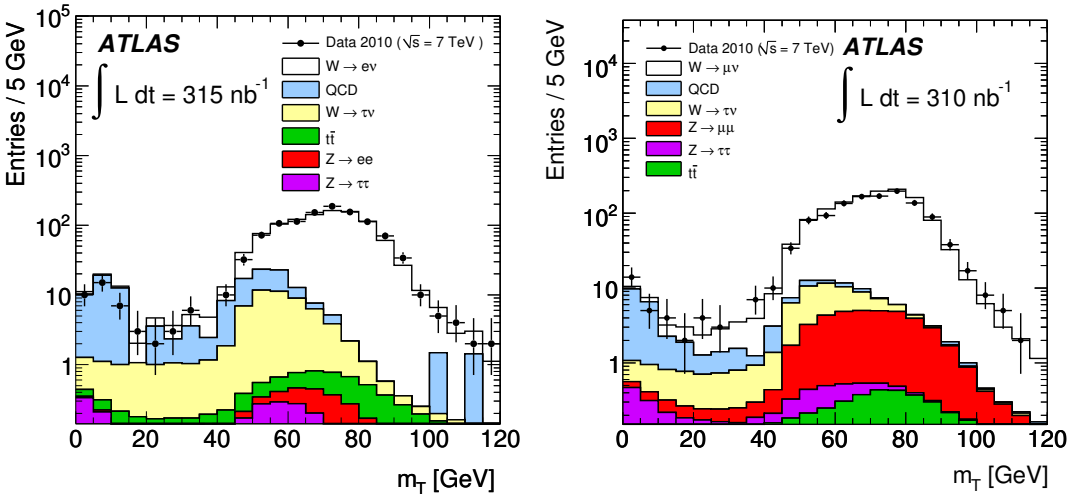

(a) (b)

Figure 4. Distributions of the transverse mass, m_{T}, of the electron-$E_{\mathrm{T}}^{\mathrm{miss}}$ system (a) and muon-$E_{\mathrm{T}}^{\mathrm{miss}}$ system (b) with a requirement of $E_{\mathrm{T}}^{\mathrm{miss}} > 25\,\mathrm{GeV}$. The data are compared to Monte-Carlo simulation, broken down into the signal and various background components. The values of the integrated luminosities for the two channels have uncertainties of ±11%, see section 3.

JHEP12(2010)060

Requirement	Number of candidates	
	$W \to e\nu$	$W \to \mu\nu$
Trigger	6.5×10^6	5.1×10^6
Lepton: e with $E_{\mathrm{T}} > 20\,\mathrm{GeV}$ or μ with $p_{\mathrm{T}} > 20\,\mathrm{GeV}$	4003	7052
Muon isolation: $\sum p_T^{\mathrm{ID}}/p_T^{\mu} < 0.2$	—	2920
$E_{\mathrm{T}}^{\mathrm{miss}} > 25\,\mathrm{GeV}$	1116	1220
$m_{\mathrm{T}} > 40\,\mathrm{GeV}$	1069	1181

Table 2. Number of $W \to e\nu$ and $W \to \mu\nu$ candidates in data, remaining after each major requirement.

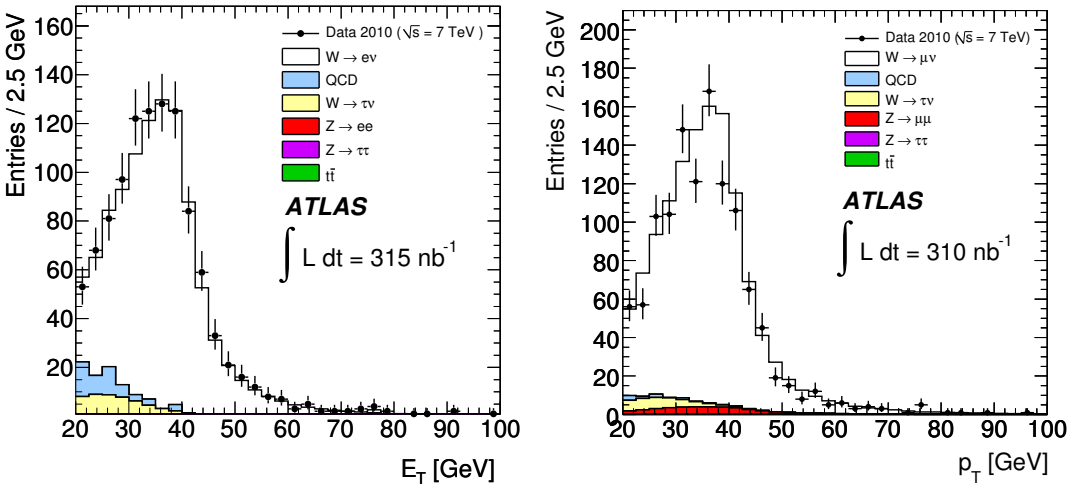

(a) (b)

Figure 5. Distributions of the electron cluster E_T (a) and muon p_{T} (b) of the W candidates after final selection. The requirements of $E_{\mathrm{T}}^{\mathrm{miss}} > 25\,\mathrm{GeV}$ and $m_{\mathrm{T}} > 40\,\mathrm{GeV}$ are applied. The data are compared to Monte-Carlo simulation, broken down into the signal and various background components. The values of the integrated luminosities for the two channels have uncertainties of $\pm 11\%$, see section 3.

Requirement	Number of candidates	
	$Z \to ee$	$Z \to \mu\mu$
Trigger	6.5×10^6	5.1×10^6
Two leptons (ee or $\mu\mu$ with $E_{\mathrm{T}}(p_{\mathrm{T}})$ >20 GeV)	83	144
Muon isolation: $\sum p_T^{\mathrm{ID}}/p_T^{\mu} < 0.2$	—	117
Opposite charge ee or $\mu\mu$ pair:	78	117
$66 < m_{\ell\ell} < 116\,\mathrm{GeV}$	70	109

Table 3. Number of $Z \to ee$ and $Z \to \mu\mu$ candidates in data, remaining after each major requirement.

JHEP12(2010)060

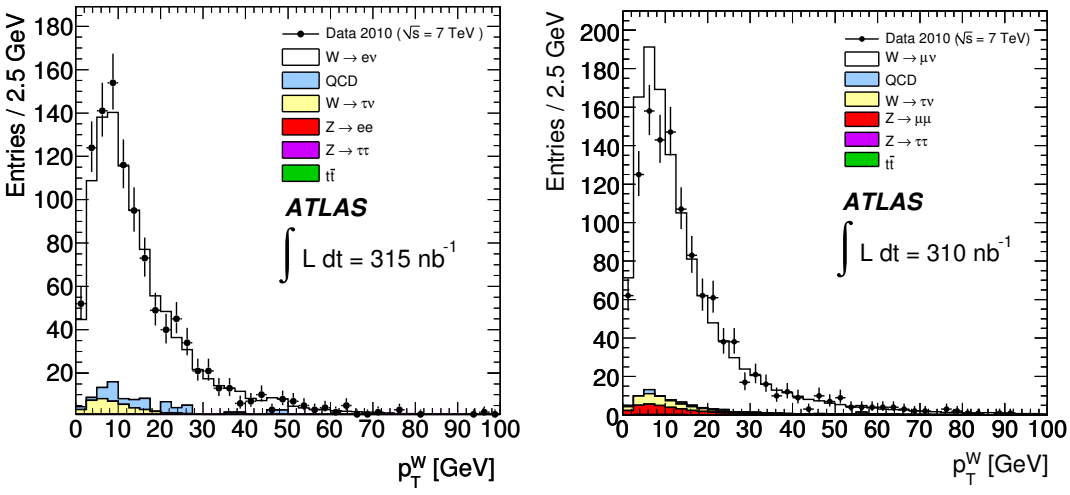

(a) (b)

Figure 6. Distributions of the transverse momentum p_{T} of the W candidates in the electron channel (a) and muon channel (b) after final selection. The requirements of $E_{\mathrm{T}}^{\mathrm{miss}} > 25\,\mathrm{GeV}$ and $m_{\mathrm{T}} > 40\,\mathrm{GeV}$ are applied. The data are compared to Monte-Carlo simulation, broken down into the signal and various background components. The values of the integrated luminosities for the two channels have uncertainties of ±11%, see section 3.

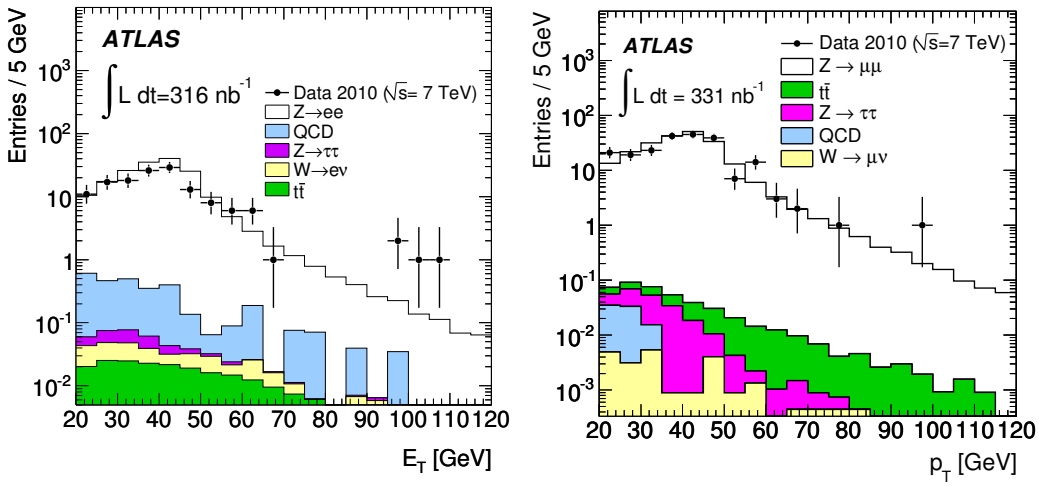

(a) (b)

Figure 7. Distributions of the electron cluster E_{T} (a) and muon p_{T} (b) of the Z candidate leptons after final selection. The data are compared to Monte-Carlo simulation, broken down into the signal and various background components. The values of the integrated luminosities for the two channels have uncertainties of ±11%, see section 3.

JHEP12(2010)060

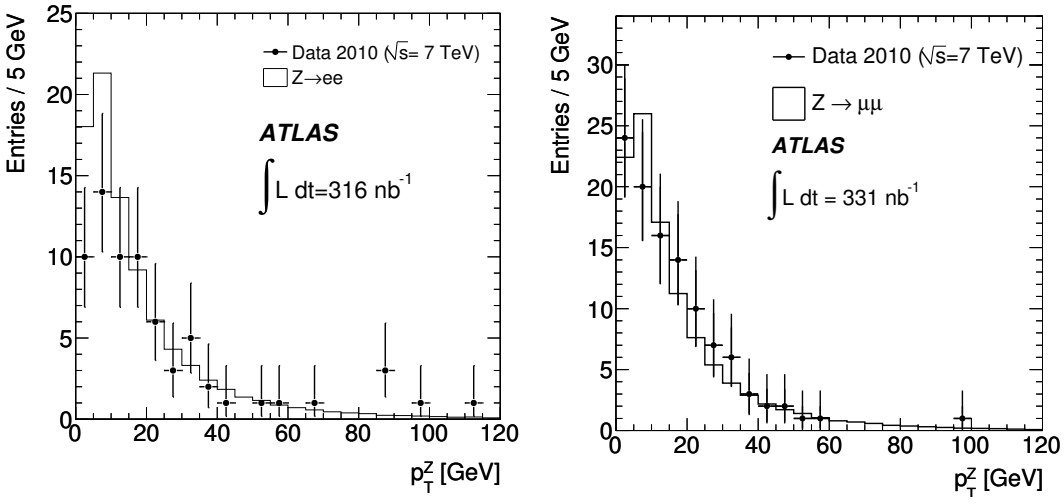

(a) (b)

Figure 8. Distributions of the transverse momentum p_{T} of the Z candidates in the electron channel (a) and muon channel (b) after final selection. The data are compared to the expectations from Monte-Carlo simulation. The values of the integrated luminosities for the two channels have uncertainties of ±11%, see section 3.

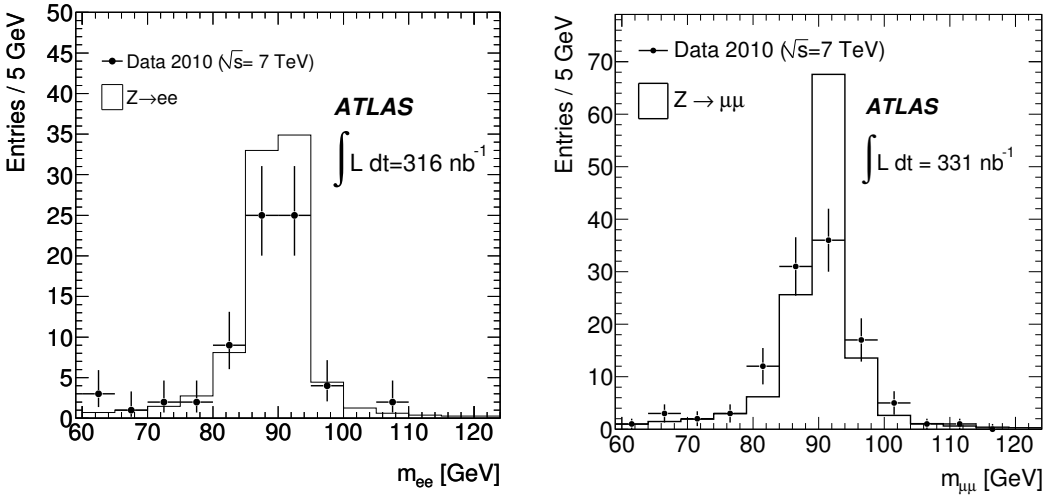

(a) (b)

Figure 9. Distributions of the invariant mass $m_{\ell\ell}$ of Z candidates in the electron (a) and muon (b) channels. The data are compared to the expectations from Monte-Carlo simulation. The values of the integrated luminosities for the two channels have uncertainties of ±11%, see section 3.

JHEP12(2010)060

6 W and Z boson signals and backgrounds

In this section, estimates of the various background components in the W and Z-candidate samples, and background-subtracted signal numbers, are presented. Except for the $Z \to \mu\mu$ final state, the QCD components of the backgrounds were estimated from the data. The electroweak and $t\bar{t}$ components were obtained for all channels from Monte-Carlo simulation.

6.1 Background estimate for the $W \to e\nu$ channel

The expected contributions from the $W \to \tau\nu$, $Z \to ee$ and $Z \to \tau\tau$ processes were estimated to be 25.9, 1.9, and 1.6 events, respectively, while from $t\bar{t}$ production 4.1 events are expected.

The QCD background was estimated using the distribution of the missing transverse energy $E_{\mathrm{T}}^{\mathrm{miss}}$ as measured in data. Events were selected by applying all cuts used in the W selection, except the $E_{\mathrm{T}}^{\mathrm{miss}}$ cut at 25 GeV. The resulting distribution is displayed in figure 10. The signal and background components in this sample were obtained from a binned maximum likelihood template fit. The shapes of the $W \to e\nu$ signal and of the dominant $W \to \tau\nu$ background were taken from Monte-Carlo simulation, whereas the shape of the QCD background was determined from data.

The background template was obtained by using the W selection, but modifying the electron identification requirements, such that the sample is dominated by background. In the template selection, the background electron candidate is required to pass the "loose" identification requirements and the track quality requirements from the "medium" electron identification. It is, however, required to fail at least one of the remaining "medium" or "tight" requirements. No requirements to reject conversions (see section 4.2) were applied. In order to suppress the residual contribution from $W \to e\nu$ signal events and to obtain an essentially signal-free sample, isolated candidates were rejected, by applying a cut on the calorimeter-based isolation variable, as described in section 5.3. Using a high-statistics QCD-dijet Monte-Carlo sample, it was verified that these requirements produce a background template similar in shape to the background expected from the W selection. The result of the fit to the data is shown in figure 10. It provides a background estimate in the signal region ($E_{\mathrm{T}}^{\mathrm{miss}} > 25$ GeV) of $N_{\mathrm{QCD}} = 28.0 \pm 3.0(\mathrm{stat})$ events, where the uncertainty contains the statistical uncertainty of the data and of the templates. This estimate is used in the extraction of the cross section in section 7.

To estimate the systematic uncertainty, the shape of the background template was varied by applying different event selection criteria, in particular by varying isolation cuts. In addition, two extreme ranges in $E_{\mathrm{T}}^{\mathrm{miss}}$ (0–25 GeV and 15–100 GeV) were considered as fit ranges. Based on these studies, the systematic uncertainty on the QCD background was estimated to be $\pm$ 10 events.

As an alternative estimate, the calorimeter isolation variable, $\sum_i^{\Delta R<0.3} E_{\mathrm{T}}^i / E_{\mathrm{T}}$, as defined in section 5.3, was used as discriminating variable. Due to the limited statistics and the few background events, the fit was performed after applying the "loose" instead of the "tight" electron identification, while the requirements on $E_{\mathrm{T}}^{\mathrm{miss}}$ and m_{T} were kept. Using this method, the number of QCD background events was estimated to be $48.0 \pm 17.0(\mathrm{stat})$.

JHEP12(2010)060

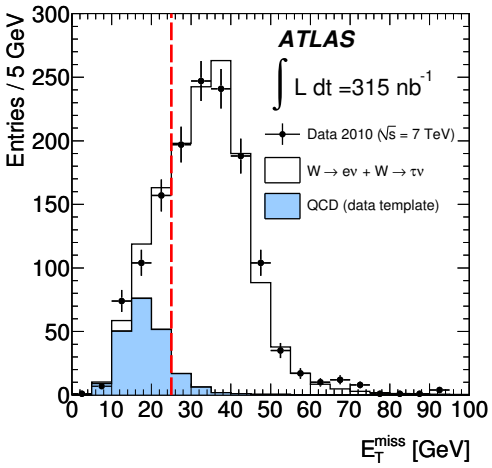

Figure 10. The distribution of $E_{\mathrm{T}}^{\mathrm{miss}}$ after applying all W selection cuts, except the $E_{\mathrm{T}}^{\mathrm{miss}}$ cut. The data are shown together with the results of a template fit for signal (including the dominant $W \to \tau\nu$ electroweak background contribution) and the QCD background. The dashed line indicates the cut on $E_{\mathrm{T}}^{\mathrm{miss}}$, as applied in the W analysis. The uncertainty of the integrated luminosity is $\pm 11\%$, see section 3.

The large error results from the large uncertainty on the estimation of the jet rejection factor for the "tight" requirement with respect to the "loose" requirement. As a further cross-check the background was also estimated from the dijet Monte-Carlo simulation, including the normalisation factor discussed in section 5.2, and was found to be 30.8±6.1(stat) events, which is in agreement with the estimates presented above.

6.2 Background estimate for the $W \to \mu\nu$ channel

For the muon channel, the expected contributions from $Z \to \mu\mu$, $W \to \tau\nu$, and $Z \to \tau\tau$ decays are 38.4, 33.6, and 1.4 events, respectively, while the $t\bar{t}$ contribution is expected to be 4.2 events.

The QCD background is primarily composed of heavy-quark decays, with smaller contributions from pion and kaon decays and hadrons faking muons. Given the large uncertainty in the dijet cross section and the difficulty to properly simulate fake prompt muons, the QCD background has been derived from data using the two methods described in the following.

In the baseline method, the QCD background was estimated from a comparison of the number of events seen in data (N_{iso}) after the full W selection, to the number of events observed (N_{loose}) if the muon isolation requirement is not applied. The number of events in the two samples can be expressed as:

$$\begin{aligned} N_{\mathrm{loose}} &= N_{\mathrm{nonQCD}} + N_{\mathrm{QCD}} \\ N_{\mathrm{iso}} &= \epsilon^{\mathrm{iso}}_{\mathrm{nonQCD}} N_{\mathrm{nonQCD}} + \epsilon^{\mathrm{iso}}_{\mathrm{QCD}} N_{\mathrm{QCD}}, \end{aligned} \tag{6.1}$$

JHEP12(2010)060

where N_{nonQCD} includes the W signal and the background from the other, non-QCD, physics processes and $\epsilon^{\text{iso}}_{\text{nonQCD}}$ and $\epsilon^{\text{iso}}_{\text{QCD}}$ denote the corresponding efficiencies of the muon isolation requirement for the two event classes. If these efficiencies are known, the equations can be solved for N_{QCD}. The muon isolation efficiency for non-QCD events was measured in the data $Z \to \mu\mu$ sample, while the efficiency for QCD events was estimated from a sample of muons with transverse momenta in the range of 15 - 20 GeV, which is dominated by dijet events (see figure 1(b)). The efficiency factor was extrapolated to higher p_{T} values relevant for the W-signal selection using Monte-Carlo simulation. A decrease of 22% was observed. The full variation was assigned as a systematic uncertainty on this efficiency determination. This method yields a background estimate in the W signal region of $21.1 \pm 4.5(\text{stat}) \pm 8.7(\text{syst})$ events. The systematic uncertainty is dominated by the uncertainty on the isolation efficiency for QCD events.

This estimate was cross-checked using a method where a similarity relationship in the plane of $E_{\text{T}}^{\text{miss}}$ versus lepton isolation was exploited [44]. The plane was divided into four separate regions and the number of background events in the signal region (high $E_{\text{T}}^{\text{miss}}$ and low values of the isolation variable) was estimated from non-isolated events at high $E_{\text{T}}^{\text{miss}}$ by applying the corresponding scale factor observed at low $E_{\text{T}}^{\text{miss}}$. The calculation was corrected for the contributions from the signal and the electroweak backgrounds and takes into account the correlation between the two variables, as predicted by Monte-Carlo simulation. This method yields a background estimate of $13.5 \pm 0.9(\text{stat}) \pm 12.7(\text{syst})$ events, in agreement with the baseline estimate.

As a further cross-check the background was also estimated from the dijet Monte-Carlo simulation, after applying the normalisation factor discussed in section 5.2, and was found to be $9.7 \pm 0.4(\text{stat})$, which is in agreement with the estimates presented above.

The muon channel is also subject to background contamination from cosmic-ray muons that overlap in time with a collision event. Looking at cosmic-ray muons from non-collision bunches and events that pass the full W selection but fail the primary vertex selection, this background component was estimated to be 1.7 ± 0.8 events.

6.3 Background estimate for the $Z \to ee$ channel

Within the invariant mass window $66 < m_{ee} < 116$ GeV, the contributions from the $W \to e\nu$, $Z \to \tau\tau$, and $t\bar{t}$ processes were determined to be 0.11, 0.06, and 0.10 events, respectively, from the Monte-Carlo simulation.

A data-driven estimate of the QCD background was made. The lepton requirement was relaxed from "medium" to "loose" (as described in section 4.2) and the invariant-mass distribution of the resulting electron-positron pairs was used as a template. A fit consisting of a Breit-Wigner convolved with a Gaussian function, to model the signal, and a second-order polynomial, to model the background, was made to the mass distribution within the mass window $50 < m_{ee} < 130$ GeV. The number of loose electron background candidate events within the mass window $66 < m_{ee} < 116$ GeV was estimated to be $48.5 \pm 6.0(\text{stat})$ events. A data-derived "loose" to "medium" rejection factor for the leptons was determined to be $0.137 \pm 0.001(\text{stat})$ and was then used to estimate the expected number of lepton pairs which both pass the nominal $Z \to ee$ requirements. By applying this data-derived rejection

JHEP12(2010)060

factor to each lepton in this "loose" pair, a QCD-background estimate totalling $0.91 \pm 0.11(\text{stat})$ events in the opposite-charge distribution within the Z-mass window was derived. This same procedure was applied to the $Z \to ee$ and corresponding background Monte-Carlo samples, resulting in an estimated QCD background of $0.87 \pm 0.04(\text{stat})$ events, in agreement with the data-derived result.

A systematic uncertainty on the number of background events within the invariant mass window was assessed by selecting pairs of candidate leptons of varying levels of electron identification, e.g. pairs of lepton candidates before the "loose" selection, one "loose" and one "medium" lepton candidate, and using the corresponding rejection factors measured from the data. The fit stability was verified by changing the bin size of the invariant mass distribution and replacing the second-order polynomial function by a first-order one. The systematic uncertainties of the rejection factors were evaluated by exploring their kinematic dependencies as well as the background composition and signal contamination of the samples used to derive these factors at the various levels of electron identification. The total estimated QCD background within the invariant mass window $66 < m_{ee} < 116\,\text{GeV}$ is $0.91 \pm 0.11(\text{stat}) \pm 0.41(\text{sys})$.

The number of same-charge lepton pairs that otherwise satisfy all other requirements is a good indicator of the level of background in the selection. In the electron channel, three same-charge lepton pairs satisfy all Z-boson selection requirements within the invariant mass window. This is in agreement with the expectation based on Monte-Carlo simulation (see section 4.2) from which 2.3 same-charge lepton pairs are expected from $Z \to ee$ decays. In addition 0.9 events are expected from QCD background.

6.4 Background estimate for the $Z \to \mu\mu$ channel

Within the invariant mass window $66 < m_{\mu\mu} < 116\,\text{GeV}$, the contributions from $t\bar{t}$, $Z \to \tau\tau$, and $W \to \mu\nu$ are expected to be 0.11, 0.09, and 0.01 events, respectively.

For this channel, also the QCD background was determined from Monte-Carlo simulation and 0.04 events are predicted from a simulation of $b\bar{b}$ production. Given the large uncertainty on the prediction of absolute rates from Monte-Carlo simulation, a 100% uncertainty is assigned to this estimate. This is considered to be a conservative assumption because the QCD background to both the single and di-muon samples was found to be overestimated by the same factor of about 1.6. An estimate of the QCD background from data is still limited by the statistical uncertainty, e.g. no same-charge muon pair was found to satisfy all Z-boson selection requirements in the invariant mass window considered and only few events are observed reversing the isolation requirement. Compared to the contributions described above, all other background sources are negligible.

6.5 Background-subtracted W and Z candidate events

The numbers of observed candidate events for the $W \to \ell\nu$ and $Z \to \ell\ell$ channels, the estimated background events from both the QCD processes and electroweak plus $t\bar{t}$ processes and the number of background-subtracted signal events are summarised in tables 4 and 5 together with their statistical and systematic uncertainties. The systematic uncertainties receive contributions from experimental systematic uncertainties (see section 7.2),

JHEP12(2010)060

ℓ	Observed candidates	Background (EW+$t\bar{t}$)	Background (QCD)	Background-subtracted signal N_W^{sig}
e^+	637	$18.8 \pm 0.2 \pm 1.7$	$14.0 \pm 2.1 \pm 7.1$	$604.2 \pm 25.2 \pm 7.6$
e^-	432	$14.7 \pm 0.2 \pm 1.3$	$14.0 \pm 2.1 \pm 7.1$	$403.2 \pm 20.8 \pm 7.5$
$e^\pm$	1069	$33.5 \pm 0.2 \pm 3.0$	$28.0 \pm 3.0 \pm 10.0$	$1007.5 \pm 32.7 \pm 10.8$
μ^+	710	$42.5 \pm 0.2 \pm 2.9$	$12.0 \pm 3.0 \pm 4.6$	$655.6 \pm 26.6 \pm 6.2$
μ^-	471	$35.1 \pm 0.2 \pm 2.4$	$10.9 \pm 2.4 \pm 4.1$	$425.0 \pm 21.7 \pm 5.4$
$\mu^\pm$	1181	$77.6 \pm 0.3 \pm 5.4$	$22.8 \pm 4.6 \pm 8.7$	$1080.6 \pm 34.4 \pm 11.2$

Table 4. Numbers of observed candidate events for the $W \to \ell\nu$ channel, electroweak ($W \to \tau\nu$, $Z \to \ell\ell$, $Z \to \tau\tau$) plus $t\bar{t}$, and QCD background events, as well as background-subtracted signal events. For the muon channel, the QCD background also contains a small cosmic-ray component. For the electron channel, the QCD background is assumed to be charge independent. The background fits were also performed separately for W^+ and W^- production and were found to agree within uncertainties. The first uncertainty is statistical. The second uncertainty represents the systematics (as described in the text). In addition to what is quoted in this table, a $\pm 11\%$ uncertainty on the luminosity determination is applicable to the electroweak plus $t\bar{t}$ backgrounds.

ℓ	Observed candidates	Background (EW+$t\bar{t}$)	Background (QCD)	Background-subtracted signal N_Z^{sig}
$e^\pm$	70	$0.27 \pm 0.00 \pm 0.03$	$0.91 \pm 0.11 \pm 0.41$	$68.8 \pm 8.4 \pm 0.4$
$\mu^\pm$	109	$0.21 \pm 0.01 \pm 0.01$	$0.04 \pm 0.01 \pm 0.04$	$108.8 \pm 10.4 \pm 0.0$

Table 5. Numbers of observed candidate events for the $Z \to \ell\ell$ channel, electroweak ($W \to \ell\nu$, $Z \to \tau\tau$) plus $t\bar{t}$, and QCD background events, as well as background-subtracted signal events. The first uncertainty is statistical. The second uncertainty represents the systematics (as described in the text). In addition to what is quoted in this table, a $\pm 11\%$ uncertainty on the luminosity determination is applicable to the electroweak plus $t\bar{t}$ backgrounds.

from theoretical uncertainties on the predicted cross sections for W, Z and $t\bar{t}$ production (see sections 3 and 7.6), and from uncertainties on the parton distribution functions (see section 7.4). The statistical component of the background uncertainty is included in the systematic uncertainty of the background-subtracted signal. The luminosity determination uncertainty of $\pm 11\%$ is used in all channels but is only applicable to the electroweak and $t\bar{t}$ backgrounds as they are determined from Monte-Carlo simulation. The resulting correlation of the luminosity systematic uncertainty is fully taken into account in the calculation of the cross sections in section 7.

JHEP12(2010)060

7 Cross-section measurements

7.1 Methodology

The production cross sections for the W and Z bosons times the branching ratios for decays into leptons can be expressed as:

$$\sigma^{\text{tot}}_{W(Z)} \cdot BR(W(Z) \to \ell\nu\ (\ell\ell)) = \frac{N^{\text{sig}}_{W(Z)}}{A_{W(Z)} \cdot C_{W(Z)} \cdot L_{W(Z)}}, \tag{7.1}$$

where

- N^{sig}_{W} and N^{sig}_{Z} denote the numbers of background-subtracted signal events passing the selection criteria of the analyses in the W and Z channels, as defined in section 5.4.

- A_W and A_Z denote the acceptances for the W and Z-boson decays under consideration, defined as the fraction of decays satisfying the geometrical and kinematical constraints at the generator level (fiducial acceptance). These quantities can only be determined from Monte-Carlo simulations and are defined here before the decay leptons emit photons via QED final state radiation.

- C_W and C_Z denote the ratios between the total number of generated events which pass the final selection requirements after reconstruction and the total number of generated events within the fiducial acceptance, as defined in section 5. These correction factors include the efficiencies for triggering, reconstructing, and identifying the W and Z-boson decays falling within the acceptance.

- L_W and L_Z denote the integrated luminosities for the channels of interest.

The resulting cross sections, as defined by eq. (7.1), define measured total inclusive cross sections. For the W boson they are measured separately for W^+, W^- and W production. The total cross sections are denoted as $\sigma^{\text{tot}}_{W^+}$, $\sigma^{\text{tot}}_{W^-}$ and σ^{tot}_{W}. The corresponding Z cross section in the invariant mass range $66 < m_{\ell\ell} < 116\,\text{GeV}$ is referred to as σ^{tot}_{Z}.

These total cross sections are derived from the measurements of the cross sections in the fiducial region, which are denoted as fiducial cross sections $\sigma^{\text{fid}}_{W(Z)}$. They are related to the total cross sections via

$$\sigma^{\text{fid}}_{W(Z)} \cdot BR(W(Z) \to \ell\nu\ (\ell\ell)) = \sigma^{\text{tot}}_{W(Z)} \cdot BR(W(Z) \to \ell\nu\ (\ell\ell))\ \cdot A_{W(Z)} = \frac{N^{\text{sig}}_{W(Z)}}{C_{W(Z)} \cdot L_{W(Z)}}. \tag{7.2}$$

By definition, no acceptance correction factors are needed for the measurement of the fiducial cross sections. Therefore these cross sections are not affected by significant theoretical uncertainties. Hence, future improvements on the predictions of A_W and A_Z can be used to extract improved total cross-section measurements. Cross-section results in this paper are presented below for both the electron and muon channels as well as for their combination.

JHEP12(2010)060

7.2 The correction factors C_W and C_Z

The central values of the correction factors C_W and C_Z are computed using Monte-Carlo simulation. Only in the case of the trigger efficiencies for muons, corrections determined from data are applied. To assess the uncertainties affecting these factors, the following decomposition is used:

$$C_W = \epsilon^W_{\text{event}} \cdot \alpha^W_{\text{reco}} \cdot \epsilon^W_{\text{lep}} \cdot \epsilon^W_{\text{trig}} \qquad (7.3)$$
$$C_Z = \epsilon^Z_{\text{event}} \cdot \alpha^Z_{\text{reco}} \cdot (\epsilon^Z_{\text{lep}})^2 \cdot [1 - (1 - \epsilon^Z_{\text{trig}})^2],$$

where the individual factors account for event selection efficiencies (ϵ event), e.g. primary vertex requirements, lepton reconstruction and identification efficiencies (ϵ_{lep}) and the trigger efficiency with respect to selected lepton candidates (ϵ_{trig}). The exact definitions of these terms for electron and muon final states are given below in the respective subsections. The factor α_{reco} accounts for all differences observed between the efficiencies of applying the kinematic and geometrical cuts at generator level and reconstruction level. It includes for example effects due to the detector resolution on the lepton transverse momenta/energies and on the missing transverse energy. This factor also includes basic reconstruction efficiencies. The choice mentioned above of calculating the acceptance factors for leptons before they emit final-state radiation of photons also affects this correction factor in a significant way, in particular for electron final states. Finally, this factor includes migration and combinatorial effects and therefore may have values larger than unity.

7.2.1 Electron final states

For electrons, the efficiency of the L1 trigger with its nominal threshold of 10 GeV was measured to be close to 100%, using minimum-bias data and samples obtained with lower-threshold electron triggers at lower luminosities.

The term ϵ_{lep} refers to the "tight" and "medium" electron identification efficiencies for the W and Z selection, respectively. They are defined with respect to all reconstructed electron candidates and were determined from Monte-Carlo simulation. A strong E_{T} and η dependence is observed for these efficiencies, which arises mainly from material interactions in the inner detector. It is a significant source of systematic uncertainty for C_W and C_Z.

This uncertainty was evaluated by combining the results from dedicated simulations, including additional material in the inner detector and in front of the electromagnetic calorimeter, with those obtained from direct measurements of the efficiencies from data. These measurements were performed with limited statistical precision using as probes unbiased electrons selected together with a well identified tag electron in $Z \to ee$ candidate events, and with better accuracy using as probes unbiased electrons in selected $W \to e\nu$ candidate events with large and isolated $E_{\text{T}}^{\text{miss}}$, as discussed in section 4.2. All these direct measurements are in agreement with the nominal values, within the estimated overall systematic uncertainties quoted in table 6 of 5.2% and 4.2%, for the "tight" and "medium" electron identification efficiencies, respectively.

The factor α_{reco} includes in addition to the electron and $E_{\text{T}}^{\text{miss}}$ resolution effects the basic reconstruction efficiency, e.g. the probability for an electron that an electromagnetic

JHEP12(2010)060

	$W \to e\nu$		$Z \to ee$		$W \to \mu\nu$		$Z \to \mu\mu$	
	Central value	Rel. uncertainty	Central value	Rel. uncertainty	Central value	Rel. uncertainty	Central value	Rel. uncertainty
ϵ_{event}	1.000	$< 0.2\%$	1.000	$< 0.2\%$	0.998	$<0.2\%$	0.998	$<0.2\%$
ϵ_{lep}	0.749	5.2%	0.943	4.2%	0.886	2.7%	0.894	2.7%
ϵ_{trig}	0.998	$< 0.2\%$	0.998	$< 0.2\%$	0.815	1.9%	0.811	1.9%
α_{reco}	0.882	3.9%	0.732	3.2%	1.051	2.3 %	1.007	0.7 %
C_W, C_Z	0.659	7.0%	0.651	9.4%	0.758	4.0%	0.773	5.5%

Table 6. Efficiency factors per lepton and α_{reco} as well as their relative uncertainties which enter the calculation of the correction factors C_W and C_Z for both lepton channels. The trigger efficiencies were measured from data. The other efficiencies and their uncertainties were determined from Monte-Carlo simulation and have been validated with data, as described in the text. It should be noted that for Z bosons the trigger and identification efficiencies are given per lepton, according to the definition given in eq. (7.3).

cluster in the calorimeter is reconstructed in a fiducial region of the detector and is loosely matched to a reconstructed track. This includes losses of leptons due to imperfect regions of the detector within the geometrical acceptance. In the case of $Z \to ee$ candidates, the value of α_{reco} is significantly lower than for $W \to e\nu$ candidates because both electrons must fall outside the imperfect regions of the detector and also because 3.3% of the $Z \to ee$ candidates fail the requirement of a pair of oppositely charged leptons, as discussed in section 6.3.

The central values as well as the relative uncertainties of the efficiencies and of α_{reco} are summarised for both $W \to e\nu$ and $Z \to ee$ final states in table 6.

7.2.2 Muon final states

For the muon channels, the trigger efficiency was measured in data relative to reconstructed muons, using a control sample selected with an independent jet trigger. Combined reconstructed muons above 20 GeV are selected by applying the same criteria as adopted for the W selection. Tracks are then extrapolated to the trigger chamber planes and the efficiency is measured by looking at associated trigger signals in the barrel or end-cap regions separately. The ratio of the event trigger efficiency measured in data and predicted by Monte-Carlo simulation is 0.929 ± 0.010 (stat) ± 0.015 (syst) in the W channel and 0.981 ± 0.003 (stat) ± 0.006 (syst) in the Z channel. These values are significantly different from 1 and therefore a correction is applied to the central values of C_W and C_Z. The systematic uncertainty is derived from changing the tolerance on the association between tracks and trigger signals, by checking the stability of the 20 GeV threshold in the plateau region and by comparing measurements obtained using different muon reconstruction algorithms.

The term ϵ_{lep} includes the combined-muon reconstruction efficiency relative to the inner detector track ($\epsilon = 0.924 \pm 0.023$) and the efficiencies of quality ($\epsilon = 0.966 \pm 0.001$) and isolation ($\epsilon = 0.993 \pm 0.010$) requirements. The combined-muon reconstruction efficiency was determined by Monte-Carlo simulation and cross-checked to be in agreement with data, as explained in section 4.3. The isolation efficiency was measured in data using a sample

JHEP12(2010)060

of muons from Z decays and found to be in agreement with Monte-Carlo simulation within $\pm 1\%$. This difference was assigned as a systematic uncertainty.

The factor α_{reco} includes in addition to the muon and $E_{\text{T}}^{\text{miss}}$ resolution effects the efficiency for the reconstruction of a track in the inner detector ($\epsilon = 0.989 \pm 0.010$). The dominant systematic uncertainties on α_{reco} result from the uncertainties on the muon momentum scale and resolution (as derived in section 4.3) and, for the W analysis, from uncertainties on the $E_{\text{T}}^{\text{miss}}$ scale and resolution.

The central values, as well as the relative uncertainties, of the efficiencies and of α_{reco} are also summarised for both $W \to \mu\nu$ and $Z \to \mu\mu$ final states in table 6.

7.2.3 C_W and C_Z and their uncertainties

The central values of the correction factors C_W and C_Z, shown in table 6, were determined to a large extent using Monte-Carlo simulation. For muons, data-driven corrections for the trigger efficiencies are included. The uncertainties of C_W and C_Z receive contributions from the uncertainties of the efficiencies discussed above and from uncertainties on the correction factor α_{reco}. A breakdown of the various components is given in tables 7 and 8 for electron and muon final states, respectively. The decomposition was made in such a way that the correlations between the different contributions are negligible. For electrons, the main contributions result from uncertainties on the electron reconstruction efficiency and from material effects in the inner detector as well as from uncertainties on the electron energy scale and resolution. For muons, the uncertainties on the reconstruction efficiency and on the $E_{\text{T}}^{\text{miss}}$ scale and resolution are dominant.

The uncertainties on C_W linked to uncertainties on the scale of the missing transverse energy were determined from a variation of the response of cells in topological clusters within the range given in section 4.4. These changes propagate to an uncertainty of $\pm 1.5\%$ on the number of accepted $W \to \ell\nu$ events. Other sources of uncertainty, namely the imperfect modelling of the overall $E_{\text{T}}^{\text{miss}}$ response (low energy hadrons) and resolution, of the underlying event and pile-up effects, lead to acceptance changes at the level of $\pm 1\%$, resulting in a total uncertainty of $\pm$ 2% on C_W.

In addition uncertainties arising from QED final-state radiation and theoretical uncertainties, resulting predominantly from structure function parametrisations, have been considered. The purely theoretical uncertainty on the QED final-state radiation emission is very small, typically smaller than 0.2% [45, 46]. It can be neglected compared to the other uncertainties discussed in section 7.4. In the case of electrons and collinear emission of QED photons, however, there is an experimental uncertainty arising from the transport of low-energy photons through the detector material and the response of the electromagnetic calorimeter which was estimated to be $< 0.3\%$ on C_W and C_Z. Finally, using the prescription described in section 7.4, the relative uncertainties on C_W and C_Z resulting from structure function parametrisations were estimated to be small, at the level of $\pm 0.3\%$. From a comparison between PYTHIA and MC@NLO, no significant additional theoretical uncertainty needs to be assigned to C_W and C_Z to account for any NLO physics that is not included in the PYTHIA generator.

JHEP12(2010)060

Parameter	$\delta C_W/C_W(\%)$	$\delta C_Z/C_Z(\%)$
Trigger efficiency	<0.2	<0.2
Material effects, reconstruction and identification	5.6	8.8
Energy scale and resolution	3.3	1.9
$E_{\mathrm{T}}^{\mathrm{miss}}$ scale and resolution	2.0	-
Problematic regions in the calorimeter	1.4	2.7
Pile-up	0.5	0.2
Charge misidentification	0.5	0.5
FSR modelling	0.3	0.3
Theoretical uncertainty (PDFs)	0.3	0.3
Total uncertainty	7.0	9.4

Table 7. Summary of the different terms contributing to the uncertainty on C_W and C_Z for electron final states. The decomposition has been made such that correlations between the various contributions are negligible.

Parameter	$\delta C_W/C_W(\%)$	$\delta C_Z/C_Z(\%)$
Trigger efficiency	1.9	0.7
Reconstruction efficiency	2.5	5.0
Momentum scale	1.2	0.5
Momentum resolution	0.2	0.5
$E_{\mathrm{T}}^{\mathrm{miss}}$ scale and resolution	2.0	-
Isolation efficiency	1.0	2.0
Theoretical uncertainty (PDFs)	0.3	0.3
Total uncertainty	4.0	5.5

Table 8. Summary of the different terms contributing to the uncertainty on C_W and C_Z for muon final states. The decomposition has been made such that correlations between the various contributions are negligible.

As can be seen from the numbers given in tables 7 and 8, the total uncertainties on C_W and C_Z are larger for electrons than for muons. This is mainly due to the higher sensitivity of electrons to material effects in the inner detector and the current knowledge of the electron energy scale compared to the muon momentum scale.

7.3 Measured fiducial cross sections

According to eq. (7.2), the correction factors C_W and C_Z, the number of observed events, and the integrated luminosity are the elements for the extraction of the fiducial cross sections. All relevant numbers are summarised, separated for W^+, W^-, W and Z production and decay in the electron and muon channels in tables 9 and 10, respectively. Using these numbers, the fiducial cross sections reported in table 11 are obtained.

JHEP12(2010)060

	W^+				W^-				W			
Electron channel												
	value	stat	syst	lumi	value	stat	syst	lumi	value	stat	syst	lumi
N_W^{sig}	604.2	25.2	7.6	2.0	403.2	20.8	7.5	1.5	1007.5	32.7	10.8	3.5
L_W [nb^{-1}]	315	-	-	35	315	-	-	35	315	-	-	35
C_W	0.656	-	0.046	-	0.662	-	0.046	-	0.659	-	0.046	-
A_W	0.466	-	0.014	-	0.457	-	0.014	-	0.462	-	0.014	-
Muon channel												
	value	stat	syst	lumi	value	stat	syst	lumi	value	stat	syst	lumi
N_W^{sig}	655.6	26.6	6.2	4.7	425.0	21.7	5.4	3.9	1080.6	34.4	11.2	8.5
L_W [nb^{-1}]	310	-	-	34	310	-	-	34	310	-	-	34
C_W	0.765	-	0.031	-	0.748	-	0.030	-	0.758	-	0.030	-
A_W	0.484	-	0.015	-	0.475	-	0.014	-	0.480	-	0.014	-

Table 9. Summary of input quantities for the calculation of the W^+, W^- and W boson production cross sections. For each channel, the observed numbers of signal events after background subtraction, the correction factors C_W, the acceptance factors A_W and the integrated luminosities are given, with their statistical, systematic, and luminosity uncertainties.

	Z/γ^*							
	Electron channel				**Muon channel**			
	value	stat	syst	lumi	value	stat	syst	lumi
N_Z^{sig}	68.8	8.4	0.4	0.0	108.8	10.4	0.0	0.0
L_Z [nb^{-1}]	316	-	-	35	331	-	-	35
C_Z	0.651	-	0.061	-	0.773	-	0.043	-
A_Z	0.446	-	0.018	-	0.486	-	0.019	-

Table 10. Summary of input quantities for the calculation of the Z/γ^* boson production cross section. For the electron and muon channels, the observed numbers of signal events after background subtraction, the correction factors C_Z, the acceptance factors A_Z and the integrated luminosities are given, with their statistical, systematic, and luminosity uncertainties.

	$\sigma^{\text{fid}}_{W^{(\pm)}} \cdot \text{BR}(W \to e\nu)$ [nb]	$\sigma^{\text{fid}}_{W^{(\pm)}} \cdot \text{BR}(W \to \mu\nu)$ [nb]
W^+	$2.92 \pm 0.12\,(\text{stat}) \pm 0.21\,(\text{syst}) \pm 0.32\,(\text{lumi})$	$2.77 \pm 0.11\,(\text{stat}) \pm 0.12\,(\text{syst}) \pm 0.30\,(\text{lumi})$
W^-	$1.93 \pm 0.10\,(\text{stat}) \pm 0.14\,(\text{syst}) \pm 0.21\,(\text{lumi})$	$1.83 \pm 0.09\,(\text{stat}) \pm 0.08\,(\text{syst}) \pm 0.20\,(\text{lumi})$
W	$4.85 \pm 0.16\,(\text{stat}) \pm 0.34\,(\text{syst}) \pm 0.53\,(\text{lumi})$	$4.60 \pm 0.15\,(\text{stat}) \pm 0.20\,(\text{syst}) \pm 0.51\,(\text{lumi})$
	$\sigma^{\text{fid}}_{Z/\gamma^*} \cdot \text{BR}(Z/\gamma^* \to ee)$ [nb], $66 < m_{ee} < 116\,\text{GeV}$	$\sigma^{\text{fid}}_{Z/\gamma^*} \cdot \text{BR}(Z/\gamma^* \to \mu\mu)$ [nb], $66 < m_{\mu\mu} < 116\,\text{GeV}$
Z/γ^*	$0.33 \pm 0.04\,(\text{stat}) \pm 0.03\,(\text{syst}) \pm 0.04\,(\text{lumi})$	$0.43 \pm 0.04\,(\text{stat}) \pm 0.02\,(\text{syst}) \pm 0.05\,(\text{lumi})$

Table 11. Measured fiducial cross sections times leptonic branching ratios for W^+, W^-, W and Z/γ^* production in the electron and muon final states.

JHEP12(2010)060

Even with the rather low integrated luminosity of about 320 nb^{-1}, these W cross-section measurements are already dominated by systematic uncertainties, most prominently by the luminosity uncertainty of $\pm 11\%$ and to a lesser degree by the experimental uncertainties discussed in the previous section. As already mentioned, these cross sections are only very weakly affected by theoretical uncertainties related to the calculation of acceptance corrections. The calculation of these correction factors and of the related uncertainties is discussed in the next section.

7.4 Acceptances and uncertainties

The total cross sections are derived from the measured fiducial cross sections by applying the factors A_W and A_Z for the phase-space requirements applied in the analysis:

- $W \to e\nu$: $E_{\mathrm{T}}^{e} > 20\,\mathrm{GeV}$, $|\eta| < 2.47$, excluding $1.37 < |\eta| < 1.52$, $p_{\mathrm{T}}^{\nu} > 25\,\mathrm{GeV}$, $m_T > 40\,\mathrm{GeV}$;
- $W \to \mu\nu$: $p_{\mathrm{T}}^{\mu} > 20\,\mathrm{GeV}$, $|\eta| < 2.4$, $p_{\mathrm{T}}^{\nu} > 25\,\mathrm{GeV}$, $m_T > 40\,\mathrm{GeV}$;
- $Z \to ee$: $E_{\mathrm{T}}^{e} > 20\,\mathrm{GeV}$, $|\eta| < 2.47$, excluding $1.37 < |\eta| < 1.52$, $66 < m_{ee} < 116\,\mathrm{GeV}$;
- $Z \to \mu\mu$: $p_{\mathrm{T}}^{\mu} > 20\,\mathrm{GeV}$, $|\eta| < 2.4$, $66 < m_{\mu\mu} < 116\,\mathrm{GeV}$.

The calculation of A_W and A_Z is based on Monte-Carlo simulation. Losses due to QED final-state radiation [45, 46] are included in the correction factors C_W and C_Z, evaluated with a full simulation of the detector response.

The acceptances are calculated using the PYTHIA Monte-Carlo generator with the modified leading order parton distribution function set MRST LO* [47] and the corresponding ATLAS MC09 tune [48]. The central values of the acceptances are provided in table 12, separated for W^+, W^-, W and Z/γ^* production. In addition, the ratio A_W/A_Z is given, which is relevant for the measurement of the cross-section ratio (see section 7.7). The statistical uncertainties resulting from the Monte-Carlo samples are negligible.

The systematic uncertainties on the acceptances are dominated by the limited knowledge of the proton PDFs and the modelling of the W and Z boson production at the LHC. These uncertainties therefore were derived by combining three different components:

- The uncertainties within one PDF set were derived using the CTEQ 6.6 PDF [49] error eigenvector sets at the 90% C.L. limit, in combination with the MC@NLO acceptance calculation. The relative uncertainties on the acceptances were found to be $\pm 1.0\%$ for W^+, $\pm 1.8\%$ for W^-, and $\pm 1.6\%$ for Z/γ^*-boson production.
- Larger uncertainties were found between different PDF sets. They have been estimated using PYTHIA, based on the maximal difference between the MRST LO*, CTEQ 6.6 and HERAPDF 1.0 [50] sets. The relative uncertainties on the acceptances were found to be $\pm 2.7\%$ for W^+, $\pm 0.9\%$ for W^-, and $\pm 2.0\%$ for Z/γ^*-boson production.

JHEP12(2010)060

MC	A_{W^+} $W^+ \to e^+\nu$	A_{W^-} $W^- \to e^-\nu$	A_W $W \to e\nu$	A_Z $Z/\gamma^* \to e^+e^-$	A_W/A_Z
PYTHIA MRST LO*	0.466	0.457	0.462	0.446	1.036
PYTHIA CTEQ6.6	0.479	0.458	0.471	0.455	1.035
PYTHIA HERAPDF1.0	0.477	0.461	0.470	0.451	1.042
MC@NLO HERAPDF1.0	0.475	0.454	0.465	0.440	1.057
MC@NLO CTEQ6.6	0.478	0.452	0.465	0.445	1.045
	A_{W^+} $W^+ \to \mu^+\nu$	A_{W^-} $W^- \to \mu^-\nu$	A_W $W \to \mu\nu$	A_Z $Z/\gamma^* \to \mu^+\mu^-$	A_W/A_Z
PYTHIA MRSTLO*	0.484	0.475	0.480	0.486	0.988
PYTHIA CTEQ6.6	0.499	0.477	0.490	0.496	0.987
PYTHIA HERAPDF1.0	0.496	0.479	0.489	0.492	0.994
MC@NLO HERAPDF1.0	0.494	0.472	0.483	0.479	1.008
MC@NLO CTEQ6.6	0.496	0.470	0.483	0.485	0.996

Table 12. Summary of acceptance values A_W for $W \to e\nu$ and $W \to \mu\nu$ (separated for charges and combined) and A_Z for $Z/\gamma^* \to ee$ and $Z/\gamma^* \to \mu\mu$ as well as the ratio A_W/A_Z using various Monte-Carlo simulations.

- The uncertainties due to the modelling of W and Z production were derived from the difference obtained between the PYTHIA and MC@NLO simulations, using the same PDF set, CTEQ 6.6. In this case the relative uncertainties on the acceptances were found to be $\pm 0.4\%$ for W^+, $\pm 1.4\%$ for W^-, and $\pm 2.3\%$ for Z/γ^*-boson production.

Adding these components in quadrature results in systematic uncertainties on the acceptance values for W^+, W^- and Z/γ^* production of $\pm 3.2\%$, $\pm 2.7\%$ and $\pm 3.8\%$, respectively. Approximate numbers of $\pm 3\%$ and $\pm 4\%$ are used in the following as the overall relative systematic uncertainties for the PYTHIA acceptance values A_W and A_Z, respectively.

The uncertainties on the ratios of acceptances cannot be naively calculated via error propagation since the theoretical uncertainties exhibit significant correlations and the PDF uncertainties are expected to cancel partially. Using the same combination of the three sources of uncertainties, as discussed for the individual acceptances, the uncertainties on the ratios are estimated to be $\pm 3.0\%$ for A_{W^+}/A_Z, $\pm 2.5\%$ for A_{W^-}/A_Z, and $\pm 1.5\%$ for the charge combined ratio A_W/A_Z.

7.5 Measured total cross sections

The total cross sections are obtained by dividing the measured fiducial cross sections by the acceptance factors. The results are summarized in table 13, separated for the electron and muon final states.

Assuming lepton universality, the measured total cross sections in the two lepton final states can be combined to decrease the statistical uncertainty. For the combination, it is assumed that the uncertainties on the integrated luminosity, on the acceptance factors A_W and A_Z and the uncertainty resulting from the hadronic part of the $E_{\mathrm{T}}^{\mathrm{miss}}$ measurement are fully correlated between the electron and muon channels. All other uncertainties are

JHEP12(2010)060

	$\sigma^{\rm tot}_{W^{(\pm)}} \cdot$ BR$(W \to e\nu)$ [nb]	$\sigma^{\rm tot}_{W^{(\pm)}} \cdot$ BR$(W \to \mu\nu)$ [nb]
W^+	$6.27 \pm 0.26\,(\text{stat}) \pm 0.48\,(\text{syst}) \pm 0.69\,(\text{lumi})$	$5.71 \pm 0.23\,(\text{stat}) \pm 0.30\,(\text{syst}) \pm 0.63\,(\text{lumi})$
W^-	$4.23 \pm 0.22\,(\text{stat}) \pm 0.33\,(\text{syst}) \pm 0.47\,(\text{lumi})$	$3.86 \pm 0.20\,(\text{stat}) \pm 0.20\,(\text{syst}) \pm 0.42\,(\text{lumi})$
W	$10.51 \pm 0.34\,(\text{stat}) \pm 0.81\,(\text{syst}) \pm 1.16\,(\text{lumi})$	$9.58 \pm 0.30\,(\text{stat}) \pm 0.50\,(\text{syst}) \pm 1.05\,(\text{lumi})$
	$\sigma^{\rm tot}_{Z/\gamma^*} \cdot$ BR$(Z/\gamma^* \to ee)$ [nb], $66 < m_{ee} < 116\,\text{GeV}$	$\sigma^{\rm tot}_{Z/\gamma^*} \cdot$ BR$(Z/\gamma^* \to \mu\mu)$ [nb], $66 < m_{\mu\mu} < 116\,\text{GeV}$
Z/γ^*	$0.75 \pm 0.09\,(\text{stat}) \pm 0.08\,(\text{syst}) \pm 0.08\,(\text{lumi})$	$0.87 \pm 0.08\,(\text{stat}) \pm 0.06\,(\text{syst}) \pm 0.10\,(\text{lumi})$

Table 13. Measured total cross sections times leptonic branching ratios for W^+, W^-, W and Z/γ^* production in the electron and muon final states.

assumed to be uncorrelated. For the W production cross sections the following results are obtained:

$$\begin{aligned}
\sigma^{\rm tot}_{W^+} \cdot \text{BR}(\text{W} \to \ell\nu) &= 5.93 \pm 0.17\,(\text{stat}) \pm 0.30\,(\text{syst}) \pm 0.65\,(\text{lumi})\ \text{nb}, \\
\sigma^{\rm tot}_{W^-} \cdot \text{BR}(\text{W} \to \ell\nu) &= 4.00 \pm 0.15\,(\text{stat}) \pm 0.20\,(\text{syst}) \pm 0.44\,(\text{lumi})\ \text{nb}, \\
\sigma^{\rm tot}_{W} \cdot \text{BR}(\text{W} \to \ell\nu) &= 9.96 \pm\ 0.23\,(\text{stat}) \pm\ 0.50\,(\text{syst}) \pm\ 1.10\,(\text{lumi})\ \text{nb}.
\end{aligned}$$

For the Z/γ^* production cross section, measured in the mass range $66 < m_{\ell\ell} < 116\,\text{GeV}$, the combined result is:

$$\sigma^{\rm tot}_{Z/\gamma^*} \cdot \text{BR}(Z/\gamma^* \to \ell\ell) = 0.82 \pm 0.06\,(\text{stat}) \pm 0.05\,(\text{syst}) \pm 0.09\,(\text{lumi})\text{nb}$$
$$(66 < m_{\ell\ell} < 116\,\text{GeV}).$$

It should be noted that the pure Z-boson cross section is expected to be 2% lower in the mass range considered.

Due to the additional uncertainties on A_W and A_Z the relative systematic uncertainties have slightly increased, as compared to the fiducial cross sections. For the total W production cross section, the relative uncertainties are ±3.3%(stat), ±7.7%(syst) and ±11%(lumi). For the Z/γ^* production cross section the statistical uncertainty is still larger than the experimental systematic uncertainty. The relative uncertainties are ±7.2%(stat), ±4.8%(syst) and ±11%(lumi).

7.6 Comparison to theoretical calculations

A comparison of the measured cross-section values for W and Z production to theoretical predictions including next-to-next-to-leading order QCD corrections are shown in figure 11. The calculations were performed using the programs FEWZ [8, 9] and ZWPROD [5, 6] with the MSTW 08 NNLO structure function parameterisation [51]. The following results were obtained:

$\sigma^{NNLO}_{W^+ \to \ell^+\nu} = 6.16 \pm 0.31$ nb, $\sigma^{NNLO}_{W^- \to \ell^-\nu} = 4.30 \pm 0.21$ nb, $\sigma^{NNLO}_{W \to \ell\nu} = 10.46 \pm 0.52$ nb and
$\sigma^{NNLO}_{Z/\gamma^* \to \ell^+\ell^-} = 0.96 \pm 0.05$ nb, for $66 < m_{\ell\ell} < 116\,GeV$.

JHEP12(2010)060

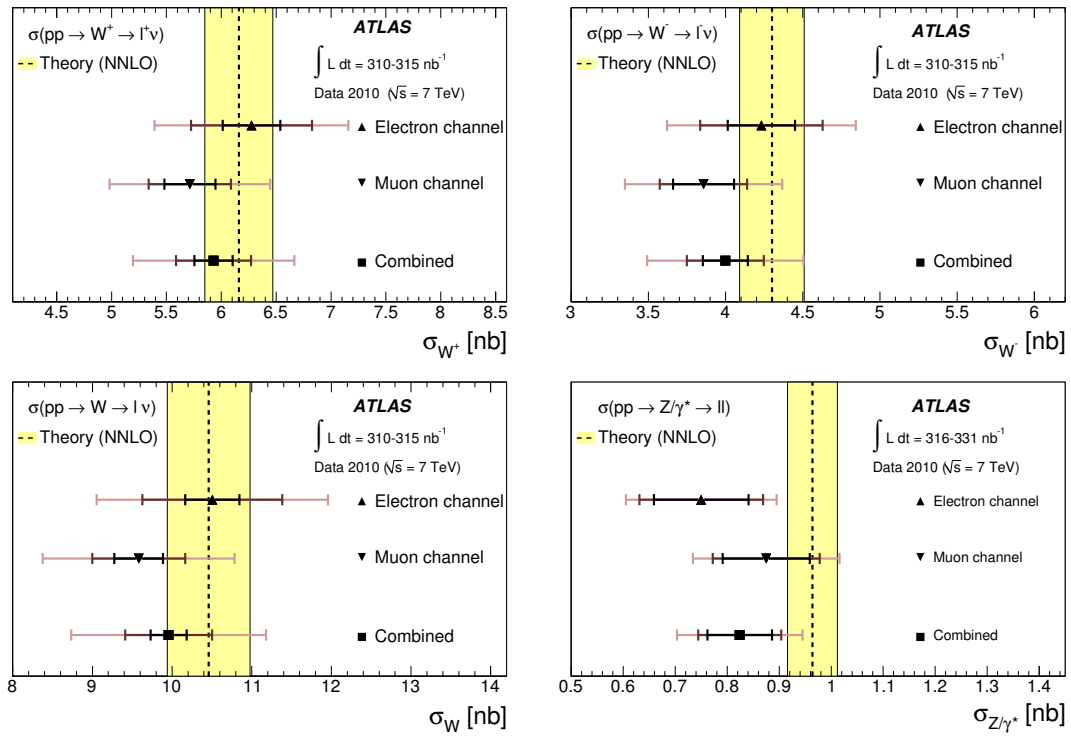

Figure 11. The measured values of $\sigma_W \cdot \mathrm{BR}\ (W \to \ell\nu)$ for W^+, W^- and for their sum and of $\sigma_{Z/\gamma^*} \cdot \mathrm{BR}\ (Z/\gamma^* \to \ell\ell)$ compared to the theoretical predictions based on NNLO QCD calculations (see text). Results are shown for the electron and muon final states as well as for their combination. The error bars represent successively the statistical, the statistical plus systematic and the total uncertainties (statistical, systematic and luminosity). All uncertainties are added in quadrature. The quoted luminosity range spans the values used for the electron and muon channels. The systematic uncertainty on these numbers is ±11%, see section 3.

An overall uncertainty of the NNLO W and Z-boson cross sections of ±5% was estimated using the MSTW 08 NNLO PDF error eigenvectors at the 90% C.L. limit, variations of α_s in the range 0.1145 – 0.1176, and variations of the renormalisation and factorisation scales by factors of two around the nominal scales $\mu_R = \mu_F = m_{W/Z}$. Within the uncertainties, the calculations for W production agree well with the measured cross sections. In particular, the expected asymmetry between the W^+ and W^- cross sections is confirmed. For the Z cross section, the present measurements are below the theoretical predictions, but are still consistent within uncertainties.

In figures 12 and 13, the combined electron and muon measurements at $\sqrt{s} = 7\,\mathrm{TeV}$ are compared to the theoretical predictions and to previous measurements of the total W and Z-production cross sections by the UA1 [10] and UA2 [11] experiments at $\sqrt{s} = 0.63\,\mathrm{TeV}$ at the CERN Sp$\overline{\mathrm{p}}$S and by the CDF [14] and D0 [16, 17] experiments at $\sqrt{s} = 1.8\,\mathrm{TeV}$ and $\sqrt{s} = 1.96\,\mathrm{TeV}$ at the Fermilab Tevatron colliders and to the recent W production cross-section measurement by the PHENIX [18] experiment in proton-proton collisions at $\sqrt{s} = 0.5\,\mathrm{TeV}$ at the RHIC collider. The theoretical predictions are in good agreement

JHEP12(2010)060

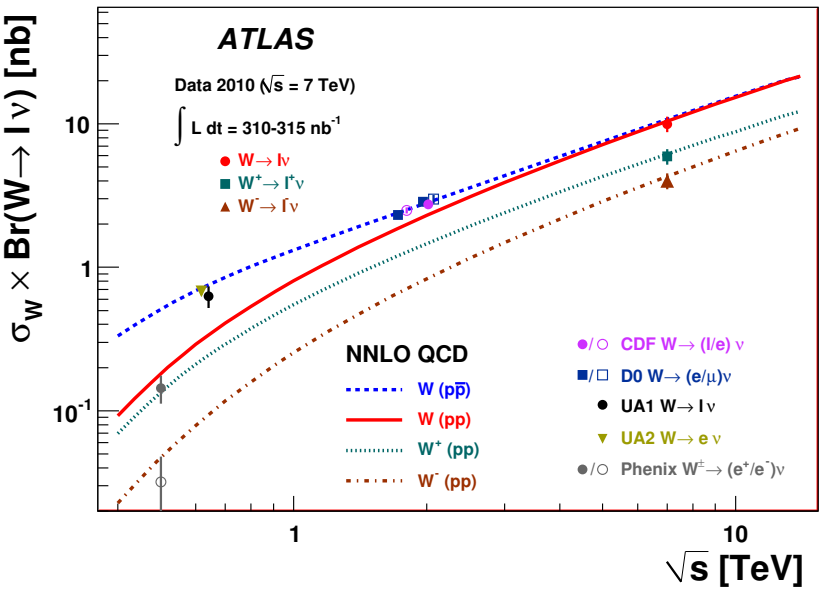

Figure 12. The measured values of $\sigma_W \cdot \mathrm{BR}\ (W \to \ell\nu)$ for W^+, W^- and for their sum compared to the theoretical predictions based on NNLO QCD calculations (see text). Results are shown for the combined electron-muon results. The predictions are shown for both proton-proton (W^+, $W^-$and their sum) and proton-antiproton colliders (W) as a function of $\sqrt{s}$. In addition, previous measurements at proton-antiproton and proton-proton colliders are shown. The data points at the various energies are staggered to improve readability. The CDF and D0 measurements are shown for both Tevatron collider energies, $\sqrt{s} = 1.8\,\mathrm{TeV}$ and $\sqrt{s} = 1.96\,\mathrm{TeV}$. All data points are displayed with their total uncertainty. The theoretical uncertainties are not shown. The quoted luminosity range spans the values used for the electron and muon channels. The systematic uncertainty on these numbers is $\pm 11\%$, see section 3.

with all measurements. The energy dependence of the total W and Z production cross sections is well described.

7.7 The ratio of the W to Z cross sections

The measurement of the ratio of the W to Z cross sections times branching ratios,

$$R \;=\; \frac{\sigma_W \cdot BR(W \to \ell\nu)}{\sigma_Z \cdot BR(Z \to \ell\ell)}, \tag{7.4}$$

constitutes an important test of the Standard Model. It can be measured with a higher relative precision than the individual cross sections since both experimental and theoretical uncertainties partially cancel. In addition, it is sensitive to new physics processes which change the W or Z production rates or the $W \to \ell\nu$ branching ratio.

Based on the theoretical cross-section calculations presented in section 7.6 the ratios of the W^+, W^-, W to the Z/γ^* cross sections are predicted to be:

$$R^{NNLO}_{W^+/Z} = 6.387^{+0.077}_{-0.057}, \quad R^{NNLO}_{W^-/Z} = 4.445^{+0.036}_{-0.054}, \quad \text{and} \quad R^{NNLO}_{W/Z} = 10.840 \pm 0.054.$$

JHEP12(2010)060

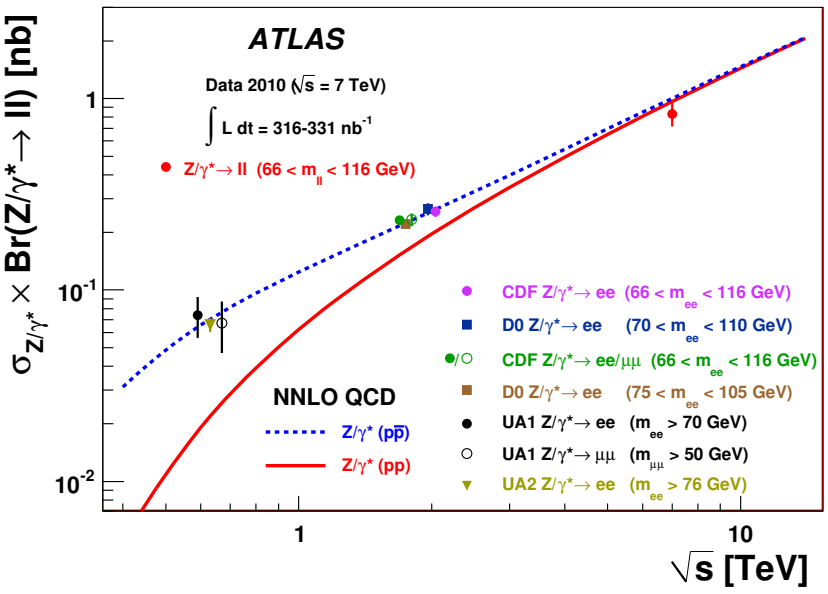

Figure 13. The measured value of $\sigma_{Z/\gamma^*} \times \mathrm{BR}\,(Z/\gamma^* \to \ell\ell)$ where the electron and muon channels have been combined, compared to the theoretical predictions based on NNLO QCD calculations (see text). The predictions are shown for both proton-proton and proton-antiproton colliders as a function of $\sqrt{s}$. In addition, previous measurements at proton-antiproton colliders are shown. The data points at the various energies are staggered to improve readability. The CDF and D0 measurements are shown for both Tevatron collider energies, $\sqrt{s} = 1.8\,\mathrm{TeV}$ and $\sqrt{s} = 1.96\,\mathrm{TeV}$. All data points are displayed with their total uncertainty. The theoretical uncertainties are not shown. The quoted luminosity range spans the values used for the electron and muon channels. The systematic uncertainty on these numbers is ±11%, see section 3.

In terms of the experimental quantities defined in the previous sections, the ratio R can be written as

$$R = \frac{N_W^{\mathrm{sig}}}{N_Z^{\mathrm{sig}}} \cdot \frac{A_Z}{A_W} \cdot \frac{C_Z}{C_W}. \tag{7.5}$$

In particular, the integrated luminosity and the related uncertainty cancel. The uncertainties on the ratio of the acceptance factors have already been discussed in section 7.4. The uncertainty on the ratio of the correction factors C_Z/C_W was evaluated separately for the electron and the muon channels. For both electrons and muons, the correlation between the uncertainties on α^W_{reco} and α^Z_{reco} was taken to be one for the contribution of the lepton energy scale and resolution and zero for the uncertainties resulting from the $E_{\mathrm{T}}^{\mathrm{miss}}$ scale (hadronic recoil), which affects only α^W_{reco}. In addition, in the case of electrons, a correlation between the "tight" (applied in the W analysis) and "medium" (applied in the Z analysis) electron identification criteria is relevant and was taken into account. The total uncertainty on C_W/C_Z was estimated to be ±6.0% for the electron channel and ±3.8% for the muon channel.

JHEP12(2010)060

	$R^{e}_{W^{(\pm)}/Z}$	$R^{\mu}_{W^{(\pm)}/Z}$
W^+	8.4 ± 1.1 (stat) ± 0.6 (syst)	6.5 ± 0.7 (stat) ± 0.3 (syst)
W^-	5.7 ± 0.7 (stat) ± 0.4 (syst)	4.4 ± 0.5 (stat) ± 0.2 (syst)
W	14.0 ± 1.8 (stat) ± 0.9 (syst)	11.0 ± 1.1 (stat) ± 0.5 (syst)

Table 14. Measured cross-section ratios $R^{e,\mu}_{W^+/Z}$, $R^{e,\mu}_{W^-/Z}$ and $R^{e,\mu}_{W/Z}$ in the electron and muon final states.

Using the measured cross-section values presented in section 7.5 the results given in table 14 are obtained for the cross-section ratios for the electron and muon channels. The combination of the two lepton flavours leads to:

$$R^{\ell}_{W^+/Z} = 7.0 \pm 0.6 \text{ (stat)} \pm 0.3 \text{ (syst)},$$
$$R^{\ell}_{W^-/Z} = 4.7 \pm 0.4 \text{ (stat)} \pm 0.2 \text{ (syst)},$$
$$R^{\ell}_{W/Z} = 11.7 \pm 0.9 \text{ (stat)} \pm 0.4 \text{ (syst)}.$$

The results are shown in figure 14 and compared to the theoretical predictions. Within the large uncertainties, which are still dominated by the statistical uncertainties, the theoretical predictions agree with the measured ratios. Due to the low value of the measured $Z \to ee$ cross section, the ratios in the electron channel are above the theoretical expectations. However, it should be noted that the three ratio measurements are correlated via the common low $Z \to ee$ cross-section value and are still compatible within uncertainties with the theory value.

Updated measurements using larger data samples will provide interesting constraints on Γ_W and allow for a precise test of the Standard Model predictions. For such measurements the ratios would have to be normalised to the pure Z boson contribution and electroweak corrections would need to be addressed more carefully.

8 Measurement of the $W \to \ell\nu$ charge asymmetry

The measurement of the charge asymmetry of the W-bosons produced at hadron colliders provides important information about parton distribution functions. Inclusive measurements have been performed at the Tevatron [52, 53] and the data have been included in global fits of parton distributions [51, 54].

The W-boson charge asymmetry is obtained from the charge of the decay leptons. The lepton charge asymmetry measured in this paper is defined via the fiducial cross sections, $\sigma^{\text{fid}}_{W^+}$ and $\sigma^{\text{fid}}_{W^-}$ (see section 7.1 for the definition):

$$A_\ell = \frac{\sigma^{\text{fid}}_{W^+} - \sigma^{\text{fid}}_{W^-}}{\sigma^{\text{fid}}_{W^+} + \sigma^{\text{fid}}_{W^-}}. \tag{8.1}$$

This formula represents a generic definition of the W boson charge asymmetry. For the η dependent measurements presented in the following, the fiducial cross sections refer to the corresponding η bins. The cuts on transverse momenta are those defined in section 5.4.

JHEP12(2010)060

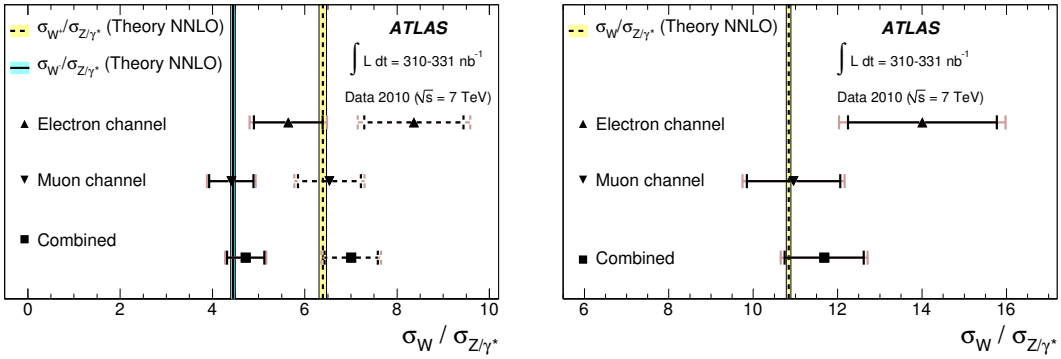

Figure 14. The measured ratios between the W^+ and W^- and the Z/γ^* cross section (left) in the electron and muon decay channels as well as the combined result (right) compared to the theoretical predictions based on NNLO QCD calculations (see text). The error bars represent successively the statistical and the total uncertainties (statistical and systematic). The uncertainties are added in quadrature. The range quoted for the luminosity values covers the integrated luminosities used for the various analyses ($W \to e\nu$, $W \to \mu\nu$, $Z \to ee$, and $Z \to \mu\mu$). The systematic uncertainty on these numbers is $\pm 11\%$, see section 3.

Given the difference in the cross-section measurements for W^+ and W^- presented in the previous section, the overall asymmetry is different from zero. This reflects the different content of u and d valence quarks in the proton. In addition, the asymmetry is expected to depend on the lepton pseudorapidity. This dependence on η provides valuable constraints on the parton distribution functions of the proton, since different η bins probe different average values of the momentum fractions x of the partons producing the W boson. As the W lepton asymmetry is mainly sensitive to valence quark distributions [55], it provides complementary information to that obtained from measurements of structure functions in deep inelastic scattering at HERA [50, 56–58], which do not strongly constrain the ratio between u and d quarks in the kinematic regime probed at the LHC.

The η distributions of reconstructed electrons and muons after the final W selection cuts (see section 5.4) are shown in figure 15. It should be noted that common η acceptance cuts for electrons and muons are used and the asymmetry is measured over the pseudorapidity range $0 < |\eta| < 1.37$ and $1.52 < |\eta| < 2.4$, which allows for a combination of the results of the two lepton flavours. The Monte Carlo simulation is found to be in good agreement with the measured η distributions.

The lepton charge asymmetry is measured in two bins of pseudorapidity. For the calculation of the asymmetry, the correction factors C_W were calculated separately for the two charges and for each of the $|\eta|$ bins and all background contributions are subtracted. For the ratio defined in eq. (8.1), the luminosity uncertainty cancels and C_W-related uncertainties appear to be dominant. Also for some of those, e.g. efficiency uncertainties, cancellations appear as long as they affect positive and negative charged leptons in a symmetric way. Given the different production rates between the two lepton charges, the charge misidentification might lead to a bias in the result. For electrons it is of the order of 0.1% for the

JHEP12(2010)060

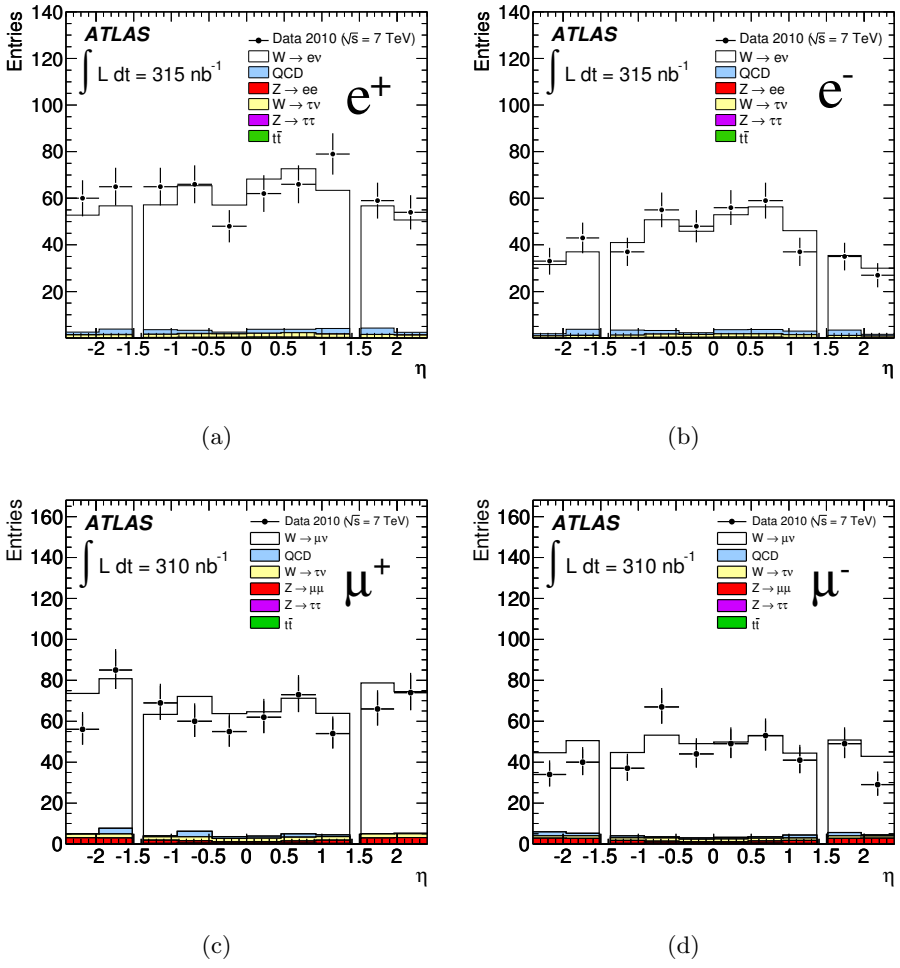

Figure 15. Pseudorapidity distributions of e^+ (a), e^- (b), μ^+ (c) and μ^- (d) candidates satisfying all W requirements (see section 5.4). The data are compared to the Monte Carlo simulation, broken down into the signal and various background components. The Monte-Carlo distributions are normalised to the integrated luminosity of the data, as described in section 5.2. The values of the integrated luminosities for the two channels have uncertainties of ±11%, see section 3.

barrel and 1.3% for the end-cap regions and has been implicitly taken into account in the C_W corrections applied. For muons, the charge misidentification is found to be negligible.

The results obtained for the different η bins as well as after integration over the full pseudorapidity interval are listed in table 15 together with their statistical and systematic uncertainties. Consistent results are obtained for the two lepton channels. The precision of the measurements is limited for both channels by the statistical uncertainties.

For the electron channel, major contributions to the systematic uncertainties result from uncertainties on the electron identification and charge misidentification (±2.0%), electron energy scale (±1.0%), and on the QCD (±1.5%) and electroweak backgrounds (±0.5%). The systematic uncertainty on the QCD background is much larger than that on

JHEP12(2010)060

η range	Electron channel A_e	Muon channel A_μ	Combination A_ℓ
$\lvert\eta\rvert < 1.37$	$0.15 \pm 0.04 \pm 0.00$	$0.12 \pm 0.04 \pm 0.01$	$0.14 \pm 0.03 \pm 0.01$
$1.52 < \lvert\eta\rvert < 2.4$	$0.29 \pm 0.05 \pm 0.02$	$0.32 \pm 0.05 \pm 0.02$	$0.31 \pm 0.04 \pm 0.01$
$\lvert\eta\rvert < 1.37$ and $1.52 < \lvert\eta\rvert < 2.4$	$0.21 \pm 0.03 \pm 0.01$	$0.19 \pm 0.03 \pm 0.01$	$0.20 \pm 0.02 \pm 0.01$

Table 15. The measured lepton asymmetries integrated over the full pseudorapidity range, as well as separately for the barrel and end-cap regions. The quoted uncertainties are statistical (first) and systematic (second).

the electroweak background because of the larger relative uncertainty on the QCD background. In addition, potential distortions of the asymmetry are much larger from the QCD background than from the electroweak background, which predominantly consists of $W \to \tau\nu$ decays exhibiting an asymmetry similar to that expected in $W \to e\nu$ decays. The systematic uncertainty on the electron identification and misidentification is determined by comparing the variation of the asymmetry as a function of identification requirements in data to the same variation as predicted by Monte Carlo simulation.

For the muon channel, the systematic uncertainty is derived from uncertainties on the muon momentum scale and resolution ($\pm 5.0\%$), from uncertainties on the trigger efficiency ($\pm 2.7\%$), and on the QCD ($\pm 0.8\%$) and electroweak backgrounds ($\pm 0.5\%$). The muon momentum scale and resolution may depend significantly on charge. Scale and resolution uncertainties on the muon momentum measurement are considered to be anti-correlated, since they could affect in opposite directions the bending of tracks of opposite sign.

The measured lepton asymmetries are displayed in figure 16 as a function of $|\eta|$ and compared to theoretical predictions obtained with NLO calculations, namely MC@NLO [29] and DYNNLO [59] which have been interfaced to various PDF parameterisations of the respective order. The parton distribution functions MSTW 08 [51], CTEQ 6.6 [49] and HERAPDF 1.0 [50] were used. The predictions of these calculations for the integrated asymmetry ($|\eta| < 1.37$ and $1.52 < |\eta| < 2.4$) are $0.218^{+0.008}_{-0.009}$ (MC@NLO, CTEQ 6.6), 0.202 ± 0.019 (MC@NLO, HERAPDF 1.0), and $0.184^{+0.011}_{-0.012}$ (DYNNLO, MSTW 08). The bands shown for the theoretical predictions display the uncertainties extracted from a variation of the error eigenvector sets of the PDFs at the 90% C.L. limit. Within the large uncertainties, the theoretical predictions agree with the present measurements. However, the data do not provide sufficient separation power to discriminate between various models.

9 Summary

The ATLAS collaboration presents first measurements of the $W \to \ell\nu$ and $Z \to \ell\ell$ production cross sections in proton-proton collisions at $\sqrt{s} = 7\,\text{TeV}$. The results are based on data corresponding to an integrated luminosity of approximately 320 nb^{-1}. The total inclusive W-boson production cross sections times the leptonic branching ratios for the combined

JHEP12(2010)060

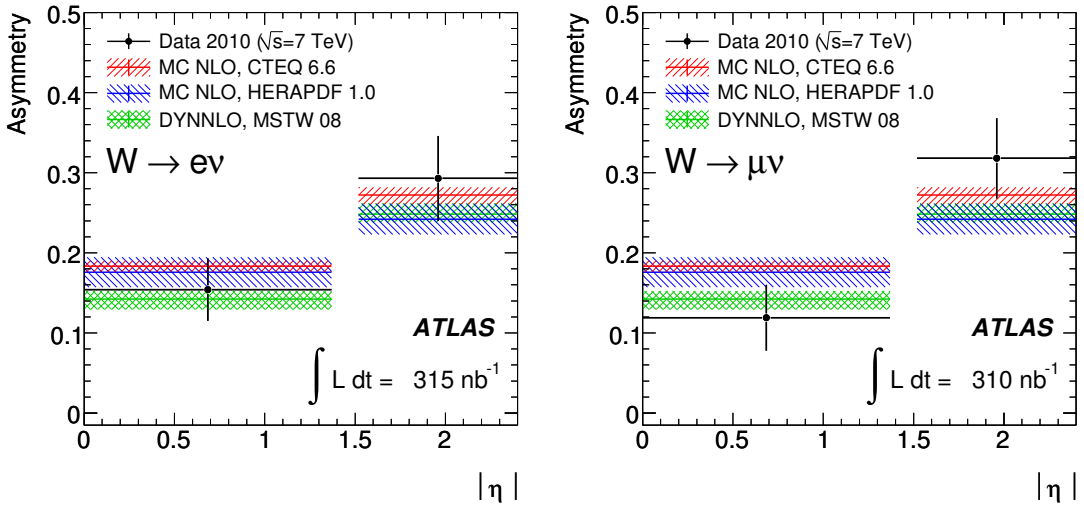

(a) (b)

Figure 16. Lepton charge asymmetries for the electron (a) and muon (b) channels. Superimposed are several theoretical predictions (see text). The bands show the uncertainties extracted from a variation of the error eigenvector sets of the PDFs at the 90% C.L. limit. The values of the integrated luminosities for the two channels have uncertainties of ±11%, see section 3.

electron-muon channels are measured to be:

$$\begin{aligned}
\sigma^{\text{tot}}_{W^+} \cdot \text{BR}(\text{W} \to \ell\nu) &= 5.93 \pm 0.17\,(\text{stat}) \pm 0.30\,(\text{syst}) \pm 0.65\,(\text{lumi})\ \text{nb}, \\
\sigma^{\text{tot}}_{W^-} \cdot \text{BR}(\text{W} \to \ell\nu) &= 4.00 \pm 0.15\,(\text{stat}) \pm 0.20\,(\text{syst}) \pm 0.44\,(\text{lumi})\ \text{nb}, \\
\sigma^{\text{tot}}_{W} \cdot \text{BR}(\text{W} \to \ell\nu) &= 9.96 \pm 0.23\,(\text{stat}) \pm 0.50\,(\text{syst}) \pm 1.10\,(\text{lumi})\ \text{nb}.
\end{aligned}$$

For the Z/γ^* production cross section, measured in the mass range $66 < m_{\ell\ell} < 116\,\text{GeV}$, the result for the combination of the electron and muon decay channels is:

$$\sigma^{\text{tot}}_{Z/\gamma^*} \cdot \text{BR}(Z/\gamma^* \to \ell\ell) = 0.82 \pm 0.06\,(\text{stat}) \pm 0.05\,(\text{syst}) \pm 0.09\,(\text{lumi})\ \text{nb}.$$

The ratio of the W to Z-boson cross sections is measured to be

$$R_{W/Z} = 11.7 \pm 0.9\ (\text{stat}) \pm 0.4\ (\text{syst}).$$

Theoretical predictions, based on NNLO QCD calculations, are in good agreement with all measurements.

In addition, a measurement of the charge asymmetry of W-boson production is presented for the first time in proton-proton collisions at $\sqrt{s} = 7\,\text{TeV}$. The charge asymmetry, defined via the fiducial cross sections, integrated over the acceptance region $|\eta| < 1.37$ and $1.52 < |\eta| < 2.4$, is measured to be

$$A_\ell = \frac{(\sigma^{\text{fid}}_{W^+} - \sigma^{\text{fid}}_{W^-})}{(\sigma^{\text{fid}}_{W^+} + \sigma^{\text{fid}}_{W^-})} = 0.20 \pm 0.02\ (\text{stat}) \pm 0.01\ (\text{syst}).$$

JHEP12(2010)060

This measurement demonstrates clearly the expected charge asymmetry for W boson production in proton-proton collisions. Theoretical predictions are in agreement with this measurement, which, at present, is still statistically limited.

Despite the rather low integrated luminosity used in the analyses presented here, the accuracy of the cross-section measurements is, however, already dominated by systematic uncertainties, most prominently by the luminosity uncertainty of $\pm 11\%$ and to a lesser degree by the experimental uncertainties on lepton identification. The latter uncertainties are expected to improve significantly with more data. In particular, high-statistics Z-boson samples can be used to perform measurements of efficiencies and to reduce the corresponding uncertainties. The luminosity uncertainty is dominated by the $\pm 10\%$ uncertainty on the beam currents in the machine and is also expected to improve with more precise and dedicated measurements.

Acknowledgments

We wish to thank CERN for the efficient commissioning and operation of the LHC during this initial high-energy data-taking period as well as the support staff from our institutions without whom ATLAS could not be operated efficiently.

We acknowledge the support of ANPCyT, Argentina; YerPhI, Armenia; ARC, Australia; BMWF, Austria; ANAS, Azerbaijan; SSTC, Belarus; CNPq and FAPESP, Brazil; NSERC, NRC and CFI, Canada; CERN; CONICYT, Chile; CAS, MOST and NSFC, China; COLCIENCIAS, Colombia; MEYS (MSMT), MPO and CCRC, Czech Republic; DNRF, DNSRC and Lundbeck Foundation, Denmark; ARTEMIS, European Union; IN2P3-CNRS, CEA-DSM/IRFU, France; GNAS, Georgia; BMBF, DFG, HGF, MPG and AvH Foundation, Germany; GSRT, Greece; ISF, MINERVA, GIF, DIP and Benoziyo Center, Israel; INFN, Italy; MEXT and JSPS, Japan; CNRST, Morocco; FOM and NWO, Netherlands; RCN, Norway; MNiSW, Poland; GRICES and FCT, Portugal; MERYS (MECTS), Romania; MES of Russia and ROSATOM, Russian Federation; JINR; MSTD, Serbia; MSSR, Slovakia; ARRS and MVZT, Slovenia; DST/NRF, South Africa; MICINN, Spain; SRC and Wallenberg Foundation, Sweden; SER, SNSF and Cantons of Bern and Geneva, Switzerland; NSC, Taiwan; TAEK, Turkey; STFC, the Royal Society and Leverhulme Trust, United Kingdom; DOE and NSF, United States of America.

The crucial computing support from all WLCG partners is acknowledged gratefully, in particular from CERN and the ATLAS Tier-1 facilities at TRIUMF (Canada), NDGF (Denmark, Norway, Sweden), CC-IN2P3 (France), KIT/GridKA (Germany), INFN-CNAF (Italy), NL-T1 (Netherlands), PIC (Spain), ASGC (Taiwan), RAL (UK) and BNL (USA) and in the Tier-2 facilities worldwide.

JHEP12(2010)060

References

[1] J. Kubar-Andre and F.E. Paige, *Gluon Corrections to the Drell-Yan Model*, *Phys. Rev.* **D 19** (1979) 221 [SPIRES].

[2] G. Altarelli, R.K. Ellis and G. Martinelli, *Large Perturbative Corrections to the Drell-Yan Process in QCD*, *Nucl. Phys.* **B 157** (1979) 461 [SPIRES].

[3] J. Kubar, M. Le Bellac, J.L. Meunier and G. Plaut, *QCD Corrections to the Drell-Yan Mechanism and the Pion Structure Function*, *Nucl. Phys.* **B 175** (1980) 251 [SPIRES].

[4] P.J. Rijken and W.L. van Neerven, *Order α_s^2 contributions to the Drell-Yan cross-section at fixed target energies*, *Phys. Rev.* **D 51** (1995) 44 [hep-ph/9408366] [SPIRES].

[5] R. Hamberg, W.L. van Neerven and T. Matsuura, *A Complete calculation of the order α_s^2 correction to the Drell-Yan K factor*, *Nucl. Phys.* **B 359** (1991) 343 [*Erratum ibid.* **B 644** (2002) 403] [SPIRES].

[6] W.L. van Neerven and E.B. Zijlstra, *The O (α_s^2) corrected Drell-Yan K factor in the DIS and MS scheme*, *Nucl. Phys.* **B 382** (1992) 11 [*Erratum ibid.* **B 680** (2004) 513] [SPIRES].

[7] R.V. Harlander and W.B. Kilgore, *Next-to-next-to-leading order Higgs production at hadron colliders*, *Phys. Rev. Lett.* **88** (2002) 201801 [hep-ph/0201206] [SPIRES].

[8] K. Melnikov and F. Petriello, *Electroweak gauge boson production at hadron colliders through $O(\alpha_s^2)$*, *Phys. Rev.* **D 74** (2006) 114017 [hep-ph/0609070] [SPIRES].

[9] K. Melnikov and F. Petriello, *The W boson production cross section at the LHC through $O(\alpha_s^2)$*, *Phys. Rev. Lett.* **96** (2006) 231803 [hep-ph/0603182] [SPIRES].

[10] UA1 collaboration, C. Albajar et al., *Intermediate Vector Boson Cross-Sections at the CERN Super Proton Synchrotron Collider and the Number of Neutrino Types*, *Phys. Lett.* **B 198** (1987) 271 [SPIRES].

[11] UA2 collaboration, J. Alitti et al., *A Measurement of the W and Z production cross-sections and a determination of Γ_W at the CERN $\bar{p}p$ collider*, *Phys. Lett.* **B 276** (1992) 365 [SPIRES].

[12] CDF collaboration, F. Abe et al., *Measurement of $\sigma \cdot B(W \to e\nu)$ and $\sigma \cdot B(Z^0 \to e^+e^-)$ in $p\bar{p}$ collisions at $\sqrt{s} = 1.8$ TeV*, *Phys. Rev. Lett.* **76** (1996) 3070 [hep-ex/9509010] [SPIRES].

[13] CDF collaboration, F. Abe et al., *Measurement of Z^0 and Drell-Yan production cross section using dimuons in $\bar{p}p$ collisions at $\sqrt{s} = 1.8$ TeV*, *Phys. Rev.* **D 59** (1999) 052002 [SPIRES].

[14] CDF collaboration, A. Abulencia et al., *Measurements of Inclusive W and Z Cross Sections in $p\bar{p}$ Collisions at $\sqrt{s} = 1.96$ TeV*, *J. Phys.* **G 34** (2007) 2457 [hep-ex/0508029] [SPIRES].

[15] D0 collaboration, B. Abbott et al., *Extraction of the width of the W boson from measurements of $\sigma(p\bar{p} \to W + X) \times B(W \to e\nu)$ and $\sigma(p\bar{p} \to Z + X) \times B(Z \to ee)$ and their ratio*, *Phys. Rev.* **D 61** (2000) 072001 [hep-ex/9906025] [SPIRES].

[16] D0 collaboration, *Measurement of the Cross Section for W and Z Production to Electron Final States with the DØ Detector at $\sqrt{s} = 1.96$ TeV*, D0 conference notes: 4403-CONF.

[17] D0 collaboration, *Measurement of the Cross-section for Inclusive W Production in the Muon Channel at $\sqrt{s} = 1.96$ TeV Using the DØ Detector*, D0 conference notes: 4750-CONF.

[18] PHENIX collaboration, A. Adare et al., *Cross Section and Parity Violating Spin Asymmetries of $W^{\pm}$ Boson Production in Polarized p+p Collisions at $\sqrt{s} = 500$ GeV*, arXiv:1009.0505 [SPIRES].

[19] STAR collaboration, M.M. Aggarwal et al., *Measurement of the parity-violating longitudinal single-spin asymmetry for $W^{\pm}$ boson production in polarized proton-proton collisions at $\sqrt{s} = 500$ GeV*, arXiv:1009.0326 [SPIRES].

JHEP12(2010)060

[20] L. Evans, and P. Bryant eds., *LHC Machine*, 2008 *JINST* **3** S08001 [SPIRES].

[21] ATLAS collaboration, G. Aad et al., *The ATLAS Experiment at the CERN Large Hadron Collider*, 2008 *JINST* **3** S08003 [SPIRES].

[22] ATLAS collaboration, *Readiness of the ATLAS Liquid Argon Calorimeter for LHC Collisions*, *Eur. Phys. J. C* (2010).

[23] S. van der Meer, *Calibration of the effective beam height in the ISR*, CERN-ISR-PO-68-31 (1968).

[24] ATLAS collaboration, *Luminosity Determination using the ATLAS Detector*, ATLAS conference note: ATLAS-CONF-2010-060.

[25] GEANT4 collaboration, S. Agostinelli et al., *GEANT4: A simulation toolkit*, *Nucl. Instrum. Meth.* **A 506** (2003) 250 [SPIRES].

[26] ATLAS collaboration, *The ATLAS Simulation Infrastructure*, arXiv:1005.4568 [SPIRES].

[27] Particle Data Group collaboration, K. Nakamura et al., *Review of particle physics*, *J. Phys.* **G 37** (2010) 075021 [SPIRES].

[28] T. Sjöstrand, S. Mrenna and P.Z. Skands, *PYTHIA 6.4 Physics and Manual*, *JHEP* **05** (2006) 026 [hep-ph/0603175] [SPIRES].

[29] S. Frixione and B.R. Webber, *Matching NLO QCD computations and parton shower simulations*, *JHEP* **06** (2002) 029 [hep-ph/0204244] [SPIRES].

[30] S. Frixione, P. Nason and B.R. Webber, *Matching NLO QCD and parton showers in heavy flavour production*, *JHEP* **08** (2003) 007 [hep-ph/0305252] [SPIRES].

[31] R. Bonciani, S. Catani, M.L. Mangano and P. Nason, *NLL resummation of the heavy-quark hadroproduction cross-section*, *Nucl. Phys.* **B 529** (1998) 424 [hep-ph/9801375] [SPIRES].

[32] S. Moch and P. Uwer, *Theoretical status and prospects for top-quark pair production at hadron colliders*, *Phys. Rev.* **D 78** (2008) 034003 [arXiv:0804.1476] [SPIRES].

[33] M. Beneke, M. Czakon, P. Falgari, A. Mitov and C. Schwinn, *Threshold expansion of the $gg(q\bar{q}) \to Q\bar{Q} + X$ cross section at α_s^4*, *Phys. Lett.* **B 690** (2010) 483 [arXiv:0911.5166] [SPIRES].

[34] S. Frixione, P. Nason and C. Oleari, *Matching NLO QCD computations with Parton Shower simulations: the POWHEG method*, *JHEP* **11** (2007) 070 [arXiv:0709.2092] [SPIRES].

[35] ATLAS collaboration, G. Aad et al., *Charged-particle multiplicities in pp interactions at $\sqrt{s} = 900$ GeV measured with the ATLAS detector at the LHC*, *Phys. Lett.* **B 688** (2010) 21 [arXiv:1003.3124] [SPIRES].

[36] T. Cornelissen et al., *Concepts, Design and Implementation of the ATLAS New Tracking (NEWT)*, ATLAS note: ATLAS-SOFT-PUB-2007-007.

[37] ATLAS collaboration, *Electron and photon reconstruction and identification in ATLAS: expected performance at high energy and results at $\sqrt{s} = 900$ GeV*, ATLAS conference note: ATLAS-CONF-2010-005.

[38] ATLAS collaboration, G. Aad et al., *Expected Performance of the ATLAS Experiment - Detector, Trigger and Physics*, CERN-OPEN-2008-020 [arXiv:0901.0512] [SPIRES].

[39] ATLAS collaboration, *Muon Reconstruction Performance*, ATLAS conference note: ATLAS-CONF-2010-064.

[40] W. Lampl et al., *Calorimeter Clustering Algorithms: Description and Performance*, ATLAS note: ATL-LARG-PUB-2008-002.

JHEP12(2010)060

[41] T. Barillari et al., *Local Hadron Calibration*, ATLAS note: ATL-LARG-PUB-2009-001.

[42] ATLAS collaboration, *ATLAS Calorimeter Response to Single Isolated Hadrons and Estimation of the Calorimeter Jet Scale Uncertainty*, ATLAS conference note: ATLAS-CONF-2010-052.

[43] ATLAS collaboration, *Data-Quality Requirements and Event Cleaning for Jets and Missing Transverse Energy Reconstruction with the ATLAS Detector in Proton-Proton Collisions at a Center-of-Mass Energy of $\sqrt{s} = 7$ TeV*, ATLAS conference note: ATLAS-CONF-2010-038.

[44] K. Lohwasser, *The W Charge Asymmetry: Measurement of the Proton Structure with the ATLAS detector*, PhD thesis, University of Oxford (2010), http://cdsweb.cern.ch/record/1265829.

[45] G. Nanava, Q. Xu and Z. Was, *Matching NLO parton shower matrix element with exact phase space: case of $W \to l\nu(\gamma)$ and $\gamma^* \to \pi^+\pi^-(\gamma)$*, arXiv:0906.4052 [SPIRES].

[46] P. Golonka and Z. Was, *PHOTOS Monte Carlo: A Precision tool for QED corrections in Z and W decays*, *Eur. Phys. J.* **C 45** (2006) 97 [hep-ph/0506026] [SPIRES].

[47] A. Sherstnev and R.S. Thorne, *Parton Distributions for LO Generators*, *Eur. Phys. J.* **C 55** (2008) 553 [arXiv:0711.2473] [SPIRES].

[48] ATLAS collaboration, *ATLAS Monte Carlo tunes for MC09*, ATLAS public note: ATL-PHYS-PUB-2010-002.

[49] P.M. Nadolsky et al., *Implications of CTEQ global analysis for collider observables*, *Phys. Rev.* **D 78** (2008) 013004 [arXiv:0802.0007] [SPIRES].

[50] H1 and ZEUS collaboration, F.D. Aaron et al., *Combined Measurement and QCD Analysis of the Inclusive ep Scattering Cross Sections at HERA*, *JHEP* **01** (2010) 109 [arXiv:0911.0884] [SPIRES].

[51] A.D. Martin, W.J. Stirling, R.S. Thorne and G. Watt, *Parton distributions for the LHC*, *Eur. Phys. J.* **C 63** (2009) 189 [arXiv:0901.0002] [SPIRES].

[52] CDF collaboration, F. Abe et al., *Measurement of the lepton charge asymmetry in W boson decays produced in $p\bar{p}$ collisions*, *Phys. Rev. Lett.* **81** (1998) 5754 [hep-ex/9809001] [SPIRES].

[53] H.-L. Lai et al., *New parton distributions for collider physics*, *Phys. Rev.* **D 82** (2010) 074024 [arXiv:1007.2241] [SPIRES].

[54] J. Pumplin et al., *New generation of parton distributions with uncertainties from global QCD analysis*, *JHEP* **07** (2002) 012 [hep-ph/0201195] [SPIRES].

[55] E.L. Berger, F. Halzen, C.S. Kim and S. Willenbrock, *Weak boson production at Tevatron energies*, *Phys. Rev.* **D 40** (1989) 83 [SPIRES].

[56] ZEUS collaboration, S. Chekanov et al., *Measurement of charged current deep inelastic scattering cross sections with a longitudinally polarised electron beam at HERA*, *Eur. Phys. J.* **C 61** (2009) 223 [arXiv:0812.4620] [SPIRES].

[57] ZEUS collaboration, S. Chekanov et al., *Measurement of high-Q^2 neutral current deep inelastic e^-p scattering cross sections with a longitudinally polarised electron beam at HERA*, *Eur. Phys. J.* **C 62** (2009) 625 [arXiv:0901.2385] [SPIRES].

[58] H1 collaboration, C. Adloff et al., *Measurement and QCD analysis of neutral and charged current cross sections at HERA*, *Eur. Phys. J.* **C 30** (2003) 1 [hep-ex/0304003] [SPIRES].

[59] S. Catani and M. Grazzini, *An NNLO subtraction formalism in hadron collisions and its application to Higgs boson production at the LHC*, *Phys. Rev. Lett.* **98** (2007) 222002 [hep-ph/0703012] [SPIRES].

JHEP12(2010)060

The ATLAS collaboration

G. Aad[48], B. Abbott[111], J. Abdallah[11], A.A. Abdelalim[49], A. Abdesselam[118], O. Abdinov[10], B. Abi[112], M. Abolins[88], H. Abramowicz[153], H. Abreu[115], E. Acerbi[89a,89b], B.S. Acharya[164a,164b], M. Ackers[20], D.L. Adams[24], T.N. Addy[56], J. Adelman[175], M. Aderholz[99], S. Adomeit[98], C. Adorisio[36a,36b], P. Adragna[75], T. Adye[129], S. Aefsky[22], J.A. Aguilar-Saavedra[124b,a], M. Aharrouche[81], S.P. Ahlen[21], F. Ahles[48], A. Ahmad[148], H. Ahmed[2], M. Ahsan[40], G. Aielli[133a,133b], T. Akdogan[18a], T.P.A. Åkesson[79], G. Akimoto[155], A.V. Akimov [94], A. Aktas[48], M.S. Alam[1], M.A. Alam[76], S. Albrand[55], M. Aleksa[29], I.N. Aleksandrov[65], M. Aleppo[89a,89b], F. Alessandria[89a], C. Alexa[25a], G. Alexander[153], G. Alexandre[49], T. Alexopoulos[9], M. Alhroob[20], M. Aliev[15], G. Alimonti[89a], J. Alison[120], M. Aliyev[10], P.P. Allport[73], S.E. Allwood-Spiers[53], J. Almond[82], A. Aloisio[102a,102b], R. Alon[171], A. Alonso[79], J. Alonso[14], M.G. Alviggi[102a,102b], K. Amako[66], P. Amaral[29], G. Ambrosio[89a,b], C. Amelung[22], V.V. Ammosov[128], A. Amorim[124a,c], G. Amorós[167], N. Amram[153], C. Anastopoulos[139], T. Andeen[34], C.F. Anders[20], K.J. Anderson[30], A. Andreazza[89a,89b], V. Andrei[58a], M-L. Andrieux[55], X.S. Anduaga[70], A. Angerami[34], F. Anghinolfi[29], N. Anjos[124a], A. Annovi[47], A. Antonaki[8], M. Antonelli[47], S. Antonelli[19a,19b], J. Antos[144b], B. Antunovic[41], F. Anulli[132a], S. Aoun[83], R. Apolle[118], G. Arabidze[88], I. Aracena[143], Y. Arai[66], A.T.H. Arce[44], J.P. Archambault[28], S. Arfaoui[29,d], J-F. Arguin[14], T. Argyropoulos[9], E. Arik[18a,*], M. Arik[18a], A.J. Armbruster[87], K.E. Arms[109], S.R. Armstrong[24], O. Arnaez[4], C. Arnault[115], A. Artamonov[95], D. Arutinov[20], M. Asai[143], S. Asai[155], R. Asfandiyarov[172], S. Ask[27], B. Åsman[146a,146b], D. Asner[28], L. Asquith[5], K. Assamagan[24], A. Astbury[169], A. Astvatsatourov[52], G. Atoian[175], B. Aubert[4], B. Auerbach[175], E. Auge[115], K. Augsten[127], M. Aurousseau[4], N. Austin[73], G. Avolio[163], R. Avramidou[9], D. Axen[168], C. Ay[54], G. Azuelos[93,e], Y. Azuma[155], M.A. Baak[29], G. Baccaglioni[89a], C. Bacci[134a,134b], A.M. Bach[14], H. Bachacou[136], K. Bachas[29], G. Bachy[29], M. Backes[49], E. Badescu[25a], P. Bagnaia[132a,132b], Y. Bai[32a], D.C. Bailey [158], T. Bain[158], J.T. Baines[129], O.K. Baker[175], M.D. Baker[24], S Baker[77], F. Baltasar Dos Santos Pedrosa[29], E. Banas[38], P. Banerjee[93], Sw. Banerjee[169], D. Banfi[89a,89b], A. Bangert[137], V. Bansal[169], S.P. Baranov[94], S. Baranov[65], A. Barashkou[65], A. Barbaro Galtieri[14], T. Barber[27], E.L. Barberio[86], D. Barberis[50a,50b], M. Barbero[20], D.Y. Bardin[65], T. Barillari[99], M. Barisonzi[174], T. Barklow[143], N. Barlow[27], B.M. Barnett[129], R.M. Barnett[14], A. Baroncelli[134a], M. Barone [47], A.J. Barr[118], F. Barreiro[80], J. Barreiro Guimarães da Costa[57], P. Barrillon[115], R. Bartoldus[143], D. Bartsch[20], R.L. Bates[53], L. Batkova[144a], J.R. Batley[27], A. Battaglia[16], M. Battistin[29], G. Battistoni[89a], F. Bauer[136], H.S. Bawa[143], M. Bazalova[125], B. Beare[158], T. Beau[78], P.H. Beauchemin[118], R. Beccherle[50a], P. Bechtle[41], G.A. Beck[75], H.P. Beck[16], M. Beckingham[48], K.H. Becks[174], A.J. Beddall[18c], A. Beddall[18c], V.A. Bednyakov[65], C. Bee[83], M. Begel[24], S. Behar Harpaz[152], P.K. Behera[63], M. Beimforde[99], C. Belanger-Champagne[166], B. Belhorma[55], P.J. Bell[49], W.H. Bell[49], G. Bella[153], L. Bellagamba[19a], F. Bellina[29], G. Bellomo[89a,89b], M. Bellomo[119a], A. Belloni[57], K. Belotskiy[96], O. Beltramello[29], S. Ben Ami[152], O. Benary[153], D. Benchekroun[135a], C. Benchouk[83], M. Bendel[81], B.H. Benedict[163], N. Benekos[165], Y. Benhammou[153], G.P. Benincasa[124a], D.P. Benjamin[44], M. Benoit[115], J.R. Bensinger[22], K. Benslama[130], S. Bentvelsen[105], M. Beretta[47], D. Berge[29], E. Bergeaas Kuutmann[41], N. Berger[4], F. Berghaus[169], E. Berglund[49], J. Beringer[14], K. Bernardet[83], P. Bernat[115], R. Bernhard[48], C. Bernius[77], T. Berry[76], A. Bertin[19a,19b], F. Bertinelli[29], F. Bertolucci[122a,122b], M.I. Besana[89a,89b], N. Besson[136], S. Bethke[99], W. Bhimji[45], R.M. Bianchi[48], M. Bianco[72a,72b], O. Biebel[98], J. Biesiada[14], M. Biglietti[132a,132b], H. Bilokon[47], M. Binder [98], M. Bindi[19a,19b], S. Binet[115], A. Bingul[18c], C. Bini[132a,132b], C. Biscarat[177], R. Bischof[62], U. Bitenc[48], K.M. Black[57], R.E. Blair[5], J-B Blanchard[115], G. Blanchot[29], C. Blocker[22], J. Blocki[38], A. Blondel[49], W. Blum[81], U. Blumenschein[54], C. Boaretto[132a,132b],

JHEP12(2010)060

G.J. Bobbink[105], V.B. Bobrovnikov[107], A. Bocci[44], D. Bocian[38], R. Bock[29], C.R. Boddy[118], M. Boehler[41], J. Boek[174], N. Boelaert[79], S. Böser[77], J.A. Bogaerts[29], A. Bogdanchikov[107], A. Bogouch[90,*], C. Bohm[146a], J. Bohm[125], V. Boisvert[76], T. Bold[163,f], V. Boldea[25a], V.G. Bondarenko[96], M. Bondioli[163], M. Boonekamp[136], G. Boorman[76], C.N. Booth[139], P. Booth[139], J.R.A. Booth[17], S. Bordoni[78], C. Borer[16], A. Borisov[128], G. Borissov[71], I. Borjanovic[12a], S. Borroni[132a,132b], K. Bos[105], D. Boscherini[19a], M. Bosman[11], H. Boterenbrood[105], D. Botterill[129], J. Bouchami[93], J. Boudreau[123], E.V. Bouhova-Thacker[71], C. Boulahouache[123], C. Bourdarios[115], A. Boveia[30], J. Boyd[29], I.R. Boyko[65], N.I. Bozhko[128], I. Bozovic-Jelisavcic[12b], S. Braccini[47], J. Bracinik[17], A. Braem[29], E. Brambilla[72a,72b], P. Branchini[134a], G.W. Brandenburg[57], A. Brandt[7], G. Brandt[41], O. Brandt[54], U. Bratzler[156], B. Brau[84], J.E. Brau[114], H.M. Braun[174], B. Brelier[158], J. Bremer[29], R. Brenner[166], S. Bressler[152], D. Breton[115], N.D. Brett[118], P.G. Bright-Thomas[17], D. Britton[53], F.M. Brochu[27], I. Brock[20], R. Brock[88], T.J. Brodbeck[71], E. Brodet[153], F. Broggi[89a], C. Bromberg[88], G. Brooijmans[34], W.K. Brooks[31b], G. Brown[82], E. Brubaker[30], P.A. Bruckman de Renstrom[38], D. Bruncko[144b], R. Bruneliere[48], S. Brunet[61], A. Bruni[19a], G. Bruni[19a], M. Bruschi[19a], T. Buanes[13], F. Bucci[49], J. Buchanan[118], N.J. Buchanan[2], P. Buchholz[141], R.M. Buckingham[118], A.G. Buckley[45], I.A. Budagov[65], B. Budick[108], V. Büscher[81], L. Bugge[117], D. Buira-Clark[118], E.J. Buis[105], O. Bulekov[96], M. Bunse[42], T. Buran[117], H. Burckhart[29], S. Burdin[73], T. Burgess[13], S. Burke[129], E. Busato[33], P. Bussey[53], C.P. Buszello[166], F. Butin[29], B. Butler[143], J.M. Butler[21], C.M. Buttar[53], J.M. Butterworth[77], T. Byatt[77], J. Caballero[24], S. Cabrera Urbán[167], M. Caccia[89a,89b,g], D. Caforio[19a,19b], O. Cakir[3a], P. Calafiura[14], G. Calderini[78], P. Calfayan[98], R. Calkins[106], L.P. Caloba[23a], R. Caloi[132a,132b], D. Calvet[33], S. Calvet[33], A. Camard[78], P. Camarri[133a,133b], M. Cambiaghi[119a,119b], D. Cameron[117], J. Cammin[20], S. Campana[29], M. Campanelli[77], V. Canale[102a,102b], F. Canelli[30], A. Canepa[159a], J. Cantero[80], L. Capasso[102a,102b], M.D.M. Capeans Garrido[29], I. Caprini[25a], M. Caprini[25a], M. Caprio[102a,102b], D. Capriotti[99], M. Capua[36a,36b], R. Caputo[148], C. Caramarcu[25a], R. Cardarelli[133a], T. Carli[29], G. Carlino[102a], L. Carminati[89a,89b], B. Caron[2,h], S. Caron[48], C. Carpentieri[48], G.D. Carrillo Montoya[172], S. Carron Montero[158], A.A. Carter[75], J.R. Carter[27], J. Carvalho[124a,i], D. Casadei[108], M.P. Casado[11], M. Cascella[122a,122b], C. Caso[50a,50b,*], A.M. Castaneda Hernandez[172], E. Castaneda-Miranda[172], V. Castillo Gimenez[167], N.F. Castro[124b,a], G. Cataldi[72a], F. Cataneo[29], A. Catinaccio[29], J.R. Catmore[71], A. Cattai[29], G. Cattani[133a,133b], S. Caughron[34], D. Cauz[164a,164c], A. Cavallari[132a,132b], P. Cavalleri[78], D. Cavalli[89a], M. Cavalli-Sforza[11], V. Cavasinni[122a,122b], A. Cazzato[72a,72b], F. Ceradini[134a,134b], C. Cerna[83], A.S. Cerqueira[23a], A. Cerri[29], L. Cerrito[75], F. Cerutti[47], M. Cervetto[50a,50b], S.A. Cetin[18b], F. Cevenini[102a,102b], A. Chafaq[135a], D. Chakraborty[106], K. Chan[2], J.D. Chapman[27], J.W. Chapman[87], E. Chareyre[78], D.G. Charlton[17], V. Chavda[82], S. Cheatham[71], S. Chekanov[5], S.V. Chekulaev[159a], G.A. Chelkov[65], H. Chen[24], L. Chen[2], S. Chen[32c], T. Chen[32c], X. Chen[172], S. Cheng[32a], A. Cheplakov[65], V.F. Chepurnov[65], R. Cherkaoui El Moursli[135d], V. Tcherniatine[24], D. Chesneanu[25a], E. Cheu[6], S.L. Cheung[158], L. Chevalier[136], F. Chevallier[136], V. Chiarella[47], G. Chiefari[102a,102b], L. Chikovani[51], J.T. Childers[58a], A. Chilingarov[71], G. Chiodini[72a], M.V. Chizhov[65], G. Choudalakis[30], S. Chouridou[137], I.A. Christidi[77], A. Christov[48], D. Chromek-Burckhart[29], M.L. Chu[151], J. Chudoba[125], G. Ciapetti[132a,132b], A.K. Ciftci[3a], R. Ciftci[3a], D. Cinca[33], V. Cindro[74], M.D. Ciobotaru[163], C. Ciocca[19a,19b], A. Ciocio[14], M. Cirilli[87,j], M. Citterio[89a], A. Clark[49], P.J. Clark[45], W. Cleland[123], J.C. Clemens[83], B. Clement[55], C. Clement[146a,146b], R.W. Clifft[129], Y. Coadou[83], M. Cobal[164a,164c], A. Coccaro[50a,50b], J. Cochran[64], P. Coe[118], S. Coelli[89a], J. Coggeshall[165], E. Cogneras[177], C.D. Cojocaru[28], J. Colas[4], B. Cole[34], A.P. Colijn[105], C. Collard[115], N.J. Collins[17], C. Collins-Tooth[53], J. Collot[55], G. Colon[84], R. Coluccia[72a,72b],

JHEP12(2010)060

G. Comune[88], P. Conde Muiño[124a], E. Coniavitis[118], M.C. Conidi[11], M. Consonni[104], S. Constantinescu[25a], C. Conta[119a,119b], F. Conventi[102a,k], J. Cook[29], M. Cooke[34], B.D. Cooper[75], A.M. Cooper-Sarkar[118], N.J. Cooper-Smith[76], K. Copic[34], T. Cornelissen[50a,50b], M. Corradi[19a], S. Correard[83], F. Corriveau[85,l], A. Corso-Radu[163], A. Cortes-Gonzalez[165], G. Cortiana[99], G. Costa[89a], M.J. Costa[167], D. Costanzo[139], T. Costin[30], D. Côté[29], R. Coura Torres[23a], L. Courneyea[169], G. Cowan[76], C. Cowden[27], B.E. Cox[82], K. Cranmer[108], J. Cranshaw[5], M. Cristinziani[20], G. Crosetti[36a,36b], R. Crupi[72a,72b], S. Crépé-Renaudin[55], C. Cuenca Almenar[175], T. Cuhadar Donszelmann[139], S. Cuneo[50a,50b], M. Curatolo[47], C.J. Curtis[17], P. Cwetanski[61], H. Czirr[141], Z. Czyczula[175], S. D'Auria[53], M. D'Onofrio[73], A. D'Orazio[99], A. Da Rocha Gesualdi Mello[23a], P.V.M. Da Silva[23a], C Da Via[82], W. Dabrowski[37], A. Dahlhoff[48], T. Dai[87], C. Dallapiccola[84], S.J. Dallison[129,*], C.H. Daly[138], M. Dam[35], M. Dameri[50a,50b], D.S. Damiani[137], H.O. Danielsson[29], R. Dankers[105], D. Dannheim[99], V. Dao[49], G. Darbo[50a], G.L. Darlea[25b], C. Daum[105], J.P. Dauvergne [29], W. Davey[86], T. Davidek[126], N. Davidson[86], R. Davidson[71], M. Davies[93], A.R. Davison[77], E. Dawe[142], I. Dawson[139], J.W. Dawson[5,*], R.K. Daya[39], K. De[7], R. de Asmundis[102a], S. De Castro[19a,19b], P.E. De Castro Faria Salgado[24], S. De Cecco[78], J. de Graat[98], N. De Groot[104], P. de Jong[105], E. De La Cruz-Burelo[87], C. De La Taille[115], B. De Lotto[164a,164c], L. De Mora[71], L. De Nooij[105], M. De Oliveira Branco[29], D. De Pedis[132a], P. de Saintignon[55], A. De Salvo[132a], U. De Sanctis[164a,164c], A. De Santo[149], J.B. De Vivie De Regie[115], G. De Zorzi[132a,132b], S. Dean[77], G. Dedes[99], D.V. Dedovich[65], P.O. Defay[33], J. Degenhardt[120], M. Dehchar[118], M. Deile[98], C. Del Papa[164a,164c], J. Del Peso[80], T. Del Prete[122a,122b], A. Dell'Acqua[29], L. Dell'Asta[89a,89b], M. Della Pietra[102a,m], D. della Volpe[102a,102b], M. Delmastro[29], P. Delpierre[83], N. Delruelle[29], P.A. Delsart[55], C. Deluca[148], S. Demers[175], M. Demichev[65], B. Demirkoz[11], J. Deng[163], W. Deng[24], S.P. Denisov[128], C. Dennis[118], J.E. Derkaoui[135c], F. Derue[78], P. Dervan[73], K. Desch[20], P.O. Deviveiros[158], A. Dewhurst[129], B. DeWilde[148], S. Dhaliwal[158], R. Dhullipudi[24,n], A. Di Ciaccio[133a,133b], L. Di Ciaccio[4], A. Di Domenico[132a,132b], A. Di Girolamo[29], B. Di Girolamo[29], S. Di Luise[134a,134b], A. Di Mattia[88], R. Di Nardo[133a,133b], A. Di Simone[133a,133b], R. Di Sipio[19a,19b], M.A. Diaz[31a], M.M. Diaz Gomez[49], F. Diblen[18c], E.B. Diehl[87], H. Dietl[99], J. Dietrich[48], T.A. Dietzsch[58a], S. Diglio[115], K. Dindar Yagci[39], J. Dingfelder[20], C. Dionisi[132a,132b], P. Dita[25a], S. Dita[25a], F. Dittus[29], F. Djama[83], R. Djilkibaev[108], T. Djobava[51], M.A.B. do Vale[23a], A. Do Valle Wemans[124a], T.K.O. Doan[4], M. Dobbs[85], R. Dobinson [29,*], D. Dobos[42], E. Dobson[29], M. Dobson[163], J. Dodd[34], O.B. Dogan[18a,*], C. Doglioni[118], T. Doherty[53], Y. Doi[66], J. Dolejsi[126], I. Dolenc[74], Z. Dolezal[126], B.A. Dolgoshein[96], T. Dohmae[155], M. Donadelli[23b], M. Donega[120], J. Donini[55], J. Dopke[174], A. Doria[102a], A. Dos Anjos[172], M. Dosil[11], A. Dotti[122a,122b], M.T. Dova[70], J.D. Dowell[17], A. Doxiadis[105], A.T. Doyle[53], Z. Drasal[126], J. Drees[174], N. Dressnandt[120], H. Drevermann[29], C. Driouichi[35], M. Dris[9], J.G. Drohan[77], J. Dubbert[99], T. Dubbs[137], S. Dube[14], E. Duchovni[171], G. Duckeck[98], A. Dudarev[29], F. Dudziak[115], M. Dührssen [29], I.P. Duerdoth[82], L. Duflot[115], M-A. Dufour[85], M. Dunford[29], H. Duran Yildiz[3b], A. Dushkin[22], R. Duxfield[139], M. Dwuznik[37], F. Dydak [29], D. Dzahini[55], M. Düren[52], W.L. Ebenstein[44], J. Ebke[98], S. Eckert[48], S. Eckweiler[81], K. Edmonds[81], C.A. Edwards[76], I. Efthymiopoulos[49], K. Egorov[61], W. Ehrenfeld[41], T. Ehrich[99], T. Eifert[29], G. Eigen[13], K. Einsweiler[14], E. Eisenhandler[75], T. Ekelof[166], M. El Kacimi[4], M. Ellert[166], S. Elles[4], F. Ellinghaus[81], K. Ellis[75], N. Ellis[29], J. Elmsheuser[98], M. Elsing[29], R. Ely[14], D. Emeliyanov[129], R. Engelmann[148], A. Engl[98], B. Epp[62], A. Eppig[87], J. Erdmann[54], A. Ereditato[16], D. Eriksson[146a], I. Ermoline[88], J. Ernst[1], M. Ernst[24], J. Ernwein[136], D. Errede[165], S. Errede[165], E. Ertel[81], M. Escalier[115], C. Escobar[167], X. Espinal Curull[11], B. Esposito[47], F. Etienne[83], A.I. Etienvre[136], E. Etzion[153], D. Evangelakou[54], H. Evans[61], V.N. Evdokimov[128], L. Fabbri[19a,19b], C. Fabre[29], K. Facius[35], R.M. Fakhrutdinov[128], S. Falciano[132a], A.C. Falou[115],

JHEP12(2010)060

Y. Fang[172], M. Fanti[89a,89b], A. Farbin[7], A. Farilla[134a], J. Farley[148], T. Farooque[158], S.M. Farrington[118], P. Farthouat[29], D. Fasching[172], P. Fassnacht[29], D. Fassouliotis[8], B. Fatholahzadeh[158], L. Fayard[115], S. Fazio[36a,36b], R. Febbraro[33], P. Federic[144a], O.L. Fedin[121], I. Fedorko[29], W. Fedorko[29], M. Fehling-Kaschek[48], L. Feligioni[83], C.U. Felzmann[86], C. Feng[32d], E.J. Feng[30], A.B. Fenyuk[128], J. Ferencei[144b], D. Ferguson[172], J. Ferland[93], B. Fernandes[124a,o], W. Fernando[109], S. Ferrag[53], J. Ferrando[118], V. Ferrara[41], A. Ferrari[166], P. Ferrari[105], R. Ferrari[119a], A. Ferrer[167], M.L. Ferrer[47], D. Ferrere[49], C. Ferretti[87], A. Ferretto Parodi[50a,50b], F. Ferro[50a,50b], M. Fiascaris[118], F. Fiedler[81], A. Filipčič[74], A. Filippas[9], F. Filthaut[104], M. Fincke-Keeler[169], M.C.N. Fiolhais[124a,i], L. Fiorini[11], A. Firan[39], G. Fischer[41], P. Fischer [20], M.J. Fisher[109], S.M. Fisher[129], J. Flammer[29], M. Flechl[48], I. Fleck[141], J. Fleckner[81], P. Fleischmann[173], S. Fleischmann[20], T. Flick[174], L.R. Flores Castillo[172], M.J. Flowerdew[99], F. Föhlisch[58a], M. Fokitis[9], T. Fonseca Martin[16], J. Fopma[118], D.A. Forbush[138], A. Formica[136], A. Forti[82], D. Fortin[159a], J.M. Foster[82], D. Fournier[115], A. Foussat[29], A.J. Fowler[44], K. Fowler[137], H. Fox[71], P. Francavilla[122a,122b], S. Franchino[119a,119b], D. Francis[29], M. Franklin[57], S. Franz[29], M. Fraternali[119a,119b], S. Fratina[120], J. Freestone[82], S.T. French[27], R. Froeschl[29], D. Froidevaux[29], J.A. Frost[27], C. Fukunaga[156], E. Fullana Torregrosa[29], J. Fuster[167], C. Gabaldon[29], O. Gabizon[171], T. Gadfort[24], S. Gadomski[49], G. Gagliardi[50a,50b], P. Gagnon[61], C. Galea[98], E.J. Gallas[118], M.V. Gallas[29], V. Gallo[16], B.J. Gallop[129], P. Gallus[125], E. Galyaev[40], K.K. Gan[109], Y.S. Gao[143,p], V.A. Gapienko[128], A. Gaponenko[14], M. Garcia-Sciveres[14], C. García[167], J.E. García Navarro[49], R.W. Gardner[30], N. Garelli[29], H. Garitaonandia[105], V. Garonne[29], J. Garvey[17], C. Gatti[47], G. Gaudio[119a], O. Gaumer[49], B. Gaur[141], V. Gautard[136], P. Gauzzi[132a,132b], I.L. Gavrilenko[94], C. Gay[168], G. Gaycken[20], J-C. Gayde[29], E.N. Gazis[9], P. Ge[32d], C.N.P. Gee[129], Ch. Geich-Gimbel[20], K. Gellerstedt[146a,146b], C. Gemme[50a], M.H. Genest[98], S. Gentile[132a,132b], F. Georgatos[9], S. George[76], P. Gerlach[174], A. Gershon[153], C. Geweniger[58a], H. Ghazlane[135d], P. Ghez[4], N. Ghodbane[33], B. Giacobbe[19a], S. Giagu[132a,132b], V. Giakoumopoulou[8], V. Giangiobbe[122a,122b], F. Gianotti[29], B. Gibbard[24], A. Gibson[158], S.M. Gibson[118], G.F. Gieraltowski[5], L.M. Gilbert[118], M. Gilchriese[14], O. Gildemeister[29], V. Gilewsky[91], D. Gillberg[28], A.R. Gillman[129], D.M. Gingrich[2,q], J. Ginzburg[153], N. Giokaris[8], M.P. Giordani[164a,164c], R. Giordano[102a,102b], F.M. Giorgi[15], P. Giovannini[99], P.F. Giraud[136], P. Girtler[62], D. Giugni[89a], P. Giusti[19a], B.K. Gjelsten[117], L.K. Gladilin[97], C. Glasman[80], J Glatzer[48], A. Glazov[41], K.W. Glitza[174], G.L. Glonti[65], K.G. Gnanvo[75], J. Godfrey[142], J. Godlewski[29], M. Goebel[41], T. Göpfert[43], C. Goeringer[81], C. Gössling[42], T. Göttfert[99], V. Goggi[119a,119b,r], S. Goldfarb[87], D. Goldin[39], T. Golling[175], N.P. Gollub[29], S.N. Golovnia[128], A. Gomes[124a,s], L.S. Gomez Fajardo[41], R. Gonçalo[76], L. Gonella[20], C. Gong[32b], A. Gonidec[29], S. Gonzalez[172], S. González de la Hoz[167], M.L. Gonzalez Silva[26], B. Gonzalez-Pineiro[88], S. Gonzalez-Sevilla[49], J.J. Goodson[148], L. Goossens[29], P.A. Gorbounov[95], H.A. Gordon[24], I. Gorelov[103], G. Gorfine[174], B. Gorini[29], E. Gorini[72a,72b], A. Gorišek[74], E. Gornicki[38], S.A. Gorokhov[128], B.T. Gorski[29], V.N. Goryachev[128], B. Gosdzik[41], M. Gosselink[105], M.I. Gostkin[65], M. Gouanère[4], I. Gough Eschrich[163], M. Gouighri[135a], D. Goujdami[135a], M.P. Goulette[49], A.G. Goussiou[138], C. Goy[4], I. Grabowska-Bold[163,t], V. Grabski[176], P. Grafström[29], C. Grah[174], K-J. Grahn[147], F. Grancagnolo[72a], S. Grancagnolo[15], V. Grassi[148], V. Gratchev[121], N. Grau[34], H.M. Gray[34,u], J.A. Gray[148], E. Graziani[134a], O.G. Grebenyuk[121], B. Green[76], D. Greenfield[129], T. Greenshaw[73], Z.D. Greenwood[24,v], I.M. Gregor[41], P. Grenier[143], A. Grewal[118], E. Griesmayer[46], J. Griffiths[138], N. Grigalashvili[65], A.A. Grillo[137], K. Grimm[148], S. Grinstein[11], Y.V. Grishkevich[97], J.-F. Grivaz[115], L.S. Groer[158], J. Grognuz[29], M. Groh[99], E. Gross[171], J. Grosse-Knetter[54], J. Groth-Jensen[79], M. Gruwe[29], K. Grybel[141], V.J. Guarino[5], C. Guicheney[33], A. Guida[72a,72b], T. Guillemin[4], S. Guindon[54], H. Guler[85,w], J. Gunther[125], B. Guo[158], A. Gupta[30], Y. Gusakov[65], V.N. Gushchin[128], A. Gutierrez[93], P. Gutierrez[111],

JHEP12(2010)060

N. Guttman[153], O. Gutzwiller[172], C. Guyot[136], C. Gwenlan[118], C.B. Gwilliam[73], A. Haas[143], S. Haas[29], C. Haber[14], G. Haboubi[123], R. Hackenburg[24], H.K. Hadavand[39], D.R. Hadley[17], C. Haeberli[16], P. Haefner[99], R. Härtel[99], F. Hahn[29], S. Haider[29], Z. Hajduk[38], H. Hakobyan[176], J. Haller[41,x], G.D. Hallewell[83], K. Hamacher[174], A. Hamilton[49], S. Hamilton[161], H. Han[32a], L. Han[32b], K. Hanagaki[116], M. Hance[120], C. Handel[81], P. Hanke[58a], C.J. Hansen[166], J.R. Hansen[35], J.B. Hansen[35], J.D. Hansen[35], P.H. Hansen[35], T. Hansl-Kozanecka[137], P. Hansson[143], K. Hara[160], G.A. Hare[137], T. Harenberg[174], R. Harper[139], R.D. Harrington[21], O.M. Harris[138], K Harrison[17], J.C. Hart[129], J. Hartert[48], F. Hartjes[105], T. Haruyama[66], A. Harvey[56], S. Hasegawa[101], Y. Hasegawa[140], K. Hashemi[22], S. Hassani[136], M. Hatch[29], D. Hauff[99], S. Haug[16], M. Hauschild[29], R. Hauser[88], M. Havranek[125], B.M. Hawes[118], C.M. Hawkes[17], R.J. Hawkings[29], D. Hawkins[163], T. Hayakawa[67], H.S. Hayward[73], S.J. Haywood[129], E. Hazen[21], M. He[32d], S.J. Head[17], V. Hedberg[79], L. Heelan[28], S. Heim[88], B. Heinemann[14], S. Heisterkamp[35], L. Helary[4], M. Heldmann[48], M. Heller[115], S. Hellman[146a,146b], C. Helsens[11], T. Hemperek[20], R.C.W. Henderson[71], P.J. Hendriks[105], M. Henke[58a], A. Henrichs[54], A.M. Henriques Correia[29], S. Henrot-Versille[115], F. Henry-Couannier[83], C. Hensel[54], T. Henß[174], Y. Hernández Jiménez[167], A.D. Hershenhorn[152], G. Herten[48], R. Hertenberger[98], L. Hervas[29], N.P. Hessey[105], A. Hidvegi[146a], E. Higón-Rodriguez[167], D. Hill[5,*], J.C. Hill[27], N. Hill[5], K.H. Hiller[41], S. Hillert[20], S.J. Hillier[17], I. Hinchliffe[14], D. Hindson[118], E. Hines[120], M. Hirose[116], F. Hirsch[42], D. Hirschbuehl[174], J. Hobbs[148], N. Hod[153], M.C. Hodgkinson[139], P. Hodgson[139], A. Hoecker[29], M.R. Hoeferkamp[103], J. Hoffman[39], D. Hoffmann[83], M. Hohlfeld[81], M. Holder[141], T.I. Hollins[17], A. Holmes[118], S.O. Holmgren[146a], T. Holy[127], J.L. Holzbauer[88], R.J. Homer[17], Y. Homma[67], T. Horazdovsky[127], C. Horn[143], S. Horner[48], K. Horton[118], J-Y. Hostachy[55], T. Hott[99], S. Hou[151], M.A. Houlden[73], A. Hoummada[135a], D.F. Howell[118], J. Hrivnac[115], I. Hruska[125], T. Hryn'ova[4], P.J. Hsu[175], S.-C. Hsu[14], G.S. Huang[111], Z. Hubacek[127], F. Hubaut[83], F. Huegging[20], T.B. Huffman[118], E.W. Hughes[34], G. Hughes[71], R.E. Hughes-Jones[82], M. Huhtinen[29], P. Hurst[57], M. Hurwitz[14], U. Husemann[41], N. Huseynov[10], J. Huston[88], J. Huth[57], G. Iacobucci[102a], G. Iakovidis[9], M. Ibbotson[82], I. Ibragimov[141], R. Ichimiya[67], L. Iconomidou-Fayard[115], J. Idarraga[115], M. Idzik[37], P. Iengo[4], O. Igonkina[105], Y. Ikegami[66], M. Ikeno[66], Y. Ilchenko[39], D. Iliadis[154], D. Imbault[78], M. Imhaeuser[174], M. Imori[155], T. Ince[20], J. Inigo-Golfin[29], P. Ioannou[8], M. Iodice[134a], G. Ionescu[4], A. Irles Quiles[167], K. Ishii[66], A. Ishikawa[67], M. Ishino[66], R. Ishmukhametov[39], T. Isobe[155], C. Issever[118], S. Istin[18a], Y. Itoh[101], A.V. Ivashin[128], W. Iwanski[38], H. Iwasaki[66], J.M. Izen[40], V. Izzo[102a], B. Jackson[120], J.N. Jackson[73], P. Jackson[143], M.R. Jaekel[29], M. Jahoda[125], V. Jain[61], K. Jakobs[48], S. Jakobsen[35], J. Jakubek[127], D.K. Jana[111], E. Jankowski[158], E. Jansen[77], A. Jantsch[99], M. Janus[20], R.C. Jared[172], G. Jarlskog[79], L. Jeanty[57], K. Jelen[37], I. Jen-La Plante[30], P. Jenni[29], A. Jeremie[4], P. Ježˇ[35], S. Jézéquel[4], H. Ji[172], W. Ji[79], J. Jia[148], Y. Jiang[32b], M. Jimenez Belenguer[29], G. Jin[32b], S. Jin[32a], O. Jinnouchi[157], M.D. Joergensen[35], D. Joffe[39], L.G. Johansen[13], M. Johansen[146a,146b], K.E. Johansson[146a], P. Johansson[139], S. Johnert[41], K.A. Johns[6], K. Jon-And[146a,146b], G. Jones[82], M. Jones[118], R.W.L. Jones[71], T.W. Jones[77], T.J. Jones[73], O. Jonsson[29], K.K. Joo[158,y], D. Joos[48], C. Joram[29], P.M. Jorge[124a,c], S. Jorgensen[11], J. Joseph[14], V. Juranek[125], P. Jussel[62], V.V. Kabachenko[128], S. Kabana[16], M. Kaci[167], A. Kaczmarska[38], P. Kadlecik[35], M. Kado[115], H. Kagan[109], M. Kagan[57], S. Kaiser[99], E. Kajomovitz[152], S. Kalinin[174], L.V. Kalinovskaya[65], S. Kama[39], N. Kanaya[155], M. Kaneda[155], V.A. Kantserov[96], J. Kanzaki[66], B. Kaplan[175], A. Kapliy[30], J. Kaplon[29], D. Kar[43], M. Karagounis[20], M. Karagoz[118], M. Karnevskiy[41], K. Karr[5], V. Kartvelishvili[71], A.N. Karyukhin[128], L. Kashif[57], A. Kasmi[39], R.D. Kass[109], A. Kastanas[13], M. Kataoka[4], Y. Kataoka[155], E. Katsoufis[9], J. Katzy[41], V. Kaushik[6], K. Kawagoe[67], T. Kawamoto[155], G. Kawamura[81], M.S. Kayl[105], F. Kayumov[94], V.A. Kazanin[107], M.Y. Kazarinov[65], S.I. Kazi[86],

JHEP12(2010)060

J.R. Keates[82], R. Keeler[169], P.T. Keener[120], R. Kehoe[39], M. Keil[54], G.D. Kekelidze[65], M. Kelly[82], J. Kennedy[98], C.J. Kenney[143], M. Kenyon[53], O. Kepka[125], N. Kerschen[29], B.P. Kerševan[74], S. Kersten[174], K. Kessoku[155], C. Ketterer[48], M. Khakzad[28], F. Khalil-zada[10], H. Khandanyan[165], A. Khanov[112], D. Kharchenko[65], A. Khodinov[148], A.G. Kholodenko[128], A. Khomich[58a], G. Khoriauli[20], N. Khovanskiy[65], V. Khovanskiy[95], E. Khramov[65], J. Khubua[51], G. Kilvington[76], H. Kim[7], M.S. Kim[2], P.C. Kim[143], S.H. Kim[160], N. Kimura[170], O. Kind[15], P. Kind[174], B.T. King[73], M. King[67], J. Kirk[129], G.P. Kirsch[118], L.E. Kirsch[22], A.E. Kiryunin[99], D. Kisielewska[37], B. Kisielewski[38], T. Kittelmann[123], A.M. Kiver[128], H. Kiyamura[67], E. Kladiva[144b], J. Klaiber-Lodewigs[42], M. Klein[73], U. Klein[73], K. Kleinknecht[81], M. Klemetti[85], A. Klier[171], A. Klimentov[24], R. Klingenberg[42], E.B. Klinkby[44], T. Klioutchnikova[29], P.F. Klok[104], S. Klous[105], E.-E. Kluge[58a], T. Kluge[73], P. Kluit[105], S. Kluth[99], N.S. Knecht[158], E. Kneringer[62], J. Knobloch[29], B.R. Ko[44], T. Kobayashi[155], M. Kobel[43], B. Koblitz[29], M. Kocian[143], A. Kocnar[113], P. Kodys[126], K. Köneke[29], A.C. König[104], S. Koenig[81], S. König[48], L. Köpke[81], F. Koetsveld[104], P. Koevesarki[20], T. Koffas[29], E. Koffeman[105], F. Kohn[54], Z. Kohout[127], T. Kohriki[66], T. Koi[143], T. Kokott[20], G.M. Kolachev[107], H. Kolanoski[15], V. Kolesnikov[65], I. Koletsou[4], J. Koll[88], D. Kollar[29], M. Kollefrath[48], S. Kolos[163,z], S.D. Kolya[82], A.A. Komar[94], J.R. Komaragiri[142], T. Kondo[66], T. Kono[41,aa], A.I. Kononov[48], R. Konoplich[108], S.P. Konovalov[94], N. Konstantinidis[77], A. Kootz[174], S. Koperny[37], S.V. Kopikov[128], K. Korcyl[38], K. Kordas[154], V. Koreshev[128], A. Korn[14], A. Korol[107], I. Korolkov[11], E.V. Korolkova[139], V.A. Korotkov[128], O. Kortner[99], S. Kortner[99], V.V. Kostyukhin[20], M.J. Kotamäki[29], S. Kotov[99], V.M. Kotov[65], K.Y. Kotov[107], C. Kourkoumelis[8], A. Koutsman[105], R. Kowalewski[169], H. Kowalski[41], T.Z. Kowalski[37], W. Kozanecki[136], A.S. Kozhin[128], V. Kral[127], V.A. Kramarenko[97], G. Kramberger[74], O. Krasel[42], M.W. Krasny[78], A. Krasznahorkay[108], J. Kraus[88], A. Kreisel[153], F. Krejci[127], J. Kretzschmar[73], N. Krieger[54], P. Krieger[158], G. Krobath[98], K. Kroeninger[54], H. Kroha[99], J. Kroll[120], J. Kroseberg[20], J. Krstic[12a], U. Kruchonak[65], H. Krüger[20], Z.V. Krumshteyn[65], A. Kruth[20], T. Kubota[155], S. Kuehn[48], A. Kugel[58c], T. Kuhl[174], D. Kuhn[62], V. Kukhtin[65], Y. Kulchitsky[90], S. Kuleshov[31b], C. Kummer[98], M. Kuna[83], N. Kundu[118], J. Kunkle[120], A. Kupco[125], H. Kurashige[67], M. Kurata[160], L.L. Kurchaninov[159a], Y.A. Kurochkin[90], V. Kus[125], W. Kuykendall[138], M. Kuze[157], P. Kuzhir[91], O. Kvasnicka[125], R. Kwee[15], A. La Rosa[29], L. La Rotonda[36a,36b], L. Labarga[80], J. Labbe[4], C. Lacasta[167], F. Lacava[132a,132b], H. Lacker[15], D. Lacour[78], V.R. Lacuesta[167], E. Ladygin[65], R. Lafaye[4], B. Laforge[78], T. Lagouri[80], S. Lai[48], M. Lamanna[29], M. Lambacher[98], C.L. Lampen[6], W. Lampl[6], E. Lancon[136], U. Landgraf[48], M.P.J. Landon[75], H. Landsman[152], J.L. Lane[82], C. Lange[41], A.J. Lankford[163], F. Lanni[24], K. Lantzsch[29], A. Lanza[119a], V.V. Lapin[128,*], S. Laplace[4], C. Lapoire[83], J.F. Laporte[136], T. Lari[89a], A.V. Larionov [128], A. Larner[118], C. Lasseur[29], M. Lassnig[29], W. Lau[118], P. Laurelli[47], A. Lavorato[118], W. Lavrijsen[14], P. Laycock[73], A.B. Lazarev[65], A. Lazzaro[89a,89b], O. Le Dortz[78], E. Le Guirriec[83], C. Le Maner[158], E. Le Menedeu[136], M. Le Vine[24], M. Leahu[29], A. Lebedev[64], C. Lebel[93], M. Lechowski[115], T. LeCompte[5], F. Ledroit-Guillon[55], H. Lee[105], J.S.H. Lee[150], S.C. Lee[151], M. Lefebvre[169], M. Legendre[136], A. Leger[49], B.C. LeGeyt[120], F. Legger[98], C. Leggett[14], M. Lehmacher[20], G. Lehmann Miotto[29], M. Lehto[139], X. Lei[6], M.A.L. Leite[23b], R. Leitner[126], D. Lellouch[171], J. Lellouch[78], M. Leltchouk[34], V. Lendermann[58a], K.J.C. Leney[73], T. Lenz[174], G. Lenzen[174], B. Lenzi[136], K. Leonhardt[43], J. Lepidis [174], C. Leroy[93], J-R. Lessard[169], J. Lesser[146a], C.G. Lester[27], A. Leung Fook Cheong[172], J. Levêque[83], D. Levin[87], L.J. Levinson[171], M.S. Levitski[128], M. Lewandowska[21], M. Leyton[15], B. Li[32d], H. Li[172], X. Li[87], Z. Liang[39], Z. Liang[118,ab], B. Liberti[133a], P. Lichard[29], M. Lichtnecker[98], K. Lie[165], W. Liebig[173], R. Lifshitz[152], J.N. Lilley[17], H. Lim[5], A. Limosani[86], M. Limper[63], S.C. Lin[151], F. Linde[105], J.T. Linnemann[88], E. Lipeles[120], L. Lipinsky[125], A. Lipniacka[13], T.M. Liss[165], D. Lissauer[24],

JHEP12(2010)060

A. Lister[49], A.M. Litke[137], C. Liu[28], D. Liu[151,ac], H. Liu[87], J.B. Liu[87], M. Liu[32b], S. Liu[2], T. Liu[39], Y. Liu[32b], M. Livan[119a,119b], S.S.A. Livermore[118], A. Lleres[55], S.L. Lloyd[75], E. Lobodzinska[41], P. Loch[6], W.S. Lockman[137], S. Lockwitz[175], T. Loddenkoetter[20], F.K. Loebinger[82], A. Loginov[175], C.W. Loh[168], T. Lohse[15], K. Lohwasser[48], M. Lokajicek[125], J. Loken [118], R.E. Long[71], L. Lopes[124a,c], D. Lopez Mateos[34,ad], M. Losada[162], P. Loscutoff[14], M.J. Losty[159a], X. Lou[40], A. Lounis[115], K.F. Loureiro[162], L. Lovas[144a], J. Love[21], P.A. Love[71], A.J. Lowe[143], F. Lu[32a], J. Lu[2], L. Lu[39], H.J. Lubatti[138], C. Luci[132a,132b], A. Lucotte[55], A. Ludwig[43], D. Ludwig[41], I. Ludwig[48], J. Ludwig[48], F. Luehring[61], G. Luijckx[105], D. Lumb[48], L. Luminari[132a], E. Lund[117], B. Lund-Jensen[147], B. Lundberg[79], J. Lundberg[29], J. Lundquist[35], M. Lungwitz[81], A. Lupi[122a,122b], G. Lutz[99], D. Lynn[24], J. Lynn[118], J. Lys[14], E. Lytken[79], H. Ma[24], L.L. Ma[172], M. Maaßen[48], J.A. Macana Goia[93], G. Maccarrone[47], A. Macchiolo[99], B. Maček[74], J. Machado Miguens[124a,c], D. Macina[49], R. Mackeprang[35], D. MacQueen[2], R.J. Madaras[14], W.F. Mader[43], R. Maenner[58c], T. Maeno[24], P. Mättig[174], S. Mättig[41], P.J. Magalhaes Martins[124a,i], L. Magnoni[29], E. Magradze[51], C.A. Magrath[104], Y. Mahalalel[153], K. Mahboubi[48], A. Mahmood[1], G. Mahout[17], C. Maiani[132a,132b], C. Maidantchik[23a], A. Maio[124a,s], S. Majewski[24], Y. Makida[66], M. Makouski[128], N. Makovec[115], P. Mal[6], Pa. Malecki[38], P. Malecki[38], V.P. Maleev[121], F. Malek[55], U. Mallik[63], D. Malon[5], S. Maltezos[9], V. Malyshev[107], S. Malyukov[65], M. Mambelli[30], R. Mameghani[98], J. Mamuzic[12b], A. Manabe[66], A. Manara[61], L. Mandelli[89a], I. Mandić[74], R. Mandrysch[15], J. Maneira[124a], P.S. Mangeard[88], M. Mangin-Brinet[49], I.D. Manjavidze[65], A. Mann[54], W.A. Mann[161], P.M. Manning[137], A. Manousakis-Katsikakis[8], B. Mansoulie[136], A. Manz[99], A. Mapelli[29], L. Mapelli[29], L. March [80], J.F. Marchand[29], F. Marchese[133a,133b], M. Marchesotti[29], G. Marchiori[78], M. Marcisovsky[125], A. Marin[21,*], C.P. Marino[61], F. Marroquim[23a], R. Marshall[82], Z. Marshall[34,ad], F.K. Martens[158], S. Marti-Garcia[167], A.J. Martin[75], A.J. Martin[175], B. Martin[29], B. Martin[88], F.F. Martin[120], J.P. Martin[93], Ph. Martin[55], T.A. Martin[17], B. Martin dit Latour[49], M. Martinez[11], V. Martinez Outschoorn[57], A. Martini[47], A.C. Martyniuk[82], F. Marzano[132a], A. Marzin[136], L. Masetti[81], T. Mashimo[155], R. Mashinistov[94], J. Masik[82], A.L. Maslennikov[107], M. Maß[42], I. Massa[19a,19b], G. Massaro[105], N. Massol[4], A. Mastroberardino[36a,36b], T. Masubuchi[155], M. Mathes[20], P. Matricon[115], H. Matsumoto[155], H. Matsunaga[155], T. Matsushita[67], C. Mattravers[118,ae], J.M. Maugain[29], S.J. Maxfield[73], E.N. May[5], J.K. Mayer[158], A. Mayne[139], R. Mazini[151], M. Mazur[20], M. Mazzanti[89a], E. Mazzoni[122a,122b], J. Mc Donald[85], S.P. Mc Kee[87], A. McCarn[165], R.L. McCarthy[148], T.G. McCarthy[28], N.A. McCubbin[129], K.W. McFarlane[56], S. McGarvie[76], H. McGlone[53], G. Mchedlidze[51], R.A. McLaren[29], S.J. McMahon[129], T.R. McMahon[76], T.J. McMahon[17], R.A. McPherson[169,l], A. Meade[84], J. Mechnich[105], M. Mechtel[174], M. Medinnis[41], R. Meera-Lebbai[111], T. Meguro[116], R. Mehdiyev[93], S. Mehlhase[41], A. Mehta[73], K. Meier[58a], J. Meinhardt[48], B. Meirose[79], C. Melachrinos[30], B.R. Mellado Garcia[172], L. Mendoza Navas[162], Z. Meng[151,af], A. Mengarelli[19a,19b], S. Menke[99], C. Menot[29], E. Meoni[11], D. Merkl[98], P. Mermod[118], L. Merola[102a,102b], C. Meroni[89a], F.S. Merritt[30], A.M. Messina[29], I. Messmer[48], J. Metcalfe[103], A.S. Mete[64], S. Meuser[20], C. Meyer[81], J-P. Meyer[136], J. Meyer[173], J. Meyer[54], T.C. Meyer[29], W.T. Meyer[64], J. Miao[32d], S. Michal[29], L. Micu[25a], R.P. Middleton[129], P. Miele[29], S. Migas[73], A. Migliaccio[102a,102b], L. Mijović[41], G. Mikenberg[171], M. Mikestikova[125], B. Mikulec[49], M. Mikuž[74], D.W. Miller[143], R.J. Miller[88], W.J. Mills[168], C. Mills[57], A. Milov[171], D.A. Milstead[146a,146b], D. Milstein[171], S. Mima[110], A.A. Minaenko[128], M. Miñano[167], I.A. Minashvili[65], A.I. Mincer[108], B. Mindur[37], M. Mineev[65], Y. Ming[130], L.M. Mir[11], G. Mirabelli[132a], L. Miralles Verge[11], S. Misawa[24], S. Miscetti[47], A. Misiejuk[76], A. Mitra[118], J. Mitrevski[137], G.Y. Mitrofanov[128], V.A. Mitsou[167], S. Mitsui[66], P.S. Miyagawa[82], K. Miyazaki[67], J.U. Mjörnmark[79], D. Mladenov[29], T. Moa[146a,146b], M. Moch[132a,132b], P. Mockett[138], S. Moed[57], V. Moeller[27], K. Mönig[41], N. Möser[20], B. Mohn[13], W. Mohr[48], S. Mohrdieck-Möck[99],

JHEP12(2010)060

A.M. Moisseev[128,*], R. Moles-Valls[167], J. Molina-Perez[29], L. Moneta[49], J. Monk[77], E. Monnier[83], S. Montesano[89a,89b], F. Monticelli[70], R.W. Moore[2], G.F. Moorhead[86], C. Mora Herrera[49], A. Moraes[53], A. Morais[124a,c], J. Morel[54], G. Morello[36a,36b], D. Moreno[81], M. Moreno Llácer[167], P. Morettini[50a], D. Morgan[139], M. Morii[57], J. Morin[75], Y. Morita[66], A.K. Morley[29], G. Mornacchi[29], M-C. Morone[49], S.V. Morozov[96], J.D. Morris[75], H.G. Moser[99], M. Mosidze[51], J. Moss[109], A. Moszczynski[38], R. Mount[143], E. Mountricha[9], S.V. Mouraviev[94], T.H. Moye[17], E.J.W. Moyse[84], M. Mudrinic[12b], F. Mueller[58a], J. Mueller[123], K. Mueller[20], T.A. Müller[98], D. Muenstermann[42], A. Muijs[105], A. Muir[168], A. Munar[120], Y. Munwes[153], K. Murakami[66], R. Murillo Garcia[163], W.J. Murray[129], I. Mussche[105], E. Musto[102a,102b], A.G. Myagkov[128], M. Myska[125], J. Nadal[11], K. Nagai[160], K. Nagano[66], Y. Nagasaka[60], A.M. Nairz[29], D. Naito[110], K. Nakamura[155], I. Nakano[110], G. Nanava[20], A. Napier[161], M. Nash[77,ag], I. Nasteva[82], N.R. Nation[21], T. Nattermann[20], T. Naumann[41], F. Nauyock[82], G. Navarro[162], S.K. Nderitu[85], H.A. Neal[87], E. Nebot[80], P. Nechaeva[94], A. Negri[119a,119b], G. Negri[29], A. Nelson[64], S. Nelson[143], T.K. Nelson[143], S. Nemecek[125], P. Nemethy[108], A.A. Nepomuceno[23a], M. Nessi[29], S.Y. Nesterov[121], M.S. Neubauer[165], L. Neukermans[4], A. Neusiedl[81], R.M. Neves[108], P. Nevski[24], F.M. Newcomer[120], C. Nicholson[53], R.B. Nickerson[118], R. Nicolaidou[136], L. Nicolas[139], G. Nicoletti[47], B. Nicquevert[29], F. Niedercorn[115], J. Nielsen[137], T. Niinikoski[29], A. Nikiforov[15], V. Nikolaenko[128], K. Nikolaev[65], I. Nikolic-Audit[78], K. Nikolopoulos[24], H. Nilsen[48], P. Nilsson[7], Y. Ninomiya [155], A. Nisati[132a], T. Nishiyama[67], R. Nisius[99], L. Nodulman[5], M. Nomachi[116], I. Nomidis[154], H. Nomoto[155], M. Nordberg[29], B. Nordkvist[146a,146b], O. Norniella Francisco[11], P.R. Norton[129], D. Notz[41], J. Novakova[126], M. Nozaki[66], M. Nožička[41], I.M. Nugent[159a], A.-E. Nuncio-Quiroz[20], G. Nunes Hanninger[20], T. Nunnemann[98], E. Nurse[77], T. Nyman[29], S.W. O'Neale[17,*], D.C. O'Neil[142], V. O'Shea[53], F.G. Oakham[28,h], H. Oberlack[99], J. Ocariz[78], A. Ochi[67], S. Oda[155], S. Odaka[66], J. Odier[83], G.A. Odino[50a,50b], H. Ogren[61], A. Oh[82], S.H. Oh[44], C.C. Ohm[146a,146b], T. Ohshima[101], H. Ohshita[140], T.K. Ohska[66], T. Ohsugi[59], S. Okada[67], H. Okawa[163], Y. Okumura[101], T. Okuyama[155], M. Olcese[50a], A.G. Olchevski[65], M. Oliveira[124a,i], D. Oliveira Damazio[24], C. Oliver[80], J. Oliver[57], E. Oliver Garcia[167], D. Olivito[120], A. Olszewski[38], J. Olszowska[38], C. Omachi[67,ah], A. Onofre[124a,ai], P.U.E. Onyisi[30], C.J. Oram[159a], G. Ordonez[104], M.J. Oreglia[30], F. Orellana[49], Y. Oren[153], D. Orestano[134a,134b], I. Orlov[107], C. Oropeza Barrera[53], R.S. Orr[158], E.O. Ortega[130], B. Osculati[50a,50b], R. Ospanov[120], C. Osuna[11], G. Otero y Garzon[26], J.P Ottersbach[105], B. Ottewell[118], M. Ouchrif[135c], F. Ould-Saada[117], A. Ouraou[136], Q. Ouyang[32a], M. Owen[82], S. Owen[139], A Oyarzun[31b], O.K. Øye[13], V.E. Ozcan[77], K. Ozone[66], N. Ozturk[7], A. Pacheco Pages[11], C. Padilla Aranda[11], E. Paganis[139], F. Paige[24], K. Pajchel[117], S. Palestini[29], J. Palla[29], D. Pallin[33], A. Palma[124a,c], J.D. Palmer[17], M.J. Palmer[27], Y.B. Pan[172], E. Panagiotopoulou[9], B. Panes[31a], N. Panikashvili[87], V.N. Panin[107], S. Panitkin[24], D. Pantea[25a], M. Panuskova[125], V. Paolone[123], A. Paoloni[133a,133b], Th.D. Papadopoulou[9], A. Paramonov[5], S.J. Park[54], W. Park[24,aj], M.A. Parker[27], S.I. Parker[14], F. Parodi[50a,50b], J.A. Parsons[34], U. Parzefall[48], E. Pasqualucci[132a], A. Passeri[134a], F. Pastore[134a,134b], Fr. Pastore[29], G. Pásztor [49,ak], S. Pataraia[172], N. Patel[150], J.R. Pater[82], S. Patricelli[102a,102b], T. Pauly[29], L.S. Peak[150], M. Pecsy[144a], M.I. Pedraza Morales[172], S.J.M. Peeters[105], S.V. Peleganchuk[107], H. Peng[172], R. Pengo[29], A. Penson[34], J. Penwell[61], M. Perantoni[23a], K. Perez[34,ad], E. Perez Codina[11], M.T. Pérez García-Estañ[167], V. Perez Reale[34], I. Peric[20], L. Perini[89a,89b], H. Pernegger[29], R. Perrino[72a], P. Perrodo[4], S. Persembe[3a], P. Perus[115], V.D. Peshekhonov[65], E. Petereit[5], O. Peters[105], B.A. Petersen[29], J. Petersen[29], T.C. Petersen[35], E. Petit[83], A. Petridis[154], C. Petridou[154], E. Petrolo[132a], F. Petrucci[134a,134b], D Petschull[41], M. Petteni[142], R. Pezoa[31b], B. Pfeifer[48], A. Phan[86], A.W. Phillips[27], P.W. Phillips[129], G. Piacquadio[29], E. Piccaro[75], M. Piccinini[19a,19b], A. Pickford[53], R. Piegaia[26], J.E. Pilcher[30], A.D. Pilkington[82], J. Pina[124a,s], M. Pinamonti[164a,164c], J.L. Pinfold[2], J. Ping[32c], B. Pinto[124a,c],

JHEP12(2010)060

O. Pirotte[29], C. Pizio[89a,89b], R. Placakyte[41], M. Plamondon[169], W.G. Plano[82], M.-A. Pleier[24], A.V. Pleskach[128], A. Poblaguev[175], S. Poddar[58a], F. Podlyski[33], P. Poffenberger[169], L. Poggioli[115], T. Poghosyan[20], M. Pohl[49], F. Polci[55], G. Polesello[119a], A. Policicchio[138], A. Polini[19a], J. Poll[75], V. Polychronakos[24], D.M. Pomarede[136], D. Pomeroy[22], K. Pommès[29], P. Ponsot[136], L. Pontecorvo[132a], B.G. Pope[88], G.A. Popeneciu[25a], R. Popescu[24], D.S. Popovic[12a], A. Poppleton[29], J. Populе[125], X. Portell Bueso[48], R. Porter[163], C. Posch[21], G.E. Pospelov[99], S. Pospisil[127], M. Potekhin[24], I.N. Potrap[99], C.J. Potter[149], C.T. Potter[85], K.P. Potter[82], G. Poulard[29], J. Poveda[172], R. Prabhu[77], P. Pralavorio[83], S. Prasad[57], M. Prata[119a,119b], R. Pravahan[7], S. Prell[64], K. Pretzl[16], L. Pribyl[29], D. Price[61], L.E. Price[5], M.J. Price[29], P.M. Prichard[73], D. Prieur[123], M. Primavera[72a], K. Prokofiev[29], F. Prokoshin[31b], S. Protopopescu[24], J. Proudfoot[5], X. Prudent[43], H. Przysiezniak[4], S. Psoroulas[20], E. Ptacek[114], C. Puigdengoles[11], J. Purdham[87], M. Purohit[24,al], P. Puzo[115], Y. Pylypchenko[117], M. Qi[32c], J. Qian[87], W. Qian[129], Z. Qian[83], Z. Qin[41], D. Qing[159a], A. Quadt[54], D.R. Quarrie[14], W.B. Quayle[172], F. Quinonez[31a], M. Raas[104], V. Radeka[24], V. Radescu[58b], B. Radics[20], T. Rador[18a], F. Ragusa[89a,89b], G. Rahal[177], A.M. Rahimi[109], D. Rahm[24], C. Raine[53,*], B. Raith[20], S. Rajagopalan[24], S. Rajek[42], M. Rammensee[48], M. Rammes[141], M. Ramstedt[146a,146b], P.N. Ratoff[71], F. Rauscher[98], E. Rauter[99], M. Raymond[29], A.L. Read[117], D.M. Rebuzzi[119a,119b], A. Redelbach[173], G. Redlinger[24], R. Reece[120], K. Reeves[40], A. Reichold[105], E. Reinherz-Aronis[153], A Reinsch[114], I. Reisinger[42], D. Reljic[12a], C. Rembser[29], Z.L. Ren[151], P. Renkel[39], B. Rensch[35], S. Rescia[24], M. Rescigno[132a], S. Resconi[89a], B. Resende[136], P. Reznicek[126], R. Rezvani[158], A. Richards[77], R.A. Richards[88], R. Richter[99], E. Richter-Was[38,am], M. Ridel[78], S. Rieke[81], M. Rijpstra[105], M. Rijssenbeek[148], A. Rimoldi[119a,119b], L. Rinaldi[19a], R.R. Rios[39], I. Riu[11], G. Rivoltella[89a,89b], F. Rizatdinova[112], E. Rizvi[75], D.A. Roa Romero[162], S.H. Robertson[85,l], A. Robichaud-Veronneau[49], D. Robinson[27], JEM Robinson[77], M. Robinson[114], A. Robson[53], J.G. Rocha de Lima[106], C. Roda[122a,122b], D. Roda Dos Santos[29], S. Rodier[80], D. Rodriguez[162], Y. Rodriguez Garcia[15], A. Roe[54], S. Roe[29], O. Røhne[117], V. Rojo[1], S. Rolli[161], A. Romaniouk[96], V.M. Romanov[65], G. Romeo[26], D. Romero Maltrana[31a], L. Roos[78], E. Ros[167], S. Rosati[138], G.A. Rosenbaum[158], E.I. Rosenberg[64], P.L. Rosendahl[13], L. Rosselet[49], V. Rossetti[11], E. Rossi[102a,102b], L.P. Rossi[50a], L. Rossi[89a,89b], M. Rotaru[25a], J. Rothberg[138], I. Rottländer[20], D. Rousseau[115], C.R. Royon[136], A. Rozanov[83], Y. Rozen[152], X. Ruan[115], B. Ruckert[98], N. Ruckstuhl[105], V.I. Rud[97], G. Rudolph[62], F. Rühr[6], F. Ruggieri[134a], A. Ruiz-Martinez[64], E. Rulikowska-Zarebska[37], V. Rumiantsev[91,*], L. Rumyantsev[65], K. Runge[48], O. Runolfsson[20], Z. Rurikova[48], N.A. Rusakovich[65], D.R. Rust[61], J.P. Rutherfoord[6], C. Ruwiedel[20], P. Ruzicka[125], Y.F. Ryabov[121], V. Ryadovikov[128], P. Ryan[88], G. Rybkin[115], S. Rzaeva[10], A.F. Saavedra[150], I. Sadeh[153], H.F-W. Sadrozinski[137], R. Sadykov[65], F. Safai Tehrani[132a,132b], H. Sakamoto[155], P. Sala[89a], G. Salamanna[105], A. Salamon[133a], M. Saleem[111], D. Salihagic[99], A. Salnikov[143], J. Salt[167], B.M. Salvachua Ferrando[5], D. Salvatore[36a,36b], F. Salvatore[149], A. Salvucci[47], A. Salzburger[29], D. Sampsonidis[154], B.H. Samset[117], H. Sandaker[13], H.G. Sander[81], M.P. Sanders[98], M. Sandhoff[174], P. Sandhu[158], T. Sandoval[27], R. Sandstroem[105], S. Sandvoss[174], D.P.C. Sankey[129], B. Sanny[174], A. Sansoni[47], C. Santamarina Rios[85], C. Santoni[33], R. Santonico[133a,133b], H. Santos[124a], J.G. Saraiva[124a,s], T. Sarangi[172], E. Sarkisyan-Grinbaum[7], F. Sarri[122a,122b], G. Sartisohn[174], O. Sasaki[66], T. Sasaki[66], N. Sasao[68], I. Satsounkevitch[90], G. Sauvage[4], P. Savard[158,h], A.Y. Savine[6], V. Savinov[123], P. Savva [9], L. Sawyer[24,an], D.H. Saxon[53], L.P. Says[33], C. Sbarra[19a,19b], A. Sbrizzi[19a,19b], O. Scallon[93], D.A. Scannicchio[163], J. Schaarschmidt[43], P. Schacht[99], U. Schäfer[81], S. Schaetzel[58b], A.C. Schaffer[115], D. Schaile[98], M. Schaller[29], R.D. Schamberger[148], A.G. Schamov[107], V. Scharf[58a], V.A. Schegelsky[121], D. Scheirich[87], M. Schernau[163], M.I. Scherzer[14], C. Schiavi[50a,50b], J. Schieck[99], M. Schioppa[36a,36b], S. Schlenker[29], J.L. Schlereth[5], E. Schmidt[48], M.P. Schmidt[175,*],

JHEP12(2010)060

K. Schmieden[20], C. Schmitt[81], M. Schmitz[20], R.C. Scholte[105], A. Schöning[58b], M. Schott[29], D. Schouten[142], J. Schovancova[125], M. Schram[85], A. Schreiner[63], C. Schroeder[81], N. Schroer[58c], M. Schroers[174], D. Schroff[48], S. Schuh[29], G. Schuler[29], J. Schultes[174], H.-C. Schultz-Coulon[58a], J.W. Schumacher[43], M. Schumacher[48], B.A. Schumm[137], Ph. Schune[136], C. Schwanenberger[82], A. Schwartzman[143], D. Schweiger[29], Ph. Schwemling[78], R. Schwienhorst[88], R. Schwierz[43], J. Schwindling[136], W.G. Scott[129], J. Searcy[114], E. Sedykh[121], E. Segura[11], S.C. Seidel[103], A. Seiden[137], F. Seifert[43], J.M. Seixas[23a], G. Sekhniaidze[102a], D.M. Seliverstov[121], B. Sellden[146a], G. Sellers[73], M. Seman[144b], N. Semprini-Cesari[19a,19b], C. Serfon[98], L. Serin[115], R. Seuster[99], H. Severini[111], M.E. Sevior[86], A. Sfyrla[29], E. Shabalina[54], M. Shamim[114], L.Y. Shan[32a], J.T. Shank[21], Q.T. Shao[86], M. Shapiro[14], P.B. Shatalov[95], L. Shaver[6], C. Shaw[53], K. Shaw[139], D. Sherman[29], P. Sherwood[77], A. Shibata[108], P. Shield[118], S. Shimizu[29], M. Shimojima[100], T. Shin[56], A. Shmeleva[94], M.J. Shochet[30], M.A. Shupe[6], P. Sicho[125], A. Sidoti[15], A. Siebel[174], F Siegert[77], J. Siegrist[14], Dj. Sijacki[12a], O. Silbert[171], J. Silva[124a,ao], Y. Silver[153], D. Silverstein[143], S.B. Silverstein[146a], V. Simak[127], Lj. Simic[12a], S. Simion[115], B. Simmons[77], M. Simonyan[35], P. Sinervo[158], N.B. Sinev[114], V. Sipica[141], G. Siragusa[81], A.N. Sisakyan[65], S.Yu. Sivoklokov[97], J. Sjölin[146a,146b], T.B. Sjursen[13], L.A. Skinnari[14], K. Skovpen[107], P. Skubic[111], N. Skvorodnev[22], M. Slater[17], T. Slavicek[127], K. Sliwa[161], T.J. Sloan[71], J. Sloper[29], V. Smakhtin[171], S.Yu. Smirnov[96], Y. Smirnov[24], L.N. Smirnova[97], O. Smirnova[79], B.C. Smith[57], D. Smith[143], K.M. Smith[53], M. Smizanska[71], K. Smolek[127], A.A. Snesarev[94], S.W. Snow[82], J. Snow[111], J. Snuverink[105], S. Snyder[24], M. Soares[124a], R. Sobie[169,l], J. Sodomka[127], A. Soffer[153], C.A. Solans[167], M. Solar[127], J. Solc[127], E. Solfaroli Camillocci[132a,132b], A.A. Solodkov[128], O.V. Solovyanov[128], R. Soluk[2], J. Sondericker[24], N. Soni[2], V. Sopko[127], B. Sopko[127], M. Sorbi[89a,89b], M. Sosebee[7], A. Soukharev[107], S. Spagnolo[72a,72b], F. Spanò[34], P. Speckmayer[29], E. Spencer[137], R. Spighi[19a], G. Spigo[29], F. Spila[132a,132b], E. Spiriti[134a], R. Spiwoks[29], L. Spogli[134a,134b], M. Spousta[126], T. Spreitzer[158], B. Spurlock[7], R.D. St. Denis[53], T. Stahl[141], J. Stahlman[120], R. Stamen[58a], S.N. Stancu[163], E. Stanecka[29], R.W. Stanek[5], C. Stanescu[134a], S. Stapnes[117], E.A. Starchenko[128], J. Stark[55], P. Staroba[125], P. Starovoitov[91], J. Stastny[125], A. Staude[98], P. Stavina[144a], G. Stavropoulos[14], G. Steele[53], E. Stefanidis[77], P. Steinbach[43], P. Steinberg[24], I. Stekl[127], B. Stelzer[142], H.J. Stelzer[41], O. Stelzer-Chilton[159a], H. Stenzel[52], K. Stevenson[75], G.A. Stewart[53], W. Stiller[99], T. Stockmanns[20], M.C. Stockton[29], M. Stodulski[38], K. Stoerig[48], G. Stoicea[25a], S. Stonjek[99], P. Strachota[126], A.R. Stradling[7], A. Straessner[43], J. Strandberg[87], S. Strandberg[146a,146b], A. Strandlie[117], M. Strang[109], M. Strauss[111], P. Strizenec[144b], R. Ströhmer[173], D.M. Strom[114], J.A. Strong[76,*], R. Stroynowski[39], J. Strube[129], B. Stugu[13], I. Stumer[24,*], J. Stupak[148], P. Sturm[174], D.A. Soh[151,ap], D. Su[143], Y. Sugaya[116], T. Sugimoto[101], C. Suhr[106], K. Suita[67], M. Suk[126], V.V. Sulin[94], S. Sultansoy[3d], T. Sumida[29], X.H. Sun[32d], J.E. Sundermann[48], K. Suruliz[164a,164b], S. Sushkov[11], G. Susinno[36a,36b], M.R. Sutton[139], Y. Suzuki[66], Yu.M. Sviridov[128], S. Swedish[168], I. Sykora[144a], T. Sykora[126], R.R. Szczygiel[38], B. Szeless[29], T. Szymocha[38], J. Sánchez[167], D. Ta[105], S. Taboada Gameiro[29], K. Tackmann[29], A. Taffard[163], R. Tafirout[159a], A. Taga[117], Y. Takahashi[101], H. Takai[24], R. Takashima[69], H. Takeda[67], T. Takeshita[140], M. Talby[83], A. Talyshev[107], M.C. Tamsett[76], J. Tanaka[155], R. Tanaka[115], S. Tanaka[131], S. Tanaka[66], Y. Tanaka[100], K. Tani[67], G.P. Tappern[29], S. Tapprogge[81], D. Tardif[158], S. Tarem[152], F. Tarrade[24], G.F. Tartarelli[89a], P. Tas[126], M. Tasevsky[125], E. Tassi[36a,36b], M. Tatarkhanov[14], C. Taylor[77], F.E. Taylor[92], G. Taylor[137], G.N. Taylor[86], R.P. Taylor[169], W. Taylor[159b], M. Teixeira Dias Castanheira[75], P. Teixeira-Dias[76], K.K. Temming[48], H. Ten Kate[29], P.K. Teng[151], Y.D. Tennenbaum-Katan[152], S. Terada[66], K. Terashi[155], J. Terron[80], M. Terwort[41,x], M. Testa[47], R.J. Teuscher[158,l], C.M. Tevlin[82], J. Thadome[174], J. Therhaag[20], T. Theveneaux-Pelzer[78], M. Thioye[175], S. Thoma[48], J.P. Thomas[17], E.N. Thompson[84], P.D. Thompson[17], P.D. Thompson[158], R.J. Thompson[82],

JHEP12(2010)060

A.S. Thompson[53], E. Thomson[120], M. Thomson[27], R.P. Thun[87], T. Tic[125], V.O. Tikhomirov[94], Y.A. Tikhonov[107], C.J.W.P. Timmermans[104], P. Tipton[175], F.J. Tique Aires Viegas[29], S. Tisserant[83], J. Tobias[48], B. Toczek[37], T. Todorov[4], S. Todorova-Nova[161], B. Toggerson[163], J. Tojo[66], S. Tokár[144a], K. Tokunaga[67], K. Tokushuku[66], K. Tollefson[88], L. Tomasek[125], M. Tomasek[125], M. Tomoto[101], D. Tompkins[6], L. Tompkins[14], K. Toms[103], A. Tonazzo[134a,134b], G. Tong[32a], A. Tonoyan[13], C. Topfel[16], N.D. Topilin[65], I. Torchiani[29], E. Torrence[114], E. Torró Pastor[167], J. Toth[83,ak], F. Touchard[83], D.R. Tovey[139], D. Traynor[75], T. Trefzger[173], J. Treis[20], L. Tremblet[29], A. Tricoli[29], I.M. Trigger[159a], S. Trincaz-Duvoid[78], T.N. Trinh[78], M.F. Tripiana[70], N. Triplett[64], W. Trischuk[158], A. Trivedi[24,aq], B. Trocmé[55], C. Troncon[89a], M. Trottier-McDonald[142], A. Trzupek[38], C. Tsarouchas[9], J.C-L. Tseng[118], M. Tsiakiris[105], P.V. Tsiareshka[90], D. Tsionou[139], G. Tsipolitis[9], V. Tsiskaridze[51], E.G. Tskhadadze[51], I.I. Tsukerman[95], V. Tsulaia[123], J.-W. Tsung[20], S. Tsuno[66], D. Tsybychev[148], J.M. Tuggle[30], M. Turala[38], D. Turecek[127], I. Turk Cakir[3e], E. Turlay[105], P.M. Tuts[34], M.S. Twomey[138], M. Tylmad[146a,146b], M. Tyndel[129], D. Typaldos[17], H. Tyrvainen[29], E. Tzamarioudaki[9], G. Tzanakos[8], K. Uchida[20], I. Ueda[155], R. Ueno[28], M. Ugland[13], M. Uhlenbrock[20], M. Uhrmacher[54], F. Ukegawa[160], G. Unal[29], D.G. Underwood[5], A. Undrus[24], G. Unel[163], Y. Unno[66], D. Urbaniec[34], E. Urkovsky[153], P. Urquijo[49,ar], P. Urrejola[31a], G. Usai[7], M. Uslenghi[119a,119b], L. Vacavant[83], V. Vacek[127], B. Vachon[85], S. Vahsen[14], C. Valderanis[99], J. Valenta[125], P. Valente[132a], S. Valentinetti[19a,19b], S. Valkar[126], E. Valladolid Gallego[167], S. Vallecorsa[152], J.A. Valls Ferrer[167], R. Van Berg[120], H. van der Graaf[105], E. van der Kraaij[105], E. van der Poel[105], D. van der Ster[29], B. Van Eijk[105], N. van Eldik[84], P. van Gemmeren[5], Z. van Kesteren[105], I. van Vulpen[105], W. Vandelli[29], G. Vandoni[29], A. Vaniachine[5], P. Vankov[73], F. Vannucci[78], F. Varela Rodriguez[29], R. Vari[132a], E.W. Varnes[6], D. Varouchas[14], A. Vartapetian[7], K.E. Varvell[150], L. Vasilyeva[94], V.I. Vassilakopoulos[56], F. Vazeille[33], G. Vegni[89a,89b], J.J. Veillet[115], C. Vellidis[8], F. Veloso[124a], R. Veness[29], S. Veneziano[132a], A. Ventura[72a,72b], D. Ventura[138], S. Ventura [47], M. Venturi[48], N. Venturi[16], V. Vercesi[119a], M. Verducci[138], W. Verkerke[105], J.C. Vermeulen[105], L. Vertogardov[118], M.C. Vetterli[142,h], I. Vichou[165], T. Vickey[145b,as], G.H.A. Viehhauser[118], S. Viel[168], M. Villa[19a,19b], E.G. Villani[129], M. Villaplana Perez[167], E. Vilucchi[47], M.G. Vincter[28], E. Vinek[29], V.B. Vinogradov[65], M. Virchaux[136,*], S. Viret[33], J. Virzi[14], A. Vitale [19a,19b], O. Vitells[171], I. Vivarelli[48], F. Vives Vaque[11], S. Vlachos[9], M. Vlasak[127], N. Vlasov[20], A. Vogel[20], P. Vokac[127], M. Volpi[11], G. Volpini[89a], H. von der Schmitt[99], J. von Loeben[99], H. von Radziewski[48], E. von Toerne[20], V. Vorobel[126], A.P. Vorobiev[128], V. Vorwerk[11], M. Vos[167], R. Voss[29], T.T. Voss[174], J.H. Vossebeld[73], A.S. Vovenko[128], N. Vranjes[12a], M. Vranjes Milosavljevic[12a], V. Vrba[125], M. Vreeswijk[105], T. Vu Anh[81], D. Vudragovic[12a], R. Vuillermet[29], I. Vukotic[115], W. Wagner[174], P. Wagner[120], H. Wahlen[174], J. Walbersloh[42], J. Walder[71], R. Walker[98], W. Walkowiak[141], R. Wall[175], P. Waller[73], C. Wang[44], H. Wang[172], J. Wang[32d], J.C. Wang[138], S.M. Wang[151], A. Warburton[85], C.P. Ward[27], M. Warsinsky[48], R. Wastie[118], P.M. Watkins[17], A.T. Watson[17], M.F. Watson[17], G. Watts[138], S. Watts[82], A.T. Waugh[150], B.M. Waugh[77], M. Webel[48], J. Weber[42], M. Weber[129], M.S. Weber[16], P. Weber[54], A.R. Weidberg[118], J. Weingarten[54], C. Weiser[48], H. Wellenstein[22], P.S. Wells[29], M. Wen[47], T. Wenaus[24], S. Wendler[123], Z. Weng[151,at], T. Wengler[29], S. Wenig[29], N. Wermes[20], M. Werner[48], P. Werner[29], M. Werth[163], U. Werthenbach[141], M. Wessels[58a], K. Whalen[28], S.J. Wheeler-Ellis[163], S.P. Whitaker[21], A. White[7], M.J. White[27], S. White[24], S.R. Whitehead[118], D. Whiteson[163], D. Whittington[61], F. Wicek[115], D. Wicke[81], F.J. Wickens[129], W. Wiedenmann[172], M. Wielers[129], P. Wienemann[20], C. Wiglesworth[73], L.A.M. Wiik[48], A. Wildauer[167], M.A. Wildt[41,x], I. Wilhelm[126], H.G. Wilkens[29], J.Z. Will[98], E. Williams[34], H.H. Williams[120], W. Willis[34], S. Willocq[84], J.A. Wilson[17], M.G. Wilson[143], A. Wilson[87], I. Wingerter-Seez[4], S. Winkelmann[48],

JHEP12(2010)060

F. Winklmeier[29], M. Wittgen[143], M.W. Wolter[38], H. Wolters[124a,i], B.K. Wosiek[38], J. Wotschack[29], M.J. Woudstra[84], K. Wraight[53], C. Wright[53], D. Wright[143], B. Wrona[73], S.L. Wu[172], X. Wu[49], J. Wuestenfeld[42], E. Wulf[34], R. Wunstorf[42], B.M. Wynne[45], L. Xaplanteris[9], S. Xella[35], S. Xie[48], Y. Xie[32a], C. Xu[32b], D. Xu[139], G. Xu[32a], N. Xu[172], B. Yabsley[150], M. Yamada[66], A. Yamamoto[66], K. Yamamoto[64], S. Yamamoto[155], T. Yamamura[155], J. Yamaoka[44], T. Yamazaki[155], Y. Yamazaki[67], Z. Yan[21], H. Yang[87], S. Yang[118], U.K. Yang[82], Y. Yang[61], Y. Yang[32a], Z. Yang[146a,146b], S. Yanush[91], W-M. Yao[14], Y. Yao[14], Y. Yasu[66], J. Ye[39], S. Ye[24], M. Yilmaz[3c], R. Yoosoofmiya[123], K. Yorita[170], H. Yoshida[66,au], R. Yoshida[5], C. Young[143], S.P. Youssef[21], D. Yu[24], J. Yu[7], J. Yu[32c,av], J. Yuan[99], L. Yuan[32a,aw], A. Yurkewicz[148], V.G. Zaets [128], R. Zaidan[63], A.M. Zaitsev[128], Z. Zajacova[29], Yo.K. Zalite [121], V. Zambrano[47], L. Zanello[132a,132b], P. Zarzhitsky[39], A. Zaytsev[107], M. Zdrazil[14], C. Zeitnitz[174], M. Zeller[175], P.F. Zema[29], A. Zemla[38], C. Zendler[20], A.V. Zenin[128], O. Zenin[128], T. Zenis[144a], Z. Zenonos[122a,122b], S. Zenz[14], D. Zerwas[115], G. Zevi della Porta[57], Z. Zhan[32d], H. Zhang[83], J. Zhang[5], Q. Zhang[5], X. Zhang[32d], L. Zhao[108], T. Zhao[138], Z. Zhao[32b], A. Zhemchugov[65], S. Zheng[32a], J. Zhong[151,ax], B. Zhou[87], N. Zhou[163], Y. Zhou[151], C.G. Zhu[32d], H. Zhu[41], Y. Zhu[172], X. Zhuang[98], V. Zhuravlov[99], B. Zilka[144a], R. Zimmermann[20], S. Zimmermann[20], S. Zimmermann[48], M. Ziolkowski[141], R. Zitoun[4], L. Živković[34], V.V. Zmouchko[128,*], G. Zobernig[172], A. Zoccoli[19a,19b], Y. Zolnierowski[4], A. Zsenei[29], M. zur Nedden[15], V. Zutshi[106].

[1] University at Albany, 1400 Washington Ave, Albany, NY 12222, United States of America

[2] University of Alberta, Department of Physics, Centre for Particle Physics, Edmonton, AB T6G 2G7, Canada

[3] Ankara University$^{(a)}$, Faculty of Sciences, Department of Physics, TR 061000 Tandogan, Ankara; Dumlupinar University$^{(b)}$, Faculty of Arts and Sciences, Department of Physics, Kutahya; Gazi University$^{(c)}$, Faculty of Arts and Sciences, Department of Physics, 06500, Teknikokullar, Ankara; TOBB University of Economics and Technology$^{(d)}$, Faculty of Arts and Sciences, Division of Physics, 06560, Sogutozu, Ankara; Turkish Atomic Energy Authority$^{(e)}$, 06530, Lodumlu, Ankara, Turkey

[4] LAPP, Université de Savoie, CNRS/IN2P3, Annecy-le-Vieux, France

[5] Argonne National Laboratory, High Energy Physics Division, 9700 S. Cass Avenue, Argonne IL 60439, United States of America

[6] University of Arizona, Department of Physics, Tucson, AZ 85721, United States of America

[7] The University of Texas at Arlington, Department of Physics, Box 19059, Arlington, TX 76019, United States of America

[8] University of Athens, Nuclear & Particle Physics, Department of Physics, Panepistimiopouli, Zografou, GR 15771 Athens, Greece

[9] National Technical University of Athens, Physics Department, 9-Iroon Polytechniou, GR 15780 Zografou, Greece

[10] Institute of Physics, Azerbaijan Academy of Sciences, H. Javid Avenue 33, AZ 143 Baku, Azerbaijan

[11] Institut de Física d'Altes Energies, IFAE, Edifici Cn, Universitat Autònoma de Barcelona, ES - 08193 Bellaterra (Barcelona), Spain

[12] University of Belgrade$^{(a)}$, Institute of Physics, P.O. Box 57, 11001 Belgrade; Vinca Institute of Nuclear Sciences$^{(b)}$M. Petrovica Alasa 12-14, 11000 Belgrade, Serbia, Serbia

[13] University of Bergen, Department for Physics and Technology, Allegaten 55, NO - 5007 Bergen, Norway

[14] Lawrence Berkeley National Laboratory and University of California, Physics Division, MS50B-6227, 1 Cyclotron Road, Berkeley, CA 94720, United States of America

JHEP12(2010)060

[15] Humboldt University, Institute of Physics, Berlin, Newtonstr. 15, D-12489 Berlin, Germany
[16] University of Bern, Albert Einstein Center for Fundamental Physics, Laboratory for High Energy Physics, Sidlerstrasse 5, CH - 3012 Bern, Switzerland
[17] University of Birmingham, School of Physics and Astronomy, Edgbaston, Birmingham B15 2TT, United Kingdom
[18] Bogazici University[(a)], Faculty of Sciences, Department of Physics, TR - 80815 Bebek-Istanbul; Dogus University[(b)], Faculty of Arts and Sciences, Department of Physics, 34722, Kadikoy, Istanbul; [(c)]Gaziantep University, Faculty of Engineering, Department of Physics Engineering, 27310, Sehitkamil, Gaziantep, Turkey; Istanbul Technical University[(d)], Faculty of Arts and Sciences, Department of Physics, 34469, Maslak, Istanbul, Turkey
[19] INFN Sezione di Bologna[(a)]; Università di Bologna, Dipartimento di Fisica[(b)], viale C. Berti Pichat, 6/2, IT - 40127 Bologna, Italy
[20] University of Bonn, Physikalisches Institut, Nussallee 12, D - 53115 Bonn, Germany
[21] Boston University, Department of Physics, 590 Commonwealth Avenue, Boston, MA 02215, United States of America
[22] Brandeis University, Department of Physics, MS057, 415 South Street, Waltham, MA 02454, United States of America
[23] Universidade Federal do Rio De Janeiro, COPPE/EE/IF [(a)], Caixa Postal 68528, Ilha do Fundao, BR - 21945-970 Rio de Janeiro; [(b)]Universidade de Sao Paulo, Instituto de Fisica, R.do Matao Trav. R.187, Sao Paulo - SP, 05508 - 900, Brazil
[24] Brookhaven National Laboratory, Physics Department, Bldg. 510A, Upton, NY 11973, United States of America
[25] National Institute of Physics and Nuclear Engineering[(a)]Bucharest-Magurele, Str. Atomistilor 407, P.O. Box MG-6, R-077125, Romania; University Politehnica Bucharest[(b)], Rectorat - AN 001, 313 Splaiul Independentei, sector 6, 060042 Bucuresti; West University[(c)] in Timisoara, Bd. Vasile Parvan 4, Timisoara, Romania
[26] Universidad de Buenos Aires, FCEyN, Dto. Fisica, Pab I - C. Universitaria, 1428 Buenos Aires, Argentina
[27] University of Cambridge, Cavendish Laboratory, J J Thomson Avenue, Cambridge CB3 0HE, United Kingdom
[28] Carleton University, Department of Physics, 1125 Colonel By Drive, Ottawa ON K1S 5B6, Canada
[29] CERN, CH - 1211 Geneva 23, Switzerland
[30] University of Chicago, Enrico Fermi Institute, 5640 S. Ellis Avenue, Chicago, IL 60637, United States of America
[31] Pontificia Universidad Católica de Chile, Facultad de Fisica, Departamento de Fisica[(a)], Avda. Vicuna Mackenna 4860, San Joaquin, Santiago; Universidad Técnica Federico Santa María, Departamento de Física[(b)], Avda. Espãna 1680, Casilla 110-V, Valparaíso, Chile
[32] Institute of High Energy Physics, Chinese Academy of Sciences[(a)], P.O. Box 918, 19 Yuquan Road, Shijing Shan District, CN - Beijing 100049; University of Science & Technology of China (USTC), Department of Modern Physics[(b)], Hefei, CN - Anhui 230026; Nanjing University, Department of Physics[(c)], Nanjing, CN - Jiangsu 210093; Shandong University, High Energy Physics Group[(d)], Jinan, CN - Shandong 250100, China
[33] Laboratoire de Physique Corpusculaire, Clermont Université, Université Blaise Pascal, CNRS/IN2P3, FR - 63177 Aubiere Cedex, France
[34] Columbia University, Nevis Laboratory, 136 So. Broadway, Irvington, NY 10533, United States of America
[35] University of Copenhagen, Niels Bohr Institute, Blegdamsvej 17, DK - 2100 Kobenhavn 0, Denmark

JHEP12(2010)060

[36] INFN Gruppo Collegato di Cosenza[(a)]; Università della Calabria, Dipartimento di Fisica[(b)], IT-87036 Arcavacata di Rende, Italy
[37] Faculty of Physics and Applied Computer Science of the AGH-University of Science and Technology, (FPACS, AGH-UST), al. Mickiewicza 30, PL-30059 Cracow, Poland
[38] The Henryk Niewodniczanski Institute of Nuclear Physics, Polish Academy of Sciences, ul. Radzikowskiego 152, PL - 31342 Krakow, Poland
[39] Southern Methodist University, Physics Department, 106 Fondren Science Building, Dallas, TX 75275-0175, United States of America
[40] University of Texas at Dallas, 800 West Campbell Road, Richardson, TX 75080-3021, United States of America
[41] DESY, Notkestr. 85, D-22603 Hamburg and Platanenallee 6, D-15738 Zeuthen, Germany
[42] TU Dortmund, Experimentelle Physik IV, DE - 44221 Dortmund, Germany
[43] Technical University Dresden, Institut für Kern- und Teilchenphysik, Zellescher Weg 19, D-01069 Dresden, Germany
[44] Duke University, Department of Physics, Durham, NC 27708, United States of America
[45] University of Edinburgh, School of Physics & Astronomy, James Clerk Maxwell Building, The Kings Buildings, Mayfield Road, Edinburgh EH9 3JZ, United Kingdom
[46] Fachhochschule Wiener Neustadt; Johannes Gutenbergstrasse 3 AT - 2700 Wiener Neustadt, Austria
[47] INFN Laboratori Nazionali di Frascati, via Enrico Fermi 40, IT-00044 Frascati, Italy
[48] Albert-Ludwigs-Universität, Fakultät für Mathematik und Physik, Hermann-Herder Str. 3, D - 79104 Freiburg i.Br., Germany
[49] Université de Genève, section de Physique, 24 rue Ernest Ansermet, CH - 1211 Geneve 4, Switzerland
[50] INFN Sezione di Genova[(a)]; Università di Genova, Dipartimento di Fisica[(b)], via Dodecaneso 33, IT - 16146 Genova, Italy
[51] Institute of Physics of the Georgian Academy of Sciences, 6 Tamarashvili St., GE - 380077 Tbilisi; Tbilisi State University, HEP Institute, University St. 9, GE - 380086 Tbilisi, Georgia
[52] Justus-Liebig-Universität Giessen, II Physikalisches Institut, Heinrich-Buff Ring 16, D-35392 Giessen, Germany
[53] University of Glasgow, Department of Physics and Astronomy, Glasgow G12 8QQ, United Kingdom
[54] Georg-August-Universität, II. Physikalisches Institut, Friedrich-Hund Platz 1, D-37077 Göttingen, Germany
[55] Laboratoire de Physique Subatomique et de Cosmologie, CNRS/IN2P3, Université Joseph Fourier, INPG, 53 avenue des Martyrs, FR - 38026 Grenoble Cedex, France
[56] Hampton University, Department of Physics, Hampton, VA 23668, United States of America
[57] Harvard University, Laboratory for Particle Physics and Cosmology, 18 Hammond Street, Cambridge, MA 02138, United States of America
[58] Ruprecht-Karls-Universität Heidelberg: Kirchhoff-Institut für Physik[(a)], Im Neuenheimer Feld 227, D-69120 Heidelberg; Physikalisches Institut[(b)], Philosophenweg 12, D-69120 Heidelberg; ZITI Ruprecht-Karls-University Heidelberg[(c)], Lehrstuhl für Informatik V, B6, 23-29, DE - 68131 Mannheim, Germany
[59] Hiroshima University, Faculty of Science, 1-3-1 Kagamiyama, Higashihiroshima-shi, JP - Hiroshima 739-8526, Japan
[60] Hiroshima Institute of Technology, Faculty of Applied Information Science, 2-1-1 Miyake Saeki-ku, Hiroshima-shi, JP - Hiroshima 731-5193, Japan
[61] Indiana University, Department of Physics, Swain Hall West 117, Bloomington, IN 47405-7105, United States of America

JHEP12(2010)060

[62] Institut für Astro- und Teilchenphysik, Technikerstrasse 25, A - 6020 Innsbruck, Austria
[63] University of Iowa, 203 Van Allen Hall, Iowa City, IA 52242-1479, United States of America
[64] Iowa State University, Department of Physics and Astronomy, Ames High Energy Physics Group, Ames, IA 50011-3160, United States of America
[65] Joint Institute for Nuclear Research, JINR Dubna, RU - 141 980 Moscow Region, Russia
[66] KEK, High Energy Accelerator Research Organization, 1-1 Oho, Tsukuba-shi, Ibaraki-ken 305-0801, Japan
[67] Kobe University, Graduate School of Science, 1-1 Rokkodai-cho, Nada-ku, JP Kobe 657-8501, Japan
[68] Kyoto University, Faculty of Science, Oiwake-cho, Kitashirakawa, Sakyou-ku, Kyoto-shi, JP - Kyoto 606-8502, Japan
[69] Kyoto University of Education, 1 Fukakusa, Fujimori, fushimi-ku, Kyoto-shi, JP - Kyoto 612-8522, Japan
[70] Universidad Nacional de La Plata, FCE, Departamento de Física, IFLP (CONICET-UNLP), C.C. 67, 1900 La Plata, Argentina
[71] Lancaster University, Physics Department, Lancaster LA1 4YB, United Kingdom
[72] INFN Sezione di Lecce[(a)]; Università del Salento, Dipartimento di Fisica[(b)]Via Arnesano IT - 73100 Lecce, Italy
[73] University of Liverpool, Oliver Lodge Laboratory, P.O. Box 147, Oxford Street, Liverpool L69 3BX, United Kingdom
[74] Jožef Stefan Institute and University of Ljubljana, Department of Physics, SI-1000 Ljubljana, Slovenia
[75] Queen Mary University of London, Department of Physics, Mile End Road, London E1 4NS, United Kingdom
[76] Royal Holloway, University of London, Department of Physics, Egham Hill, Egham, Surrey TW20 0EX, United Kingdom
[77] University College London, Department of Physics and Astronomy, Gower Street, London WC1E 6BT, United Kingdom
[78] Laboratoire de Physique Nucléaire et de Hautes Energies, Université Pierre et Marie Curie (Paris 6), Université Denis Diderot (Paris-7), CNRS/IN2P3, Tour 33, 4 place Jussieu, FR - 75252 Paris Cedex 05, France
[79] Fysiska institutionen, Lunds universitet, Box 118, SE - 221 00 Lund, Sweden
[80] Universidad Autonoma de Madrid, Facultad de Ciencias, Departamento de Fisica Teorica, ES - 28049 Madrid, Spain
[81] Universität Mainz, Institut für Physik, Staudinger Weg 7, DE - 55099 Mainz, Germany
[82] University of Manchester, School of Physics and Astronomy, Manchester M13 9PL, United Kingdom
[83] CPPM, Aix-Marseille Université, CNRS/IN2P3, Marseille, France
[84] University of Massachusetts, Department of Physics, 710 North Pleasant Street, Amherst, MA 01003, United States of America
[85] McGill University, High Energy Physics Group, 3600 University Street, Montreal, Quebec H3A 2T8, Canada
[86] University of Melbourne, School of Physics, AU - Parkville, Victoria 3010, Australia
[87] The University of Michigan, Department of Physics, 2477 Randall Laboratory, 500 East University, Ann Arbor, MI 48109-1120, United States of America
[88] Michigan State University, Department of Physics and Astronomy, High Energy Physics Group, East Lansing, MI 48824-2320, United States of America
[89] INFN Sezione di Milano[(a)]; Università di Milano, Dipartimento di Fisica[(b)], via Celoria 16, IT - 20133 Milano, Italy

JHEP12(2010)060

[90] B.I. Stepanov Institute of Physics, National Academy of Sciences of Belarus, Independence Avenue 68, Minsk 220072, Republic of Belarus
[91] National Scientific & Educational Centre for Particle & High Energy Physics, NC PHEP BSU, M. Bogdanovich St. 153, Minsk 220040, Republic of Belarus
[92] Massachusetts Institute of Technology, Department of Physics, Room 24-516, Cambridge, MA 02139, United States of America
[93] University of Montreal, Group of Particle Physics, C.P. 6128, Succursale Centre-Ville, Montreal, Quebec, H3C 3J7 , Canada
[94] P.N. Lebedev Institute of Physics, Academy of Sciences, Leninsky pr. 53, RU - 117 924 Moscow, Russia
[95] Institute for Theoretical and Experimental Physics (ITEP), B. Cheremushkinskaya ul. 25, RU 117 218 Moscow, Russia
[96] Moscow Engineering & Physics Institute (MEPhI), Kashirskoe Shosse 31, RU - 115409 Moscow, Russia
[97] Lomonosov Moscow State University Skobeltsyn Institute of Nuclear Physics (MSU SINP), 1(2), Leninskie gory, GSP-1, Moscow 119991 Russian Federation, Russia
[98] Ludwig-Maximilians-Universität München, Fakultät für Physik, Am Coulombwall 1, DE - 85748 Garching, Germany
[99] Max-Planck-Institut für Physik, (Werner-Heisenberg-Institut), Föhringer Ring 6, 80805 München, Germany
[100] Nagasaki Institute of Applied Science, 536 Aba-machi, JP Nagasaki 851-0193, Japan
[101] Nagoya University, Graduate School of Science, Furo-Cho, Chikusa-ku, Nagoya, 464-8602, Japan
[102] INFN Sezione di Napoli$^{(a)}$; Università di Napoli, Dipartimento di Scienze Fisiche$^{(b)}$, Complesso Universitario di Monte Sant'Angelo, via Cinthia, IT - 80126 Napoli, Italy
[103] University of New Mexico, Department of Physics and Astronomy, MSC07 4220, Albuquerque, NM 87131 U.S.A., United States of America
[104] Radboud University Nijmegen/NIKHEF, Department of Experimental High Energy Physics, Heyendaalseweg 135, NL-6525 AJ, Nijmegen, Netherlands
[105] Nikhef National Institute for Subatomic Physics, and University of Amsterdam, Science Park 105, 1098 XG Amsterdam, Netherlands
[106] Department of Physics, Northern Illinois University, LaTourette Hall Normal Road, DeKalb, IL 60115, United States of America
[107] Budker Institute of Nuclear Physics (BINP), RU - Novosibirsk 630 090, Russia
[108] New York University, Department of Physics, 4 Washington Place, New York NY 10003, U.S.A., United States of America
[109] Ohio State University, 191 West Woodruff Ave, Columbus, OH 43210-1117, United States of America
[110] Okayama University, Faculty of Science, Tsushimanaka 3-1-1, Okayama 700-8530, Japan
[111] University of Oklahoma, Homer L. Dodge Department of Physics and Astronomy, 440 West Brooks, Room 100, Norman, OK 73019-0225, United States of America
[112] Oklahoma State University, Department of Physics, 145 Physical Sciences Building, Stillwater, OK 74078-3072, United States of America
[113] Palacký University, 17.listopadu 50a, 772 07 Olomouc, Czech Republic
[114] University of Oregon, Center for High Energy Physics, Eugene, OR 97403-1274, United States of America
[115] LAL, Univ. Paris-Sud, IN2P3/CNRS, Orsay, France
[116] Osaka University, Graduate School of Science, Machikaneyama-machi 1-1, Toyonaka, Osaka 560-0043, Japan

JHEP12(2010)060

[117] University of Oslo, Department of Physics, P.O. Box 1048, Blindern, NO - 0316 Oslo 3, Norway
[118] Oxford University, Department of Physics, Denys Wilkinson Building, Keble Road, Oxford OX1 3RH, United Kingdom
[119] INFN Sezione di Pavia[(a)]; Università di Pavia, Dipartimento di Fisica Nucleare e Teorica[(b)], Via Bassi 6, IT-27100 Pavia, Italy
[120] University of Pennsylvania, Department of Physics, High Energy Physics Group, 209 S. 33rd Street, Philadelphia, PA 19104, United States of America
[121] Petersburg Nuclear Physics Institute, RU - 188 300 Gatchina, Russia
[122] INFN Sezione di Pisa[(a)]; Università di Pisa, Dipartimento di Fisica E. Fermi[(b)], Largo B. Pontecorvo 3, IT - 56127 Pisa, Italy
[123] University of Pittsburgh, Department of Physics and Astronomy, 3941 O'Hara Street, Pittsburgh, PA 15260, United States of America
[124] Laboratorio de Instrumentacao e Fisica Experimental de Particulas - LIP[(a)], Avenida Elias Garcia 14-1, PT - 1000-149 Lisboa, Portugal; Universidad de Granada, Departamento de Fisica Teorica y del Cosmos and CAFPE[(b)], E-18071 Granada, Spain
[125] Institute of Physics, Academy of Sciences of the Czech Republic, Na Slovance 2, CZ - 18221 Praha 8, Czech Republic
[126] Charles University in Prague, Faculty of Mathematics and Physics, Institute of Particle and Nuclear Physics, V Holesovickach 2, CZ - 18000 Praha 8, Czech Republic
[127] Czech Technical University in Prague, Zikova 4, CZ - 166 35 Praha 6, Czech Republic
[128] State Research Center Institute for High Energy Physics, Moscow Region, 142281, Protvino, Pobeda street, 1, Russia
[129] Rutherford Appleton Laboratory, Science and Technology Facilities Council, Harwell Science and Innovation Campus, Didcot OX11 0QX, United Kingdom
[130] University of Regina, Physics Department, Canada
[131] Ritsumeikan University, Noji Higashi 1 chome 1-1, JP - Kusatsu, Shiga 525-8577, Japan
[132] INFN Sezione di Roma I[(a)]; Università La Sapienza, Dipartimento di Fisica[(b)], Piazzale A. Moro 2, IT- 00185 Roma, Italy
[133] INFN Sezione di Roma Tor Vergata[(a)]; Università di Roma Tor Vergata, Dipartimento di Fisica[(b)], via della Ricerca Scientifica, IT-00133 Roma, Italy
[134] INFN Sezione di Roma Tre[(a)]; Università Roma Tre, Dipartimento di Fisica[(b)], via della Vasca Navale 84, IT-00146 Roma, Italy
[135] Réseau Universitaire de Physique des Hautes Energies (RUPHE): Université Hassan II, Faculté des Sciences Ain Chock[(a)], B.P. 5366, MA - Casablanca; Centre National de l'Energie des Sciences Techniques Nucleaires (CNESTEN)[(b)], B.P. 1382 R.P. 10001 Rabat 10001; Université Mohamed Premier[(c)], LPTPM, Faculté des Sciences, B.P.717. Bd. Mohamed VI, 60000, Oujda; Université Mohammed V, Faculté des Sciences[(d)]4 Avenue Ibn Battouta, BP 1014 RP, 10000 Rabat, Morocco
[136] CEA, DSM/IRFU, Centre d'Etudes de Saclay, FR - 91191 Gif-sur-Yvette, France
[137] University of California Santa Cruz, Santa Cruz Institute for Particle Physics (SCIPP), Santa Cruz, CA 95064, United States of America
[138] University of Washington, Seattle, Department of Physics, Box 351560, Seattle, WA 98195-1560, United States of America
[139] University of Sheffield, Department of Physics & Astronomy, Hounsfield Road, Sheffield S3 7RH, United Kingdom
[140] Shinshu University, Department of Physics, Faculty of Science, 3-1-1 Asahi, Matsumoto-shi, JP - Nagano 390-8621, Japan
[141] Universität Siegen, Fachbereich Physik, D 57068 Siegen, Germany
[142] Simon Fraser University, Department of Physics, 8888 University Drive, CA - Burnaby, BC V5A 1S6, Canada

JHEP12(2010)060

[143] SLAC National Accelerator Laboratory, Stanford, California 94309, United States of America
[144] Comenius University, Faculty of Mathematics, Physics & Informatics[(a)], Mlynska dolina F2, SK - 84248 Bratislava; Institute of Experimental Physics of the Slovak Academy of Sciences, Dept. of Subnuclear Physics[(b)], Watsonova 47, SK - 04353 Kosice, Slovak Republic
[145] [(a)]University of Johannesburg, Department of Physics, PO Box 524, Auckland Park, Johannesburg 2006; [(b)]School of Physics, University of the Witwatersrand, Private Bag 3, Wits 2050, Johannesburg, South Africa, South Africa
[146] Stockholm University: Department of Physics[(a)]; The Oskar Klein Centre[(b)], AlbaNova, SE - 106 91 Stockholm, Sweden
[147] Royal Institute of Technology (KTH), Physics Department, SE - 106 91 Stockholm, Sweden
[148] Stony Brook University, Department of Physics and Astronomy, Nicolls Road, Stony Brook, NY 11794-3800, United States of America
[149] University of Sussex, Department of Physics and Astronomy Pevensey 2 Building, Falmer, Brighton BN1 9QH, United Kingdom
[150] University of Sydney, School of Physics, AU - Sydney NSW 2006, Australia
[151] Insitute of Physics, Academia Sinica, TW - Taipei 11529, Taiwan
[152] Technion, Israel Inst. of Technology, Department of Physics, Technion City, IL - Haifa 32000, Israel
[153] Tel Aviv University, Raymond and Beverly Sackler School of Physics and Astronomy, Ramat Aviv, IL - Tel Aviv 69978, Israel
[154] Aristotle University of Thessaloniki, Faculty of Science, Department of Physics, Division of Nuclear & Particle Physics, University Campus, GR - 54124, Thessaloniki, Greece
[155] The University of Tokyo, International Center for Elementary Particle Physics and Department of Physics, 7-3-1 Hongo, Bunkyo-ku, JP - Tokyo 113-0033, Japan
[156] Tokyo Metropolitan University, Graduate School of Science and Technology, 1-1 Minami-Osawa, Hachioji, Tokyo 192-0397, Japan
[157] Tokyo Institute of Technology, 2-12-1-H-34 O-Okayama, Meguro, Tokyo 152-8551, Japan
[158] University of Toronto, Department of Physics, 60 Saint George Street, Toronto M5S 1A7, Ontario, Canada
[159] TRIUMF[(a)], 4004 Wesbrook Mall, Vancouver, B.C. V6T 2A3; [(b)]York University, Department of Physics and Astronomy, 4700 Keele St., Toronto, Ontario, M3J 1P3, Canada
[160] University of Tsukuba, Institute of Pure and Applied Sciences, 1-1-1 Tennoudai, Tsukuba-shi, JP - Ibaraki 305-8571, Japan
[161] Tufts University, Science & Technology Center, 4 Colby Street, Medford, MA 02155, United States of America
[162] Universidad Antonio Narino, Centro de Investigaciones, Cra 3 Este No.47A-15, Bogota, Colombia
[163] University of California, Irvine, Department of Physics & Astronomy, CA 92697-4575, United States of America
[164] INFN Gruppo Collegato di Udine[(a)]; ICTP[(b)], Strada Costiera 11, IT-34014, Trieste; Università di Udine, Dipartimento di Fisica[(c)], via delle Scienze 208, IT - 33100 Udine, Italy
[165] University of Illinois, Department of Physics, 1110 West Green Street, Urbana, Illinois 61801, United States of America
[166] University of Uppsala, Department of Physics and Astronomy, P.O. Box 516, SE -751 20 Uppsala, Sweden
[167] Instituto de Física Corpuscular (IFIC) Centro Mixto UVEG-CSIC, Apdo. 22085 ES-46071 Valencia, Dept. Física At. Mol. y Nuclear; Dept. Ing. Electrónica; Univ. of Valencia, and Inst. de Microelectrónica de Barcelona (IMB-CNM-CSIC) 08193 Bellaterra, Spain
[168] University of British Columbia, Department of Physics, 6224 Agricultural Road, CA - Vancouver, B.C. V6T 1Z1, Canada

JHEP12(2010)060

[169] University of Victoria, Department of Physics and Astronomy, P.O. Box 3055, Victoria B.C., V8W 3P6, Canada
[170] Waseda University, WISE, 3-4-1 Okubo, Shinjuku-ku, Tokyo, 169-8555, Japan
[171] The Weizmann Institute of Science, Department of Particle Physics, P.O. Box 26, IL - 76100 Rehovot, Israel
[172] University of Wisconsin, Department of Physics, 1150 University Avenue, WI 53706 Madison, Wisconsin, United States of America
[173] Julius-Maximilians-University of Würzburg, Physikalisches Institute, Am Hubland, 97074 Würzburg, Germany
[174] Bergische Universität, Fachbereich C, Physik, Postfach 100127, Gauss-Strasse 20, D- 42097 Wuppertal, Germany
[175] Yale University, Department of Physics, PO Box 208121, New Haven CT, 06520-8121, United States of America
[176] Yerevan Physics Institute, Alikhanian Brothers Street 2, AM - 375036 Yerevan, Armenia
[177] Centre de Calcul CNRS/IN2P3, Domaine scientifique de la Doua, 27 bd du 11 Novembre 1918, 69622 Villeurbanne Cedex, France

[a] Also at LIP, Portugal
[b] Present address FermiLab, U.S.A.
[c] Also at Faculdade de Ciencias, Universidade de Lisboa, Portugal
[d] Also at CPPM, Marseille, France.
[e] Also at TRIUMF, Vancouver, Canada
[f] Also at FPACS, AGH-UST, Cracow, Poland
[g] Now at Universita' dell'Insubria, Dipartimento di Fisica e Matematica
[h] Also at TRIUMF, Vancouver, Canada
[i] Also at Department of Physics, University of Coimbra, Portugal
[j] Now at CERN
[k] Also at Università di Napoli Parthenope, Napoli, Italy
[l] Also at Institute of Particle Physics (IPP), Canada
[m] Also at Università di Napoli Parthenope, via A. Acton 38, IT - 80133 Napoli, Italy
[n] Louisiana Tech University, 305 Wisteria Street, P.O. Box 3178, Ruston, LA 71272, United States of America
[o] Also at Universidade de Lisboa, Portugal
[p] At California State University, Fresno, U.S.A.
[q] Also at TRIUMF, 4004 Wesbrook Mall, Vancouver, B.C. V6T 2A3, Canada
[r] Currently at Istituto Universitario di Studi Superiori IUSS, Pavia, Italy
[s] Also at Faculdade de Ciencias, Universidade de Lisboa, Portugal and at Centro de Fisica Nuclear da Universidade de Lisboa, Portugal
[t] Also at FPACS, AGH-UST, Cracow, Poland
[u] Also at California Institute of Technology, Pasadena, U.S.A.
[v] Louisiana Tech University, Ruston, U.S.A.
[w] Also at University of Montreal, Montreal, Canada
[x] Also at Institut für Experimentalphysik, Universität Hamburg, Hamburg, Germany
[y] Now at Chonnam National University, Chonnam, Korea 500-757
[z] Also at Petersburg Nuclear Physics Institute, Gatchina, Russia
[aa] Also at Institut für Experimentalphysik, Universität Hamburg, Luruper Chaussee 149, 22761 Hamburg, Germany
[ab] Also at School of Physics and Engineering, Sun Yat-sen University, China
[ac] Also at School of Physics, Shandong University, Jinan, China

JHEP12(2010)060

[ad] Also at California Institute of Technology, Pasadena, U.S.A.
[ae] Also at Rutherford Appleton Laboratory, Didcot, U.K.
[af] Also at school of physics, Shandong University, Jinan
[ag] Also at Rutherford Appleton Laboratory, Didcot , U.K.
[ah] Now at KEK
[ai] Also at Departamento de Fisica, Universidade de Minho, Portugal
[aj] University of South Carolina, Columbia, U.S.A.
[ak] Also at KFKI Research Institute for Particle and Nuclear Physics, Budapest, Hungary
[al] University of South Carolina, Dept. of Physics and Astronomy, 700 S. Main St, Columbia, SC 29208, United States of America
[am] Also at Institute of Physics, Jagiellonian University, Cracow, Poland
[an] Louisiana Tech University, Ruston, U.S.A.
[ao] Also at Centro de Fisica Nuclear da Universidade de Lisboa, Portugal
[ap] Also at School of Physics and Engineering, Sun Yat-sen University, Taiwan
[aq] University of South Carolina, Columbia, U.S.A.
[ar] Transfer to LHCb 31.01.2010
[as] Also at Oxford University, Department of Physics, Denys Wilkinson Building, Keble Road, Oxford OX1 3RH, United Kingdom
[at] Also at school of physics and engineering, Sun Yat-sen University
[au] Naruto University of Education, Tokushima, Japan
[av] Also at CEA
[aw] Also at LPNHE, Paris, France
[ax] Also at Nanjing University, China
[*] Deceased

JHEP12(2010)060